

UNIVERSITY OF CALIFORNIA, SAN DIEGO

**A Search for New Physics producing Jets, Large MT₂, and Disappearing Tracks in 13 TeV
Proton-Proton Collision at CERN's Large Hadron Collider**

A dissertation submitted in partial satisfaction of the
requirements for the degree
Doctor of Philosophy

in

Physics

by

Dylan Gilbert

Committee in charge:

Professor Avraham Yagil, Chair
Professor Frank Würthwein, Co-Chair
Professor Rommie Amaro
Professor Adam Burgasser
Professor George Fuller

2019

Copyright
Dylan Gilbert, 2019
All rights reserved.

The dissertation of Dylan Gilbert is approved, and it is acceptable in quality and form for publication on microfilm and electronically:

Co-Chair

Chair

University of California, San Diego

2019

TABLE OF CONTENTS

Signature Page	iii
Table of Contents	iv
List of Figures	vi
List of Tables	viii
Acknowledgements	ix
Vita	x
Abstract of the Dissertation	xi
Chapter 1 Introduction	1
1.1 The Standard Model of Particle Physics	1
1.1.1 A Brief Description	1
1.1.2 Feynman Diagrams	1
1.1.3 Quantum Chromodynamics, Hadronization, and Jets	2
1.1.4 Parton Distribution Functions	2
1.2 Some Problems with the Standard Model	2
1.2.1 Effective Field Theory	2
1.2.2 Gravity	2
1.2.3 The Hierarchy Problem	2
1.2.4 Astrophysical Evidence of Dark Matter	3
1.3 Supersymmetry	3
1.3.1 Theoretical Appeal	3
1.3.2 Experimental Signatures	3
1.3.3 Simplified Models	3
1.4 Other Models	4
Chapter 2 The Large Hadron Collider and the CMS Detector	5
2.1 The Large Hadron Collider	5
2.1.1 A Brief Description	5
2.1.2 Luminosity Delivered	5
2.2 The CMS Detector	6
2.2.1 Magnet	6
2.2.2 Tracker	6
2.2.3 Electromagnetic Calorimeter	6
2.2.4 Hadronic Calorimeter	7
2.2.5 Muon System	7
2.2.6 Missing Transverse Energy	7

2.3	CMS Event Reconstruction	7
2.3.1	Challenges	7
2.3.2	Vertices	8
2.3.3	Particle Flow	8
2.3.4	Jet Clustering	8
2.4	Simulation	9
2.5	Objectives	9
2.6	Limitations and Challenges	9
2.7	The Simulation Pipeline	9
Chapter 3	The Full 13 TeV M_{T2} Analysis	10
3.1	Classic Search	11
3.1.1	General Description	11
3.1.2	Signals	12
3.1.3	Backgrounds	18
3.1.4	Baseline Selection	24
3.1.5	Upgrades in 2019	24
3.1.6	Signal Contamination	30
3.1.7	Results	31
3.1.8	Limits	31
3.1.9	Future of the Classic M_{T2} Search	39
3.2	Disappearing Tracks Search	41
3.2.1	General Description	41
3.2.2	Data-Driven Background Estimate	42
3.2.3	Results	42
3.2.4	Limits	42
3.2.5	Future	43
Chapter 4	Conclusions	52
Appendix A	Full Classic Binning and Results	53
Bibliography	62

LIST OF FIGURES

Figure 1.1:	Theoretical gluino pair production cross section in simplified models.	4
Figure 3.1:	Diagrams for gluino and squark pair production, as predicted by supersymmetric extensions of the Standard Model.	13
Figure 3.2:	Diagram for the mono- ϕ model.	17
Figure 3.3:	Leptoquark pair production diagrams.	17
Figure 3.4:	M_{T2} distributions of backgrounds and an example signal point.	20
Figure 3.5:	$\Delta\phi_{min}^{1,2,3,4}$ distributions of backgrounds and an example signal point.	21
Figure 3.6:	(Left) The ratio of the number of same flavor to different flavor lepton pairs in data. (Right) A comparison of the M_{T2} shape between data Z to lepton events and simulated Z to neutrino events.	23
Figure 3.7:	Fit of r_ϕ as a function of M_{T2}	26
Figure 3.8:	Example plot of jet energy resolution template.	27
Figure 3.9:	Validation of the Rebalance and Smear jet mismeasurement background estimate in the $\Delta\phi_{min}^{1,2,3,4} < 0.3$ control region.	28
Figure 3.10:	Comparison of predicted background and observed data events in the classic search (upper) integrated over M_{T2} and (lower) for each of the medium H_T search regions.	32
Figure 3.11:	Exclusion limits for gluino pair production and decay to light quarks.	35
Figure 3.12:	Exclusion limits for gluino pair production and decay to bottom (left) and top (right) quarks.	36
Figure 3.13:	Exclusion limit at 95% CL _S for (upper left) light-flavor squark pair production, (upper right) bottom squark pair production, and (lower) top squark pair production.	37
Figure 3.14:	Exclusion limit at 95% CL _S for top squark pair production for various decay modes of the top squark.	38
Figure 3.15:	Exclusion limit at 95% CL _S for the mono- ϕ model.	39
Figure 3.16:	Upper limits at 95% CL _S on the leptoquark production cross sections as a function of leptoquark mass.	40
Figure 3.17:	Validation of the disappearing tracks background estimate in (upper) 2016 and (lower) 2017–2018 data.	43
Figure 3.18:	Comparison of the predicted background and observed data events in the disappearing track search for (upper) 2016 and (lower) 2017–2018.	44
Figure 3.19:	Diagrams for (left) gluino, (center) light-flavor squark, and (right) top squark pair production, in which the gluinos and squarks can decay via a long-lived $\tilde{\chi}^\pm$	45
Figure 3.20:	Exclusion limits at 95% CL _S for direct gluino pair production where the gluinos decay to light-flavor quarks, with $c\tau_0(\tilde{\chi}^\pm)$ = (upper left) 10 cm, (upper right) 50 cm, and (lower) 200 cm.	46
Figure 3.21:	Exclusion limits at 95% CL _S for light squark pair production with $c\tau_0(\tilde{\chi}^\pm)$ = (upper left) 10 cm, (upper right) 50 cm, and (lower) 200 cm.	47

Figure 3.22: Exclusion limits at 95% CL _S for top squark pair production with $c\tau_0(\tilde{\chi}^\pm) =$ (upper left) 10cm, (upper right) 50cm, and (lower) 200cm.	48
Figure 3.23: Exclusion limits at 95% CL _S on the $\tilde{\chi}_1^0$ mass, with $m_{\tilde{\chi}^\pm} = m_{\tilde{\chi}_1^0} + \mathcal{O}(100\text{ MeV})$, as a function of the $\tilde{\chi}^\pm$ proper decay length, for (upper) direct gluino and (lower) direct light-flavor squark pair production, for representative gluino and squark masses.	49
Figure 3.24: Exclusion limits at 95% CL _S on the $\tilde{\chi}_1^0$ mass, with $m_{\tilde{\chi}^\pm} = m_{\tilde{\chi}_1^0} + \mathcal{O}(100\text{ MeV})$, as a function of the $\tilde{\chi}^\pm$ proper decay length, for direct top squark pair pro- duction, as obtained for a representative top squark mass.	50
Figure 3.25: Exclusion limits at 95% CL _S on $\sigma/\sigma_{\text{theory}}$ as a function of the $\tilde{\chi}^\pm$ decay length, for (upper) gluino pair production where the gluinos decay to light- flavor quarks, (lower left) light-flavor squark pair production, and (lower right) top squark pair production, as obtained from the search for disappear- ing tracks.	51

LIST OF TABLES

Table 3.1: Summary table of baseline event selection.	24
Table A.1: Table of the classic monojet regions.	53
Table A.2: Table of the Very Low H_T classic regions.	54
Table A.3: Table of the Low H_T classic regions.	55
Table A.4: Table of the Medium H_T classic regions, with $N_{\text{jet}} < 7$	56
Table A.5: Table of the Medium H_T classic regions, with $N_{\text{jet}} \geq 7$	57
Table A.6: Table of the High H_T classic regions, with $N_{\text{jet}} < 7$	58
Table A.7: Table of the High H_T classic regions, with $N_{\text{jet}} \geq 7$	59
Table A.8: Table of the Ultra-High H_T classic regions, with $N_{\text{jet}} < 7$	60
Table A.9: Table of the Ultra-High H_T classic regions, with $N_{\text{jet}} \geq 7$	61

ACKNOWLEDGEMENTS

Thousands of physicists, engineers, and technicians around the world have worked for decades to design, build, and operate CERN’s LHC and the CMS detector. My work would have been impossible without their efforts.

My advisors Avi Yagil and Frank Würthwein showed great patience and faith in me along the way, for which I am profoundly thankful.

Mario Masciovecchio deserves special thanks for providing the bulk of my technical training, and working with me at all hours of the day and night, transcending timezones, for years. He also developed the prototype short track definition.

Slava Krutelyov, Ryan Kelley, Ian MacNeill, Bobak Hashemi, Dominick Olivito, Mark Derdzinski, Giovanni Zevi Della Porta, and Daniel Klein also provided helpful training.

Bennett Marsh, as part of and in addition to maintaining the “classic” portion of the analysis, wrote a lot of helpful code, offered many useful tips and ideas, and in general managed much of the tedious technical work for years.

Claudio Campagnari provided useful instruction in statistical analysis, and suggested the idea that finalized the disappearing track background estimate.

More generally, I must thank the rest of the Surf and Turf (SNT) group for criticism and suggestions along the way, which helped to sharpen the analysis, and the team responsible for maintaining the CMS Tier 2 computing center at UCSD, which provided most of the computing resources.

Finally, the CMS SUSY group, like SNT, provided useful criticism during analysis development.

VITA

2013 B. A. in Physics, Williams College

2019 Ph. D. in Physics, University of California, San Diego

PUBLICATIONS

The CMS collaboration, Sirunyan, A.M., et al., *Searches for physics beyond the standard model with the M_{T2} variable in hadronic final states with and without disappearing tracks in proton-proton collisions at $\sqrt{s} = 13$ TeV*, Eur. Phys. J C (2019)

ABSTRACT OF THE DISSERTATION

A Search for New Physics producing Jets, Large MT₂, and Disappearing Tracks in 13 TeV Proton-Proton Collision at CERN's Large Hadron Collider

by

Dylan Gilbert

Doctor of Philosophy in Physics

University of California, San Diego, 2019

Professor Avraham Yagil, Chair
Professor Frank Würthwein, Co-Chair

This work presents two searches for new physics characterized by pair-production of strongly interacting particles, each decaying to hadronic jets and a particle that is not detectable. The searches use the full 13 TeV proton-proton collision dataset produced by CERN's Large Hadron Collider and recorded by the CMS detector from 2016 to 2018, with total integrated luminosity 137 fb^{-1} . The presence of particles interacting too weakly to be detected is inferred using imbalance in the transverse momentum of the collision products, and sensitivity to pair-production is enhanced by requiring large values of the kinematic variable M_{T2} in events with

at least two jets. The first search is inclusive, binning events using the total hadronic transverse energy, the total number of jets, the number of jets reconstructed as originating from a bottom quark, and either the value of M_{T2} in multijet events, or the transverse momentum of the jet in monojet events. The second search extends the first, by requiring the presence of a disappearing track in the event, and adds binning in the length and transverse momentum of the disappearing track. Both searches are sensitive to a variety of extensions to the Standard Model that include dark matter candidates. Of greatest interest, the results set constraints on pair production of squarks and gluinos as predicted by R-parity conserving supersymmetric extensions of the Standard Model, in which the lightest superysmmetric particle is a neutralino. The first search is sensitive to any decay chain terminating in Standard Model hadrons plus the neutralino, while the second specifically targets, with greatly enhanced sensitivity, decay chains containing an intermediate long-lived chargino. These constraints are the most stringent yet produced by any experiment.

Chapter 1

Introduction

Introduction

1.1 The Standard Model of Particle Physics

Briefly discuss the history of particle physics (eg Millikan, Rutherford, Planck, Bohr, Dirac... QFT), culminating in the Standard Model.

Figure ??

1.1.1 A Brief Description

Describe the particles of the Standard Model, and some of their experimental relevance.

1.1.2 Feynman Diagrams

Provide a few example Feynman diagrams (eg. ee -> mu mu, gg -> top loop -> higgs -> top loop -> gamma gamma) and describe how they represent particle physics processes, and are used to calculate amplitudes.

1.1.3 Quantum Chromodynamics, Hadronization, and Jets

Describe why final state quarks and gluons experimentally produce jets. Mention that it is difficult to make precise predictions in QCD (at low energy), leading to requirement for approximate models for jet formation (pythia...). In particular, ISR is challenging.

1.1.4 Parton Distribution Functions

Describe protons as a sea of quarks and gluons with varying momenta, and why we need a PDF to calculate production rates in a hadron collider.

1.2 Some Problems with the Standard Model

Standard Model is extremely successful (electron magnetic moment, Higgs prediction) but not entirely satisfactory.

1.2.1 Effective Field Theory

Includes explicit energy cutoff, as part of renormalization. Cannot, by construction, be the final theory.

1.2.2 Gravity

Doesn't include gravity, so Planck scale is maximum possible cutoff (but could be smaller).

1.2.3 The Hierarchy Problem

Why is the Higgs mass / weak scale so much smaller than the Planck scale? Is the cutoff much smaller?

1.2.4 Astrophysical Evidence of Dark Matter

SM has no (cold) dark matter candidate. Of course may be well out of reach, but look where we can. Good reason to believe that dark matter could be produced at LHC (WIMP miracle).

1.3 Supersymmetry

SUSY is one particular model that can patches up some of the SM's issues.

1.3.1 Theoretical Appeal

Solves up hierarchy problem if at the weak scale (so, potentially accessible to LHC) and provides a dark matter candidate. (Focus on RPC SUSY, due to proton stability.)

1.3.2 Experimental Signatures

SUSY produces MET, and in strong SUSY decays, potentially lots and lots of jets. Since SUSY

1.3.3 Simplified Models

SUSY parameter space is vast, so we consider one potential discovery channel at a time.

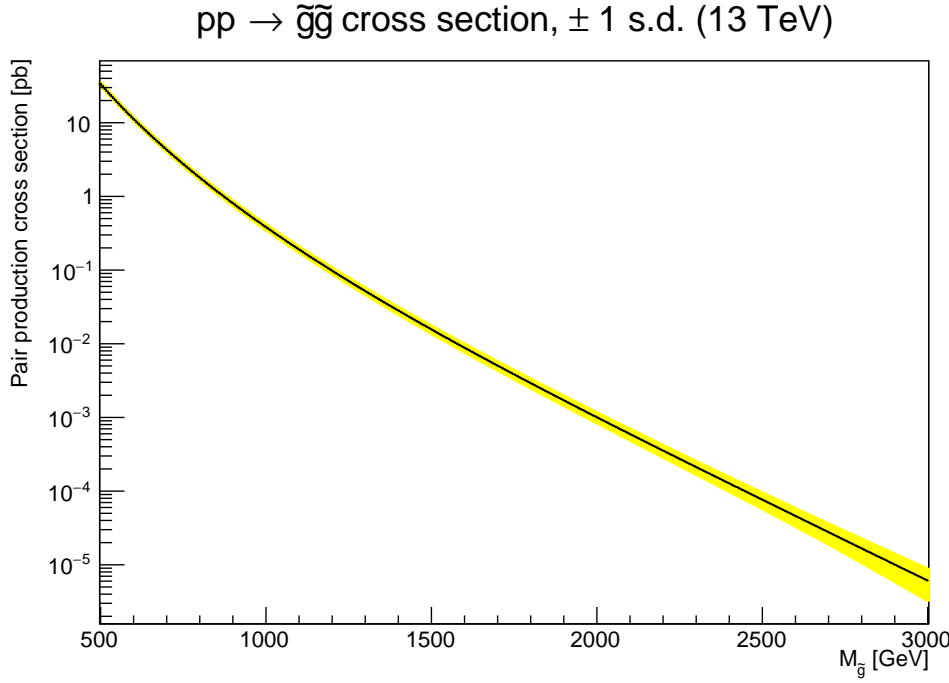


Figure 1.1: In simplified models, it is possible to calculate superpartner production cross sections from theory. Here, the theoretical gluino pair production cross section in 13 TeV proton-proton collisions is shown in black, with the one standard deviation uncertainty shown as a yellow band. The cross section drops rapidly with increasing mass. Based on cross section values used in [5], calculated in [4]. Compare Figure 5 (upper) from [4], of which this is a simplified reproduction.

1.4 Other Models

Introduce leptoquarks and mono-*phi*.

Chapter 2

The Large Hadron Collider and the CMS Detector

The CMS detector straddles proton beams produced using the LHC machine at CERN and observes the products of collisions. Its data is shared around the world and is used for this work.

2.1 The Large Hadron Collider

2.1.1 A Brief Description

Protons are accelerated and directed using electromagnetic fields. Ring is used for multiple collision chances, and must be large due to limited field strength (perhaps also mention that protons are chosen to keep synchrotron losses small).

2.1.2 Luminosity Delivered

Many, many collisions are needed to see rare events.

2.2 The CMS Detector

The LHC makes the collisions, but the CMS detector observes the products. Put overall plots distinguishing the experimental signatures for each particle type with references to the appropriate section.

2.2.1 Magnet

Strong magnet for determining charges of particles produced and assisting in ID and energy determination. Probably discuss advantages and disadvantages of CMS's (relative) compactness here, as almost entire detector is inside magnet.

2.2.2 Tracker

Tracker records positions of charged particles (current flow in silicon...). These hits are assembled into tracks (describe algorithm). Tracker is divided into pixel (higher precision) and strip (lower precision). Best possible detector would be an extremely large tracker, but the expense... Mention that tracker is not intended to shower particles, but sometimes does and refer to disappearing tracks section (probably nuclear interaction length budget plot goes here)

2.2.3 Electromagnetic Calorimeter

Photons and electrons shower in ECAL cells. What are the nice features that distinguish good and bad candidates? Heavier particles (muons, pions) are more penetrating (less brem). Mention dead cells due to radiation damage and reference dis tracks section.

2.2.4 Hadronic Calorimeter

Get everything else to shower except muons, how? Stress that even neutral hadrons are detected, and the importance of this to the dis track search.

2.2.5 Muon System

Muons are most highly penetrating (heavy, no nuclear interactions). Muons are very clean objects. What are the nice features that distinguish good and bad candidates? Describe different detector technologies.

2.2.6 Missing Transverse Energy

Sum everything up and infer the presence of undetected, “invisible” particles. Neutrinos! Also, mismeasurement, but perhaps also a small excess of something else...

M_{T2}

Describe the MT2 algorithm, its relationship to MET, and its experimental usefulness.

2.3 CMS Event Reconstruction

2.3.1 Challenges

Spray of thousands of particles, many in dense jets, from collisions distributed across a rather large beam crossing, millions of times per second. Pace is so high that travel of electrical impulses along the equipment is comparable to the collision frequency.

The Trigger System

High event rate needs to be suppressed due to computing limitations. High event rate is necessary to see rare things (how rare?).

Pileup

Obtaining a high enough event leads to many simultaneous collisions (not 1 proton collision at a time, but bunches crossing every 25 ns). Charged pileup contribution can be subtracted exactly using the tracker, but neutral pileup correction is heuristic. Effective area vs delta-beta.

2.3.2 Vertices

Use tracker to identify tracks and extrapolate them back to an origin point. These origins are vertices.

B-Tagging

Some tracks will not extrapolate back to a proton collision point but instead a point a few millimeters away: secondary vertices characteristic of b-tags. Describe other indicators used to identify b-jets and the efficiency.

2.3.3 Particle Flow

Describe particle flow algorithm and advantage relative to other techniques.

2.3.4 Jet Clustering

Jets are made from PF candidates using anti-kt. How accurately?

2.4 Simulation

The Standard Model and models of new physics predict what happens at the primary interaction, and this needs to be converted into a prediction for what happens in the detector.

2.5 Objectives

Used to study backgrounds and develop estimation techniques, and to design analyses to maximize sensitivity to expected signal signatures.

2.6 Limitations and Challenges

Ultra-detailed knowledge of the detector at the subatomic level at all locations is unachievable, and the detector's state evolves over time. QCD is irritating, and even electroweak physics is subject to theoretical uncertainties due partly to dependence on experimental inputs, and partly to calculating only to finite order. Can't run the simulation forever, and the computation is expensive.

2.7 The Simulation Pileline

Matrix elements (MadGraph) -> observed particles (pythia) -> how those particles interact with detector components (GEANT). Mention also fastsim vs fullsim (ie replacing GEANT with approximate smearing).

Chapter 3

The Full 13 TeV M_{T2} Analysis

This section presents two searches for new physics in all-hadronic final states with substantial \cancel{E}_T as inferred through large M_{T2} in 13 TeV proton-proton collisions recorded by the CMS detector [5]. The \cancel{E}_T requirement targets invisible particles, motivated by the evidence for dark matter discussed in Section 1.2.4. If dark matter is at least in part a particle associated with physics at the weak scale, then it may be produced in LHC collisions and, while not detectable itself, be inferred via an excess of events with imbalanced transverse momentum. Considering only all-hadronic events with large M_{T2} is part of a divide and conquer strategy employed by CMS. CMS analyses also search for dark matter in events containing leptons, e.g. [12], but there is no way to know whether dark matter will be found in either or both. By splitting the searches, each can optimize for its unique event topology. Likewise, CMS also considers all-hadronic events that do not necessarily have large M_{T2} [13], since while M_{T2} in many cases provides enhanced sensitivity, it can reduce sensitivity to some models, for instance in cases where the decay energy is very small, or those in which invisible particles are not produced in pairs.

The first search is inclusive, and is a continuation of previous analyses based on smaller datasets, most recently using the 35.9 fb^{-1} dataset recorded in 2016 [9]. Accordingly, it is referred to as the classic search. The second search is a new extension of the first, requiring

additionally the presence of a disappearing track in the event. Disappearing tracks have been targeted as an observable of interest by both CMS [6, 10] and ATLAS [3, 2] previously, but with lower energy or smaller datasets, and different methods. Both searches set the strongest constraints to date on a variety of hypothetical extensions to the Standard Model possessing pair-produced dark matter candidates, most notably R-parity conserving supersymmetry.

3.1 Classic Search

3.1.1 General Description

The search’s core, defining selections are for events with large missing transverse energy \cancel{E}_T as inferred via M_{T2} , large total hadronic transverse energy H_T , and no leptons.

The primary motivation for the analysis is either finding or setting constraints on particle dark matter. The experimental signature of dark matter is its undetectability; its presence can only be inferred through large imbalance of transverse energy. The M_{T2} analysis further focusses on the case of pair-produced dark matter using its eponymous observable. For reasons discussed in Section 1.3, R-parity conserving supersymmetry is a model of special interest to the theoretical community, and this model’s dark matter candidate would always appear in pairs. The M_{T2} variable tends to increase sensitivity to the pair-production scenario.

The selection of events with large H_T is motivated by the CMS trigger as discussed in Section 2.3.1, which is in turn motivated by the inferred large energy scale of new physics. The decays of heavy new particles to relatively light Standard Model particles will result in, typically, very energetic events. It is possible that the dark matter candidate is itself very heavy, nearly as massive as the new particle that decays to it; this is called the compressed scenario. In this scenario, while the events are indeed very energetic, much of the energy is lost to the invisible portion of the event, and the visible, hadronic energy can be relatively small. Accordingly, sensitivity in the compressed scenario is weaker, as many of the new physics events are too

low energy to pass the kinematic selections. The M_{T2} selection is especially inefficient, in this scenario. However, sensitivity is not negligible, and the search is sensitive to any mass splitting in many cases.

The last selection, a veto of leptons, is chiefly motivated by CMS’s divide-and-conquer strategy. Events with leptons are considered in other searches. However, the veto does allow for partial suppression of the Standard Model neutrino background, since neutrinos are often produced alongside a charged lepton in decays of the W boson, as discussed in Section 3.1.3.

Ideally, any observation of an event with large \cancel{E}_T and M_{T2} , large H_T , and no leptons, would constitute a discovery. Unfortunately, this is not the case, as the Standard Model is capable of producing events with all of these signatures. Neutrinos and simple mismeasurement of the event can produce large missing energy signatures. Events with large H_T are uncommon in the Standard Model but hardly impossible, and the vast majority of events in a proton-proton collider have no leptons. Some number of events will have all of these properties without any new physics occurring, and most of the analysis’ efforts are spent estimating how often these background processes occur, as discussed in Section 3.1.3.

3.1.2 Signals

The classic search generically targets any new physics that produces high H_T events with jets and missing energy from undetected particles. Diagrams for several candidate models are shown in Figures 3.1, ??, and 3.3. The diagrams in Figure 3.1 of gluino and squark pair production as predicted by supersymmetric extensions of the Standard Model are of greatest interest, and while the analysis is sensitive to a wide variety of similar hypothetical models, it is optimized for these. As discussed in Section 1.3.3, these models simplify the enormous parameter space of supersymmetric extensions, assuming that all superpartners except those in the process are so massive that they can be neglected entirely. The upper five diagrams all depict pair production of gluinos, the supersymmetric partner of the gluon, the mediating gauge boson

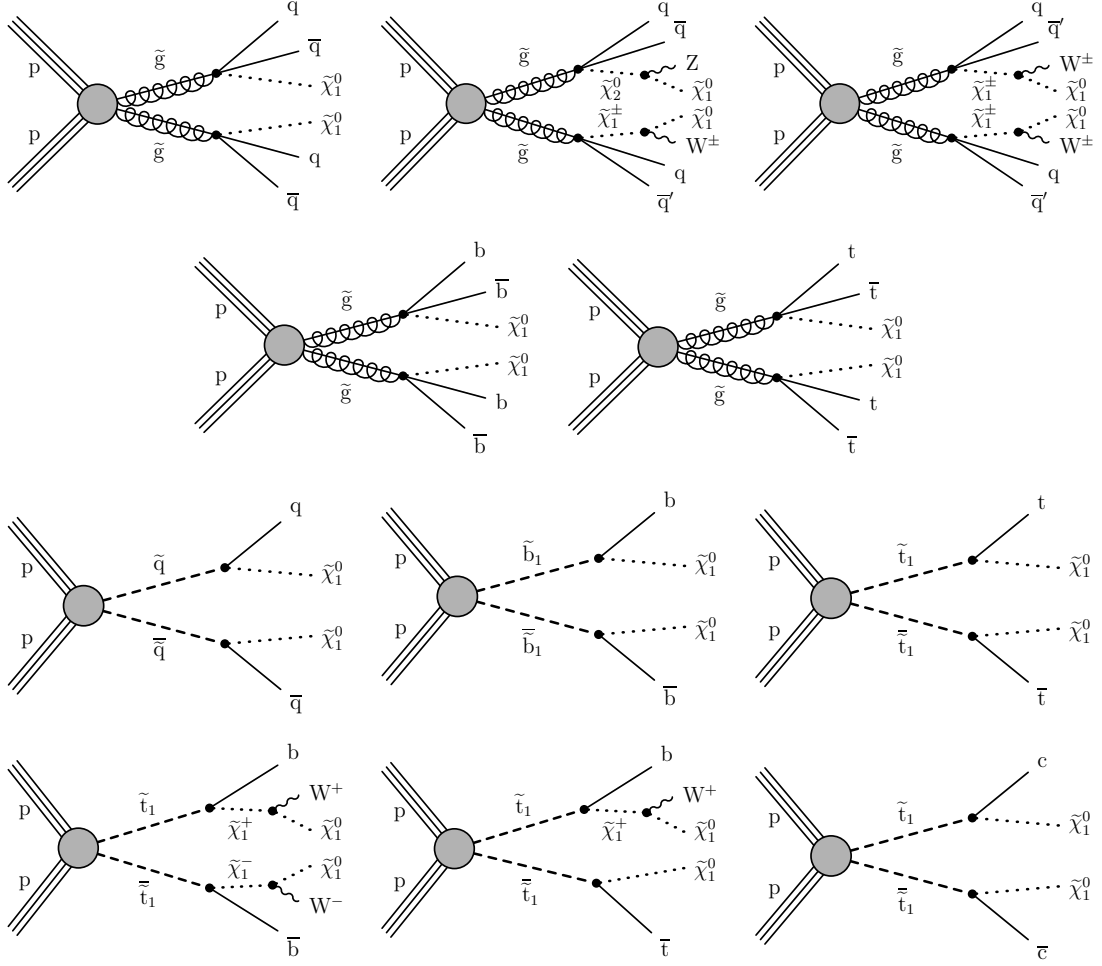


Figure 3.1: Diagrams of gluino (upper five) and squark (lower six) pair production, as predicted by supersymmetric extensions of the Standard Model. The classic search considers five potential gluino decay chains. At upper left, the gluinos decay to light flavor quarks (up, down, strange, or charm), and the lightest neutralino, $\tilde{\chi}_1^0$. At upper center, the gluinos decay to light flavor quarks, but rather than decaying directly to $\tilde{\chi}_1^0$, the gluinos decay either to the second neutralino, $\tilde{\chi}_2^0$, which subsequently decays to a Z boson and $\tilde{\chi}_1^0$, or to the lightest chargino, $\tilde{\chi}_1^\pm$, which subsequently decays to the W boson and $\tilde{\chi}_1^0$, with equal probability. At upper right, both gluinos undergo the $\tilde{\chi}_1^\pm$ to W decay chain. On the left of the second row, both gluinos decay to bottom quark pairs and $\tilde{\chi}_1^0$. On the right of the second row, both gluinos decay to top quark pairs and $\tilde{\chi}_1^0$. Additionally, the classic search considers six potential modes of squark production and decay. On the left of the third row, light flavor squarks decay to light flavor quarks and $\tilde{\chi}_1^0$. In the center of the third row, bottom squarks decay to bottom quarks and $\tilde{\chi}_1^0$. On the right of the third row, top squarks decay to top quarks and $\tilde{\chi}_1^0$. At lower left, top quarks decay to bottom squarks and $\tilde{\chi}_1^\pm$, which subsequently decay to the W boson and $\tilde{\chi}_1^0$. At lower center, top squarks may undergo either the $\tilde{\chi}_1^\pm$ decay chain, or a direct decay to a bottom squark and $\tilde{\chi}_1^0$, with equal probability. At lower right, each top squark decays to a charm squark and $\tilde{\chi}_1^0$. Taken from [5].

of the strong interaction. As each gluino decays to two quarks, each of which will typically produce a jet, gluino pair production events tend to have many jets. Many different decay chains are possible, and the analysis considers five representative benchmarks.

In the first benchmark, the gluinos decay to light flavor quarks (up, down, strange, or charm), and the lightest neutralino, $\tilde{\chi}_1^0$.

In the second benchmark, the gluinos decay to light flavor quarks, but rather than decaying directly to $\tilde{\chi}_1^0$, the gluinos can decay either to the second neutralino, $\tilde{\chi}_2^0$, which subsequently decays to a Z boson and $\tilde{\chi}_1^0$, or to the lightest chargino, $\tilde{\chi}^\pm$, which subsequently decays to the W boson and $\tilde{\chi}_1^0$. Each of these decays can occur with equal probability. Both the W and Z will themselves decay, usually to a pair of quarks, which will in turn produce jets. So, relative to the first signal model, the second tends to have greater jet multiplicity. The Z can also decay to neutrinos, and the W can decay to a neutrino and a lepton that is not reconstructed. In these scenarios, this benchmark trades some jets for an enhanced missing energy signature. If the W and/or Z decay leptonically and these leptons are successfully reconstructed, events from these signals may fail the lepton veto and instead end up in control regions, biasing the background prediction. The procedure used to handle such signal contamination of control regions is described in Section 3.1.6.

The third benchmark, in which both gluinos undergo the $\tilde{\chi}^\pm$ to W decay chain, is similar.

In the fourth benchmark, both gluinos decay to the bottom quark and $\tilde{\chi}_1^0$. As described in Section 2.3.2, it is possible to identify jets that originated from a bottom quark; such a jet is said to be “b-tagged.” The classic search bins in the number of b-tagged jets in order to enhance sensitivity to signals of this type.

In the fifth and final gluino pair-production benchmark, both gluinos decay to top quarks and $\tilde{\chi}_1^0$. The top quark decays with probability near unity to a bottom quark and a W boson. The extra W bosons, compared to the direct bottom decay model, can either add jets or leptons and neutrinos, as previously discussed. This signal tends to produce the most remarkable events of

any signal model considered, with very large H_T , N_{jet} , and $N_{\text{b-tag}}$, but also loses many events to the lepton veto as any of the four W bosons is liable to produce a lepton.

The lower six diagrams of Figure 3.1 all depict pair production of squarks, the supersymmetric partners of quarks. Squark decays directly produce only one quark each, compared to two for gluino decays, so squark pair-production events tend to have fewer jets than gluino pair-production events.

In the first squark benchmark diagram, on the left of the third row, a pair of light flavor squarks (up, down, strange, or charm) is produced and each decays to a light flavor squark and $\tilde{\chi}_1^0$.

In the second benchmark, bottom squarks are produced and decay to bottom quarks and $\tilde{\chi}_1^0$. These events tend to have b-tagged jets, but fewer than in gluino decays to bottom squarks.

In the third benchmark, top squarks are pair produced and decay to top quarks and $\tilde{\chi}_1^0$. The relationship between this process and the previous one is similar to the relationship between the fifth and fourth gluino benchmarks, respectively.

The fourth benchmark is very similar to the third. Instead of the top squark decaying directly to a top quark, which then decays to a bottom quark and W boson, the squark decays to a bottom quark directly and $\tilde{\chi}^\pm$, which subsequently produces the W. While the final state particles are identical, their kinematics can be very different depending on the distribution of masses realized in nature. For instance, if the top squark and $\tilde{\chi}^\pm$ mass splitting is very small, the bottom quark jet in this benchmark may have such low p_T in a typical event that it is difficult to reconstruct.

In the fifth benchmark, each top squark may undergo the $\tilde{\chi}^\pm$ decay chain or decay directly to a bottom squark and $\tilde{\chi}_1^0$, with equal probability, mixing the two previous models.

In the last benchmark, each top squark decays to a charm quark and $\tilde{\chi}_1^0$. This decay chain could dominate when the top squark and $\tilde{\chi}_1^0$ mass splitting is too small to allow decay to on-shell top quarks, and the mass of $\tilde{\chi}^\pm$ is larger than that of the top squark.

In each of these models, the mass of the squark or gluino and the mass of $\tilde{\chi}_1^0$ are free

parameters. Large squark and gluino masses cause low production rates, as the production cross sections drop rapidly with increasing mass, as discussed in Section 1.3.3 and shown in Figure 1.1. The mass of $\tilde{\chi}_1^0$ does not affect the production rate, except insofar as it must be lower than the masses of all other superpartners, but it does affect the character of the events. When the mass splitting between the gluino or squark and $\tilde{\chi}_1^0$ is small, only a small portion of the event’s energy ends up in the visible decay products, and most is lost to the rest energy of $\tilde{\chi}_1^0$. These events have low H_T and E_T , low N_{jet} , and when applicable, low $N_{\text{b-tag}}$, and more closely resemble background. As the mass splitting increases, more energy shifts to the visible portion of the event, making events less background-like and increasing sensitivity. The analysis considers a grid of potential mass points for each model, and this sensitivity pattern is evident in the curves shown in Section 3.1.8.

The classic search also considers non-supersymmetric models.

The first is referred to as the mono- ϕ model. In this model, a colored scalar boson much like a squark is produced singly, rather than pair-produced as in squark models in order to conserve R-parity, and decays to a quark and invisible fermion, as shown in Figure 3.2. This model has an especially low number of jets and low M_{T2} , and so would appear in more background-like bins than most supersymmetric models. In fact, it was originally proposed [1] to explain a potential excess in bins of this sort in the previous edition of the classic search, published based on 2016 data [9], and so there is some interest in whether such an excess persists in the larger dataset. While the analysis is not optimized for models of this sort, indeed M_{T2} is designed to target pair-production, it still has some residual sensitivity to any model characterized by jets and missing energy in the final state, including mono- ϕ .

The second non-supersymmetric model, and final model considered explicitly by the classic search, is leptoquark extensions of the Standard Model. As discussed in Section 1.4, while squarks can decay to a quark and $\tilde{\chi}_1^0$, leptoquarks decay to a quark and a neutrino, which is experimentally effectively indistinguishable from a low mass $\tilde{\chi}_1^0$. This last fact was first established

in a reinterpretation of the 2016 edition of the classic search [11]. Thus, it is a relatively simple exercise to reinterpret squark squark results in the low mass $\tilde{\chi}_1^0$ limit to leptoquark results. A few leptoquark production diagrams are shown in Figure 3.3.

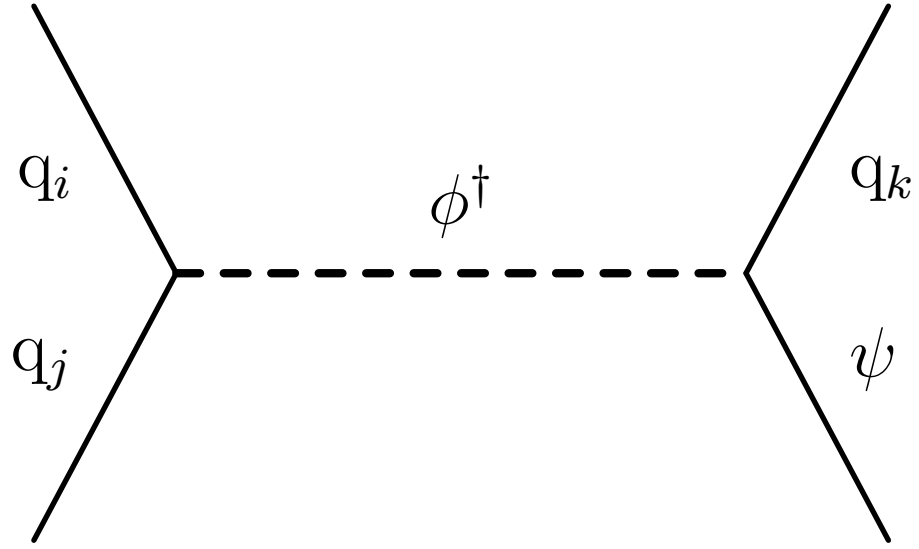


Figure 3.2: Diagram for the mono- ϕ model, in which a colored scalar ϕ is resonantly produced, and decays to an invisible massive Dirac fermion ψ and an SM quark. Note that ϕ is not pair-produced, in contrast to otherwise-similar squarks. Taken from [5].

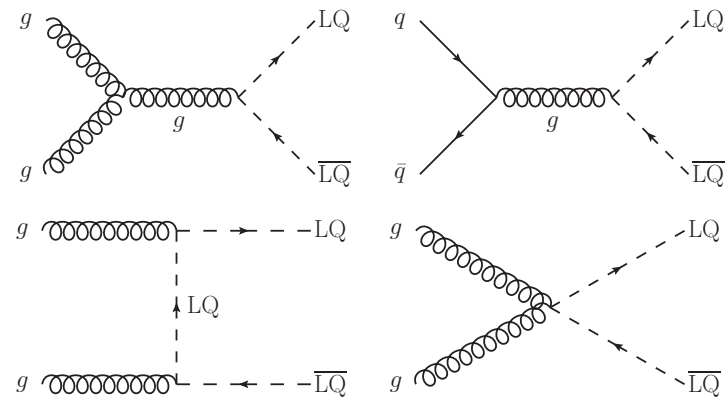


Figure 3.3: Diagrams of leptoquark pair production. Each leptoquark decays to a neutrino and a quark. Taken from [5].

3.1.3 Backgrounds

All of the targeted signals are characterized by all-hadronic events with large missing energy, but observing such an event does not constitute discovery due to the existence of backgrounds that can produce the same basic signature. These backgrounds can be broadly divided into the detector mismeasurement background, in which apparent missing energy is generated not by genuine undetected particles but by an error in reconstruction, and the neutrino background, in which the missing energy is produced by genuine neutrinos as predicted in the Standard Model. The neutrino background can be subdivided into neutrinos originating from $W^\pm \rightarrow \ell^\pm v$, in which the presence of a charged lepton allows the neutrino to be rejected with good efficiency, and those originating from $Z \rightarrow vv$, in which the final state is entirely invisible and cannot be efficiently vetoed.

Mismeasurement

The most problematic background is that caused by detector mismeasurement. Nearly every mismeasured event is a QCD multijet event, because nearly every event at a proton-proton collider is a QCD multijet event and the probability of mismeasurement is roughly flat across events. Accordingly, the mismeasurement background is also referred to as the QCD multijet background. While the detector makes mistakes only very rarely, QCD events are so relatively common that this background is still the most common in the raw dataset, before any cleaning selections. Estimating the QCD background is challenging because it requires highly detailed knowledge of the detector’s idiosyncrasies. Rather than risk falsely discovering a signal or failing to identify one that is present due to misprediction of this background, the analysis adopts selections designed to suppress it, until the background is sufficiently minor that large relative error in its prediction is acceptable.

The first and most powerful of these selections uses the M_{T2} variable described in Section 2.2.6, namely $M_{T2} > 200$ GeV, where the value is chosen to achieve the desired suppression

of the mismeasurement background. Although the M_{T2} selection is somewhat expensive in the sense that it eliminates a significant fraction of signal, especially for signals with a small mass splitting and signals like mono-*phi* that are not pair-produced, it is crucial for suppressing the mismeasurement background. At $H_T > 1500$ GeV, the mismeasurement background extends unacceptably beyond $M_{T2} \sim 200$ GeV, and the M_{T2} selection is tightened to $M_{T2} > 400$ GeV.

The second selection uses the observable

$$\Delta\phi_{min}^{1,2,3,4} = \text{Min} \left(\left| \phi_{\cancel{E}_T} - \phi_i \right| \right)$$

where ϕ_i indicates the *phi* coordinate of the *i*th p_T jet and $\phi_{\cancel{E}_T}$ is the ϕ coordinate of the missing energy vector. Stated simply, $\Delta\phi_{min}^{1,2,3,4}$ is the smallest angular separation in the transverse plane of the missing energy vector and any of the four highest p_T jets. Close overlap between a jet and the missing energy vector indicates a high probability that the jet was badly mismeasured, and is itself the source of the \cancel{E}_T in the event. The selection applied is $\Delta\phi_{min}^{1,2,3,4} > 0.3$, where the value is chosen to achieve strong background rejection without too great a loss of signal efficiency. Only the four highest energy jets are used because the probability of *some* jet overlapping the missing energy vector approaches unity as the number of jets increases, so the selection would nearly always veto high N_{jet} events, and the high N_{jet} bins are sufficiently signal-rich that aggressive background rejection is not as necessary. The effect of this selection is depicted in Figure 3.5, after an M_{T2} selection of only 100 GeV.

The last selection rejects events in which a suspiciously large fraction of the missing energy is coming from very soft objects. The minimum p_T for selected jets is 30 GeV. The missing energy vector from only jets is defined as \vec{H}_T . The missing energy vector used in the analysis, \cancel{E}_T , uses all PF candidates, including those outside jets or in jets with $p_T < 30$ GeV. If these two figures are very different, it means that a large portion of the \cancel{E}_T in the event was generated by these low p_T objects, a sign that something may have gone wrong in reconstruction.

Specifically, the selection is $\left| \vec{H}_T - \vec{E}_T \right| / |\vec{E}_T| < 0.5$.

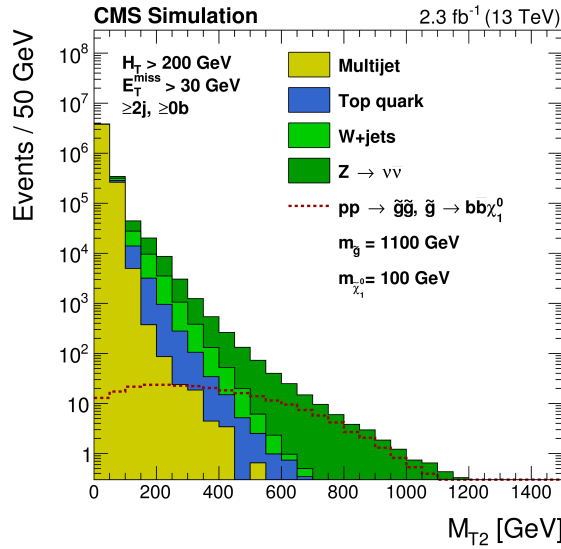


Figure 3.4: The distributions in M_{T2} of the QCD background (filled yellow) and the neutrino backgrounds (filled blue and green) are stacked and overlaid with an example signal point (bottom squark pair production, in red). Even with other mismeasurement-suppression selections applied, the mismeasurement background still dominates without $M_{T2} > 200$ GeV. Taken from [7].

The residual mismeasurement background is estimated using a procedure called Rebalance and Smear that was newly implemented for this edition of the classic analysis, and described in Section 3.1.5.

Lost Lepton

The lepton veto rejects most events containing neutrinos originating from the decay of a W boson, $W^\pm \rightarrow \ell^\pm \nu$. However, the lepton is not always successfully reconstructed, usually because the lepton is a τ that decays hadronically and is mistaken for a meson, and this residual so-called lost lepton background must be estimated. A first attempt might be to simulate events containing W bosons, scale the simulation to the desired luminosity, and count the events in which the lepton is not reconstructed. This procedure would have reasonable accuracy, but producing accurate simulations is not trivial, and the result would be subject to an array of systematic

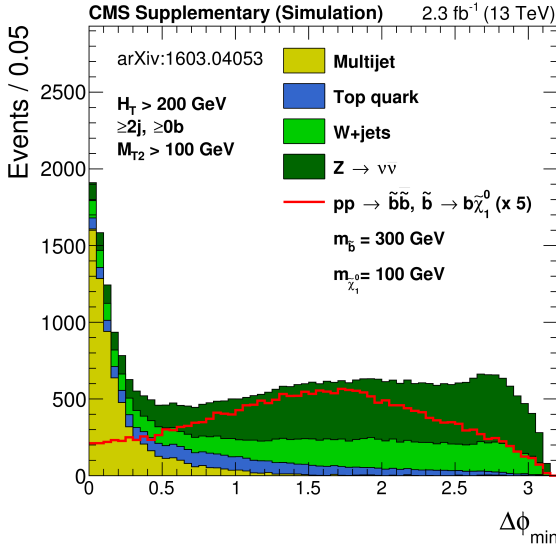


Figure 3.5: The distributions in $\Delta\phi_{min}^{1,2,3,4}$ of the QCD background (filled yellow) and the neutrino backgrounds (filled blue and green) are stacked and overlaid with an example signal point scaled up by a factor of 5 (bottom squark pair production, in red), with a the M_{T2} selection relaxed to 100 GeV. Note that most QCD lies below the cut value of 0.3. Taken from [7] supplementary materials.

errors. Schematically, if N_{LL}^{Data} is the actual number of lost lepton events in data and N_{LL}^{MC} is the number predicted by Monte Carlo simulation, the simulation will mispredict by some factor ϵ such that $N_{LL}^{Data} = \epsilon N_{LL}^{MC}$. It is possible to do better than ϵ with data driven techniques. We can also ask the simulation for its prediction of the number of W events in which the lepton is not lost, single lepton events, N_{SL}^{MC} , where we restrict the lepton to electrons and muons since τ reconstruction is much more difficult. Every part of this simulation is exactly identical to the lost lepton simulation, subject to almost the same errors, with the major exception being the predicted lepton reconstruction efficiency. Call this new error factor δ so that $N_{SL}^{Data} = \delta N_{SL}^{MC}$. Then $\epsilon/\delta = \gamma$ is the portion of the misprediction due to the simulation's imperfect knowledge of the lepton reconstruction efficiency, a small portion of the total. The ratio $R_{MC}^{0\ell/1\ell} = N_{LL}^{MC}/N_{SL}^{MC}$ is subject only to this relatively small error γ , since the fully correlated errors cancel. The prediction of N_{LL}^{Data} follows directly,

$$N_{LL}^{Data;Est} = R_{MC}^{0\ell/1\ell} N_{SL}^{Data}. \quad (3.1)$$

The input N_{SL}^{Data} is measured in a control region populated by single lepton events observed in data, in a kinematic region identical to the corresponding lost lepton signal region. The remaining systematic uncertainty is only about 15% in most signal regions.

While the lost lepton background tends to be subdominant relative to the Invisible Z background discussed in the next section, it is the largest background in certain high N_{jet} , high $N_{b\text{-tag}}$, high H_T bins as Z events do not populate these bins efficiently, while $t\bar{t}$ pair-production events do, and all $t\bar{t}$ events contain two W bosons that may decay leptonically.

Invisible Z

The $Z \rightarrow vv$ background is predicted in a similar fashion to the lost lepton background, using a control region populated with $Z \rightarrow \ell^+\ell^-$ events. Again, the leptons are restricted to pairs of electrons and pairs of muons, since τ reconstruction is much more difficult. The ratio $R_{MC}^{vv/\ell^+\ell^-}$ can be extracted from Monte Carlo simulation, and is dominated by only the lepton reconstruction efficiency uncertainty. In the Standard Model, this ratio is almost exactly 3, but it is significantly larger experimentally because it is possible for one of the leptons in $Z \rightarrow \ell^+\ell^-$ not to be well-reconstructed, causing the affected event not to be counted. The value $N_{\ell^+\ell^-}^{Data}$, unlike N_{SL}^{Data} , is not trivial to extract, since a non-negligible fraction of double lepton events come from sources other than a single Z boson, almost always one each from a pair of W bosons. $N_{\ell^+\ell^-}^{MC}$ and N_{vv}^{Data} are exclusively $Z \rightarrow \ell^+\ell^-$ and $Z \rightarrow vv$ events, respectively, and for maximal cancellation of systematic uncertainties, it is desirable that $N_{\ell^+\ell^-}^{Data}$ be purified to the greatest extent possible.

Fortunately, there is an experimental handle on the contamination. When a Z boson decays to a lepton pair, the flavor is always identical, either two electrons or two muons. When a pair of W bosons each decay to a lepton pair, their choices are uncorrelated. Half the time, the flavors will be identical as for a Z event, and half the time, one W will decay to a muon and the other to an electron. The first case is the undesired impurity in $N_{\ell^+\ell^-}^{Data}$ and the second are used to populated a different-flavor control region used to predict the impurity, N_{DF}^{Data} . It is nearly sufficient simply to

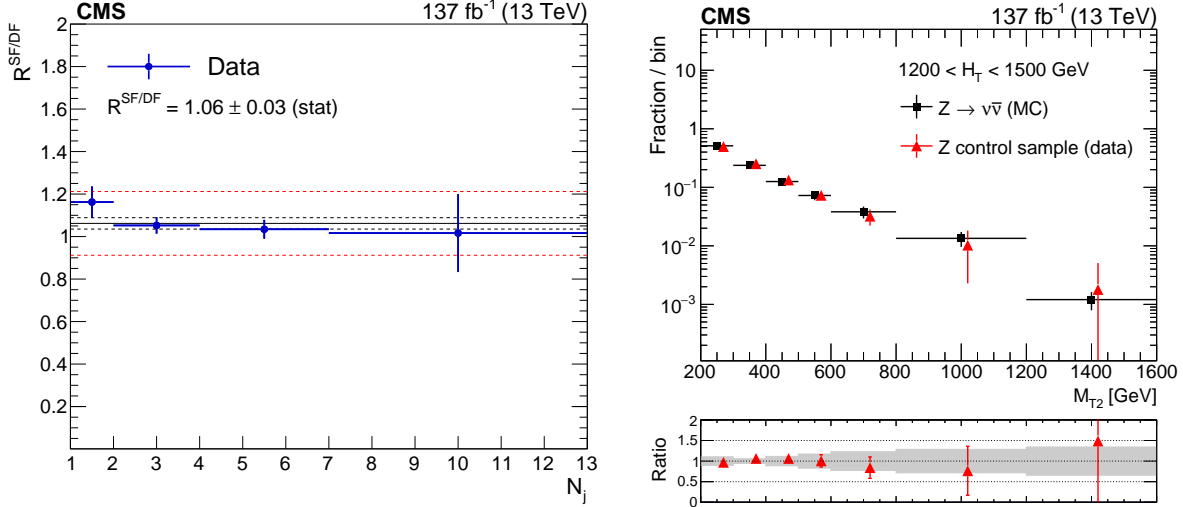


Figure 3.6: (Left) The ratio of the number of same flavor to different flavor lepton pairs in data, $R^{SF/DF}$, which is a component of the $Z \rightarrow vv$ background estimate from $Z \rightarrow \ell^+\ell^-$ events. (Right) A comparison of the M_{T2} shape between data $Z \rightarrow \ell^+\ell^-$ events and simulated $Z \rightarrow vv$ events. The two processes should be kinematically identical, and the similarity of the distributions indicates that the Monte Carlo simulation models the processes well. Taken from [5].

subtract N_{DF}^{Data} from $N_{\ell^+\ell^-}^{Data}$ since the different flavor and same flavor W events occur at the same rate. However, it is possible that the detector is slightly more or less efficient at reconstructing events where both leptons are the same flavor than events in which they are different flavors, so the different flavor count must be scaled slightly to compensate, by a factor $R^{SF/DF}$. $R^{SF/DF}$ is measured in data in $\ell^+\ell^-$ events that are kinematically inconsistent with originating from a Z decay, chiefly due to a requirement that the invariant mass of the lepton pair be at least 20 GeV away from the Z mass. One finds that $R^{SF/OF} \approx 1.06 \pm 0.15$. The final prediction is

$$N_{vv}^{Data;Est} = R_{MC}^{vv/\ell^+\ell^-} (N_{\ell^+\ell^-}^{Data} - R^{SF/OF} N_{DF}^{Data}) \quad (3.2)$$

Being irreducible, the $Z \rightarrow vv$ plus jets background is dominant in the vast majority of bins.

Observable	Selection	Notes
M_{T2}	$> 200 \text{ GeV}$	Only for multijet events. Increased to $M_{T2} > 400 \text{ GeV}$ for $H_T > 1500 \text{ GeV}$ to maintain QCD suppression.
p_T^{jet1}	$> 250 \text{ GeV}$	Only for monojet events.
H_T	$> 250 \text{ GeV}$	Motivated by available triggers. Background events at lower H_T are too common for these events to be always recorded.
\cancel{E}_T	$> 250 \text{ GeV}$	Relaxed to $\cancel{E}_T > 30 \text{ GeV}$ for $H_T > 1200 \text{ GeV}$. Motivated by available triggers.
$\Delta\phi_{min}^{1,2,3,4}$	> 0.3	Auxiliary mismeasurement suppression.
$ \vec{H}_T - \vec{\cancel{E}}_T / \cancel{E}_T$	< 0.5	Auxiliary mismeasurement suppression.
N_{lep}	$= 0$	The lepton veto; rejects the majority of $W^\pm \rightarrow \ell^\pm \nu$ background.

Table 3.1: A summary of the baseline event selection for the classic M_{T2} search. Events are required to have large H_T , no leptons, and significant missing energy unlikely to be the product of detector mismeasurement or a single undetected particle.

3.1.4 Baseline Selection

The properties of these signals and backgrounds motivate the baseline event selection summarized in Table 3.1. The M_{T2} selection primarily suppresses the mismeasurement background, by many orders of magnitude. The $\Delta\phi_{min}^{1,2,3,4}$ and H_T selections also help to suppress this background further, until it is smaller than the genuine \cancel{E}_T backgrounds. The H_T and \cancel{E}_T selections are chosen primarily so that all of the selected events pass the online trigger. Backgrounds are so common at $H_T < 250 \text{ GeV}$, and $\cancel{E}_T < 250 \text{ GeV}$ for $H_T < 1200 \text{ GeV}$, that the experiment is unable to record all of the events observed, making this part of the parameter space a poor region to search for a rare signal in any case. The lepton veto rejects most $W^\pm \rightarrow \ell^\pm \nu$ events, so that only events in which the lepton is not reconstructed remain in the signal region, as described in Section 3.1.3, and serves to narrow the analysis’ focus to the all-hadronic final state as part of CMS’s larger research program.

In addition to this baseline selection, the analysis bins in M_{T2} , H_T , N_{jet} , and $N_{\text{b-tag}}$ to enhance signal sensitivity as described in Section 3.1.5.

3.1.5 Upgrades in 2019

The classic search has been performed before at 13 TeV, once in 2015 [7] using a 2.3 fb^{-1} dataset, and again in 2016 [9] using 35.9 fb^{-1} . The update in 2019 uses the full dataset from 2016,

2017, and 2018, totaling 137 fb^{-1} . As the analysis is dominated by statistical uncertainties in its most sensitive bins, the increased statistical power is the primary improvement in the update.

The update includes two other major upgrades.

The first improves the estimate of the mismeasurement background using a technique called Rebalance and Smear.

The second leverages the increased statistics to expand the signal region binning, better targeting signal models with more extreme jet and b-tagged jet multiplicities, and M_{T2} .

Rebalance and Smear

In older versions of the classic search [7, 9], the mismeasurement background estimate used the $\Delta\phi_{min}^{1,2,3,4}$ observable and extrapolated across M_{T2} . Events at low M_{T2} and at low $\Delta\phi_{min}^{1,2,3,4}$ are both dominated by QCD mismeasurement. The suppression effect of M_{T2} is so strong that even events at low M_{T2} and *high* $\Delta\phi_{min}^{1,2,3,4}$ are QCD dominated. As essentially every low M_{T2} event is a QCD event, low M_{T2} events can be used to measure the ratio r_ϕ of QCD mismeasurement events at high and low $\Delta\phi_{min}^{1,2,3,4}$. High M_{T2} events with low $\Delta\phi_{min}^{1,2,3,4}$ can then serve as a control region for estimating the QCD mismeasurement background, $N_{\Delta\phi_{min}^{1,2,3,4} > 0.3} = r_\phi N_{\Delta\phi_{min}^{1,2,3,4} < 0.3}$. Unfortunately, r_ϕ decreases with increasing M_{T2} , so that instead the dependence must be fit to a power law at low M_{T2} and extrapolated to high M_{T2} , as shown in Figure 3.7. This procedure has obvious potential for statistical errors in the fit, systematic error in extrapolating the fit to high M_{T2} , and potential non-multijet contamination of the low $\Delta\phi_{min}^{1,2,3,4}$ control region at high M_{T2} , producing total relative error at least 40% and as large as 180%. Although the impact of these errors is controlled by suppressing the mismeasurement background as described in Section 3.1.3, it is desirable to replace this procedure with a more robust one.

Rebalance and Smear (R&S) achieves the desired improvement. R&S begins with a sample of multijet events from data with H_T on the order of hundreds of GeV and at least two jets with $p_T > 10 \text{ GeV}$, as nearly unbiased a sample of QCD events as is allowed by available triggers.

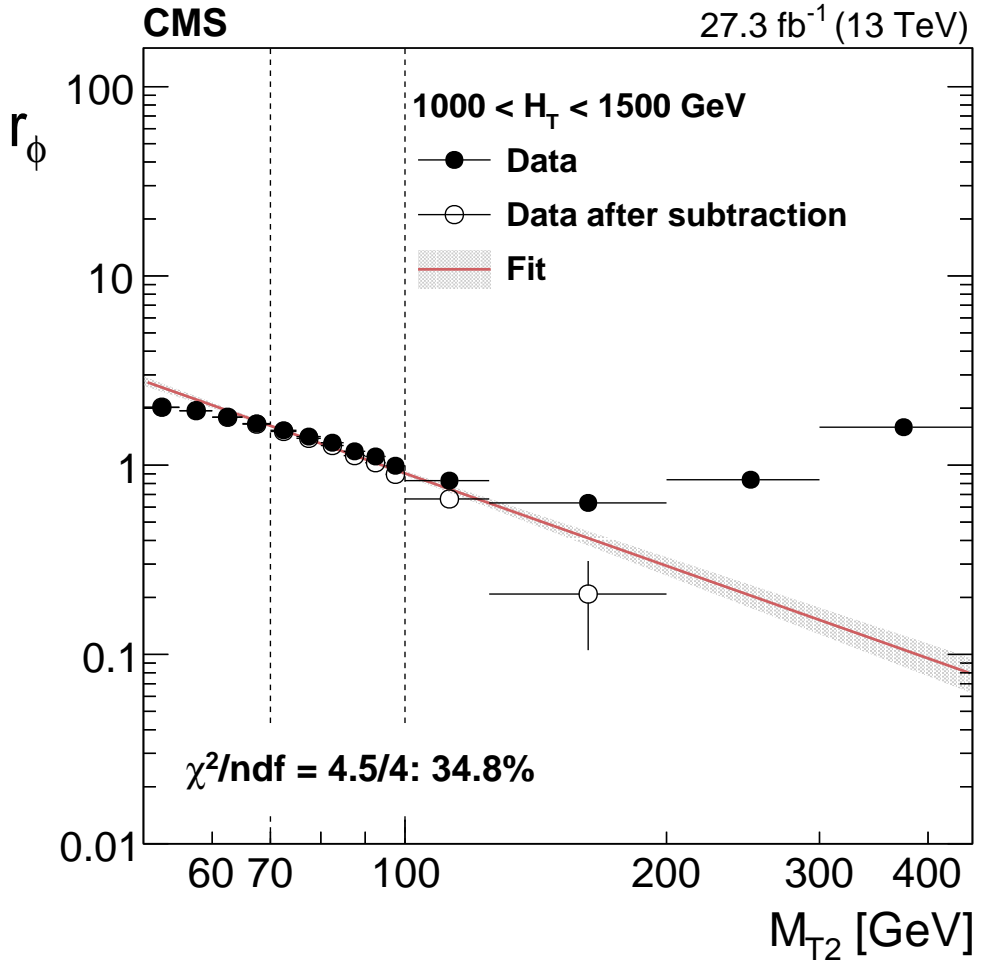


Figure 3.7: The fit of $r_\phi = N_{\Delta\phi_{min}^{1,2,3,4} > 0.3}/N_{\Delta\phi_{min}^{1,2,3,4} < 0.3}$ as a function of M_{T2} obtained in the 2016 classic search, for the $1000 < H_T < 1500$ GeV H_T band. The fit is performed in events in the M_{T2} band $70 < M_{T2} < 100$ GeV and extrapolated to the $M_{T2} > 200$ GeV signal region. Black points represent raw data, while white points represent data after the non-multijet contribution is subtracted. Taken from [9].

These events will generically have some small but nonzero \cancel{E}_T due to imperfect measurement of the jet energies, dictated by the detector's resolution, and potentially a very small contribution from genuine neutrinos produced in the hadron decay chains inside the jets. The p_T values assigned to the jets are then adjusted, finding the most likely assignment of p_T values subject to the hypothesis that the true \cancel{E}_T is very nearly zero, and that jet mismeasurements of a given size occur with probability given by jet response templates. As shown in Figure 3.8, large

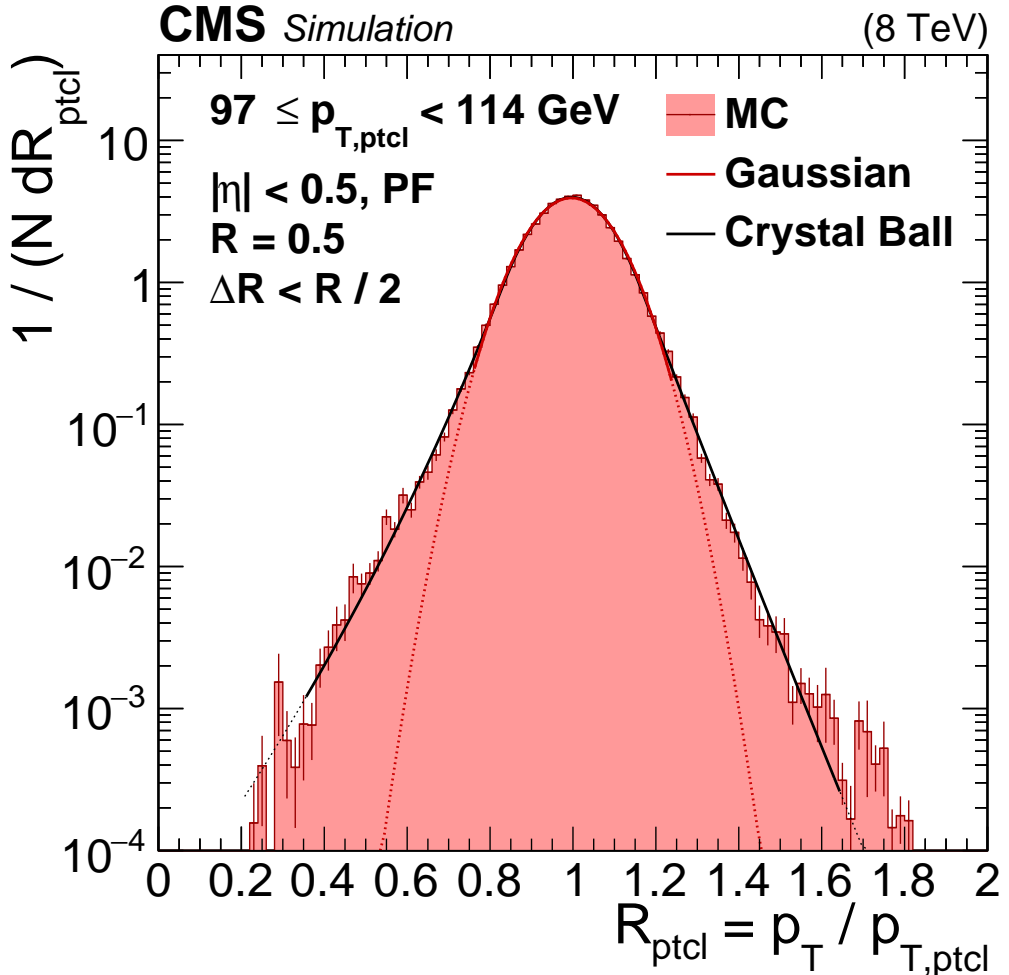


Figure 3.8: $p_{T,ptcl}$ is the “particle level” p_T , the total energy that the jet’s particle components actually had, while p_T is the energy measured by the detector. The horizontal axis is the ratio of these two quantities, and the vertical axis the probability that a jet’s measured energy will differ from its true energy by that ratio. The response curve shown here applies to jets with particle level p_T in the band $97 < p_T < 114$ GeV, and measured in the CMS barrel. Large mismeasurements of jet energy are less probable than small mismeasurements. The core is well-described by a Gaussian, but the tails are highly non-Gaussian and best described by a Crystal-Ball function. Taken from [8].

mismeasurements are rare. Thus, the Rebalancing step tries to get the p_T as close to zero as feasible without making more improbable adjustments to the jets than necessary. The output of the Rebalancing step is a large sample of real QCD events with maximally accurate jet p_T assignments.

Then, each of these events goes through a Smearing step. This step randomly assigns a

new p_T to each jet in the event according to the same jet response templates. The vast majority of the time, the new event looks as unremarkable as the original event. Rarely, the output event passes the baseline selection and represents a potential mismeasurement event that might lie in the data signal region. The Smearing can be repeated as many times for each event as is desired, subject to computing limitations. The number of Smeared events falling into each signal region, from this sample of known equivalent integrated luminosity, can then be converted into the expected number of events that would fall into the signal region in data, due to jet mismeasurement.

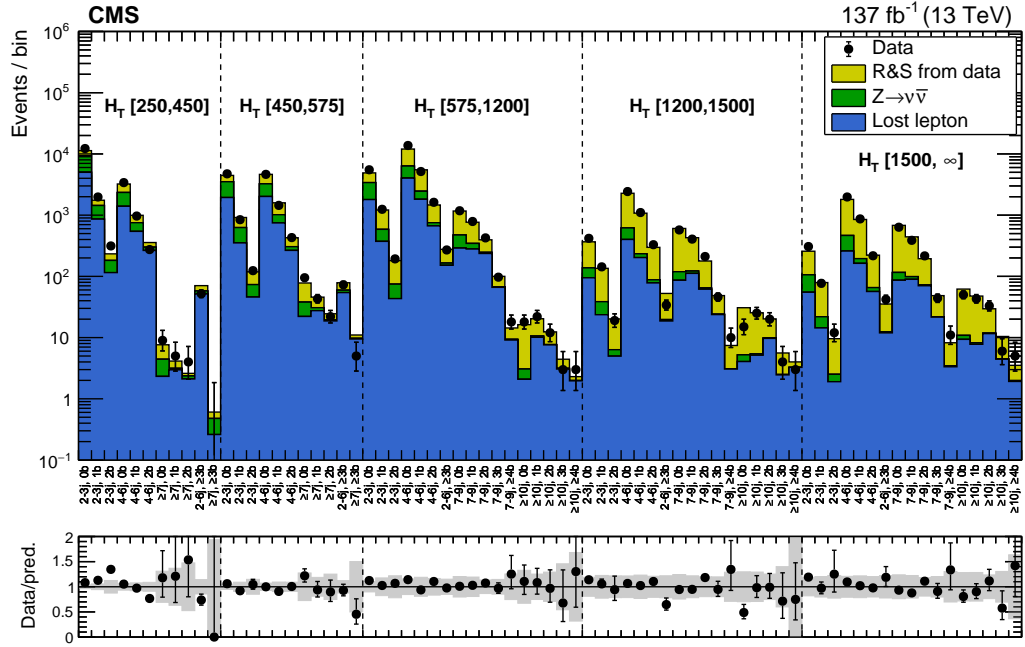


Figure 3.9: The Rebalance and Smear jet mismeasurement background estimate is validated in the $\Delta\phi_{min}^{1,2,3,4} < 0.3$ control region. The multijet mismeasurement event count predicted by Rebalance and Smear is shown in yellow, and contributes most of the event counts in this control region. The combined background estimate (filled histogram) is consistent with the data observation (black data points). Taken from [5].

Of course, many of the output events will have $\Delta\phi_{min}^{1,2,3,4} < 0.3$, falling outside of the signal into a QCD-dominated control region. This allows for a validation in data of the R&S procedure, shown in Figure 3.9. The total background estimate is consistent with data in the $\Delta\phi_{min}^{1,2,3,4} < 0.3$ control region across all of the analysis bins, with the R&S estimated counts contributing most of the predicted events.

R&S achieves a significant improvement over the old r_ϕ based system, effectively eliminating statistical error, and improving the worst case relative error on the mismeasurement estimate from 180% to less than 50%.

Expanded Binning

Although the baseline selection defines the class of events in which a signal of interest may be found, most signals will produce a significant number of events in only a subset of the phase space. For instance, a signal producing 4 top quarks in the final state (see Figure 3.1 second row, right) will almost always produce events with $N_{\text{jet}} \geq 7$, $N_{\text{b-tag}} > 0$, and $H_T \sim 1 \text{ TeV}$. If the entire set of selected events is considered together, the entire background is combined, potentially hiding a signal. If instead the phase space is divided into many separate regions, the background in each region is smaller, so that the background count is as small as possible in the small subset of regions that any given signal actually populates. This sensitivity enhancement motivates very fine binning of the signal region. The classic search uses M_{T2} , H_T , N_{jet} , and $N_{\text{b-tag}}$ as binning variables.

In the 2016 version of the classic search [9], the most extreme N_{jet} bin was $N_{\text{jet}} \geq 7$, and the most extreme $N_{\text{b-tag}}$ bin was $N_{\text{b-tag}} \geq 3$. This limitation was imposed by limited statistics. The background estimate for each bin is performed separately, and the observed counts are subject to Poisson statistical fluctuations. Binning too finely causes any potential sensitivity gains from better isolating signal to be lost to greater uncertainty in the expected background. The analysis binning was updated for the latest edition of the classic search [5], anticipating the improved statistical power. The full set of new bins, along with the predicted background counts and observed event counts in data, is available in Appendix A.

The new binning extends the old binning in three ways. First, new $N_{\text{jet}} \geq 10$ bins were added to the $H_T > 1200 \text{ GeV}$ regions. This allows for enhanced sensitivity to signals with extremely high jet multiplicity, such as the 4 top signal previously mentioned. Similarly, new

$N_{b\text{-tag}} \geq 4$ bins were added to these same regions, targeting the same signal. Sensitivity to some mass points of this signal model roughly doubled due to the addition of these bins, which have negligible background but appreciable signal. Finally, M_{T2} binning was generally made narrower and the last bin moved to larger M_{T2} values, for all signal regions, until the expected background in the last bin was on the order of 1 event. In all, there are 282 classic search bins, enhancing sensitivity to a broad array of potential signal models.

3.1.6 Signal Contamination

The data driven estimate procedures for the neutrino backgrounds used control regions defined using leptons. Signals capable of producing leptons can contaminate these control regions, increasing the observed control region counts above the actual Standard Model production rate. This leads directly to an overprediction of background. For instance, consider stop pair production followed by decay to tops, as shown in Figure 3.1 (row 3, right). Both tops will decay to a W and a bottom quark. If one of the W bosons decays leptonically and the lepton is reconstructed, the event will likely enter the single lepton control region. The lost lepton background, described in Section 3.1.3, will be overpredicted,

$$N_{LL}^{\text{Data;Est}} = R_{MC}^{0\ell/1\ell} N_{SL}^{\text{Data}} = R_{MC}^{0\ell/1\ell} \left(N_{SL}^{\text{Data;SM}} + N_{SL}^{\text{Data;BSM}} \right). \quad (3.3)$$

The background overprediction is $\Delta N = R_{MC}^{0\ell/1\ell} N_{SL}^{\text{Data;BSM}}$. For analysis purposes, the overprediction is modeled in simulation and treated as a reduction of the expected signal counts in every affected bin.

$$N_{SR}^{\text{BSM;Adjusted}} = N_{SR}^{\text{BSM;Raw}} - \Delta N \quad (3.4)$$

This adjustment has the nice property that all terms are linear in the signal strength, so that it does not need to be recalculated for every signal strength considered when performing statistical analysis of the results. The same fraction of the signal is lost at every signal strength.

As a result of this loss of sensitivity due to signal contamination, the classic analysis is less effective, all things equal, when used to search for signals that sometimes produce leptons than the naive expectation based on the leptonic versus hadronic branching ratios. This is an inevitable consequence of performing an all-hadronic search.

3.1.7 Results

The full set of results for every classic search signal region, including every background prediction and the observed count, are available in Appendix ???. The full set of results integrating over the M_{T2} binning are displayed in Figure 3.10 (upper), and the results including the M_{T2} binning for the $575 < H_T < 1200$ GeV bins, the largest set, are shown in Figure 3.10 (lower). No significant discrepancies are observed, and the results are used to set exclusion limits at 95% confidence level on the signals discussed in Section 3.1.2.

3.1.8 Limits

The statistical analysis procedure begins with maximum likelihood fits to the background-only and signal-plus-background hypotheses, for each signal model, considering each mass point separately. The likelihoods are products of Poisson probabilities for each signal region bin, with log-normal constraint terms for each systematic affecting the predicted counts. Correlation between uncertainties affecting different bins are fully accounted for. As stated in the previous section, the background-only hypothesis is consistent with the observation. So, the parameter of interest for each signal model is the maximum signal cross section that can be excluded with 95% confidence level. That is, the maximum possible production rate that the signal model could have, without requiring a combination of background and signal fluctuations more improbable than 1 in 20 to be consistent with the data. If the production cross section excluded at 95% CL exceeds the theoretical cross section for a given signal model, that signal model is said to be excluded at 95%

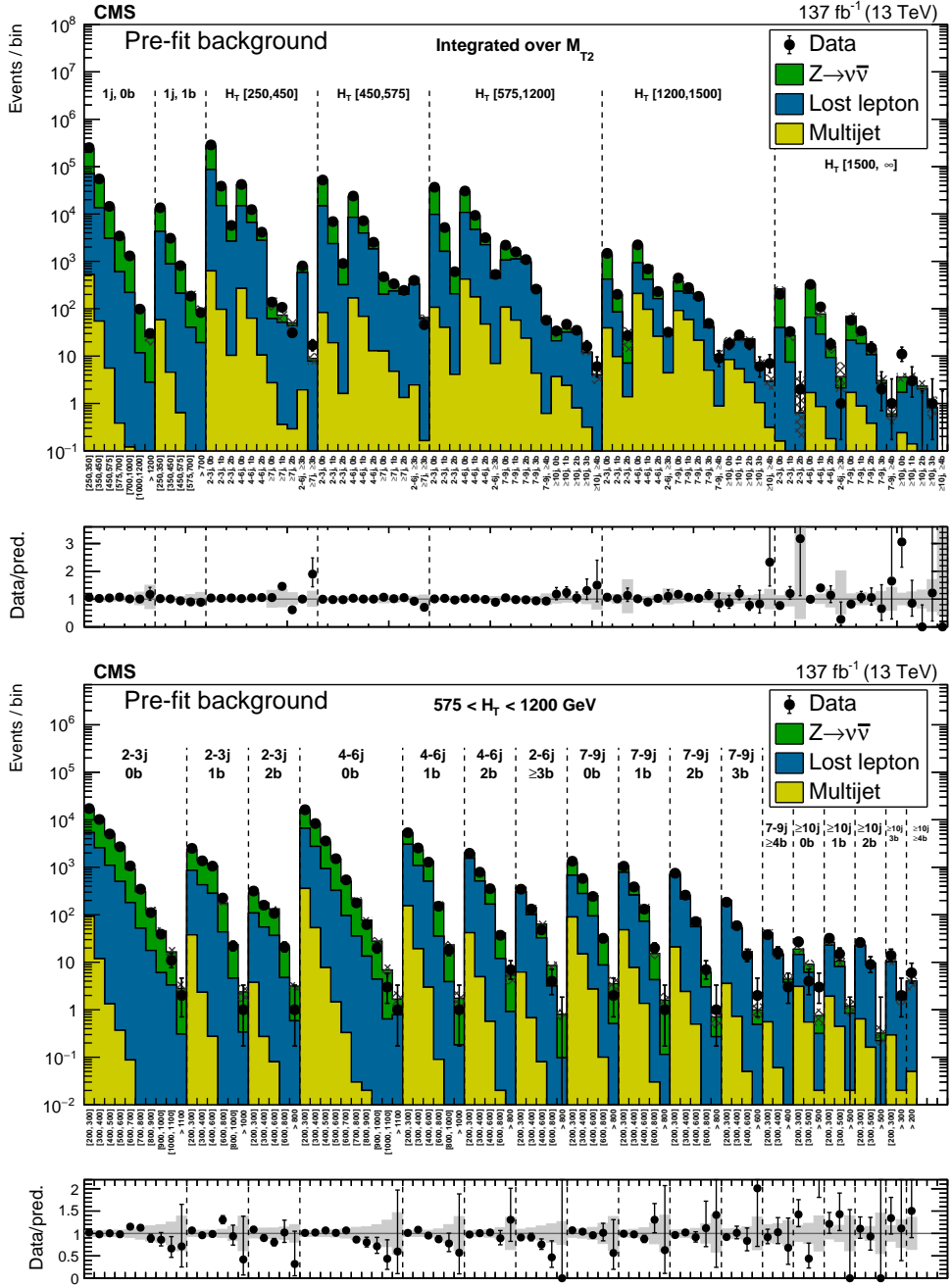


Figure 3.10: Comparison of predicted background and observed data events in the classic search (upper) integrated over M_{T2} and (lower) for each of the medium H_T search regions. Taken from [5].

CL.

The simplified supersymmetric extensions to the Standard Model shown in Figure 3.1

have only two free parameters, the masses of the pair-produced superpartner, and the mass of the lightest supersymmetric particle, the dark matter candidate $\tilde{\chi}_1^0$. Plotting the gluino or squark mass on the horizontal axis and the mass of $\tilde{\chi}_1^0$ on the vertical axis, then marking the mass points excluded at exactly 95% CL produces the exclusion curves shown in Figures 3.11–3.14. Points to the lower left of these curves are excluded, while points above and to the right are not, as they require fluctuations no more improbable than 1 in 20 to be consistent with present data.

There are multiple exclusion curves shown on each plot, some in red and some in black, as an indication of how relatively lucky or unlucky the analysis appears to have been.

The CMS dataset was only collected once, and this dataset is subject to fluctuations. Suppose that the background’s expected event count in a given region, summing across this entire dataset, is B . It is clearly possible that the actual number of background events that occur in the dataset in this bin could be around $B + \sqrt{B}$, or $B - \sqrt{B}$. In the first case, the analysis will draw unexpectedly strong limits on signals that populate this bin. In the second case, the analysis will draw unexpectedly weak limits on signals, perhaps because the inferred larger background is in truth a small genuine signal contribution that will grow in time.

The curves shown in red are the median, 1 standard deviation, and 2 standard deviation expected exclusion curves, in the background-only hypothesis. Together, these indicate the typical range of exclusion curves across many imaginary CMS datasets in which there is no signal to find. The curves in black are those that were observed in the CMS dataset as actually recorded. When the black observed curves extend out beyond the red expected curves, the analysis likely benefitted from a downward fluctuation of background. In cases where the observed curves swing inward compared to the expected curves, the analysis may have experienced an analogous unlucky upward fluctuation of background that mimicked a small signal, or alternatively there may be a genuine small signal lurking in the data that is resisting exclusion!

The general shape of the curves is set by a combination of the falling cross section with increasing gluino or squark mass shown in Figure ??, and a loss of signal efficiency and signal

versus background discriminatory power when the mass splitting between the gluino or squark and $\tilde{\chi}_1^0$ is small. On the lower right hand side of the plots lie signals that produce spectacular, energetic events, but at a very low rate due to the large mass of the gluino and squark, and accordingly small pair-production cross section. Moving up along the $\tilde{\chi}_1^0$ mass axis towards the upper right, the events remain spectacular, so the exclusion curves remain roughly vertical, limited only by the production cross section. Eventually, the mass splitting becomes small enough that the loss of signal efficiency and signal versus background discriminatory power becomes significant, and the exclusion curve turns to the left, towards lower mass squarks or gluinos and higher production rates. Decreasing the gluino or squark mass at fixed $\tilde{\chi}_1^0$ mass reduces the mass splitting, so the curve generally must also drop down somewhat along the $\tilde{\chi}_1^0$ mass axis to maintain a reasonable splitting. Eventually, the curve intercepts the $M_{\tilde{\chi}_1^0} = M_{\tilde{g}}$ or $M_{\tilde{\chi}_1^0} = M_{\tilde{q}}$ line. At this mass and below, all points are excluded even in the limit of zero mass splitting.

Figure 3.11 shows the exclusion curves for gluino pair production and decay to light quarks (upper), light quarks and the Z boson (lower left), and light quarks and the W boson (lower right). Figure 3.12 shows the exclusion curves for gluino pair production and decay to bottom (left) and top (right) quarks.

Figure 3.13 shows the exclusion curves for light-flavor squark (upper left), bottom squark (upper right), and (lower) top squark pair production in which the top squark decays to a top quark. The light-flavor figure contains two curves, one which assumes that there is only a single low mass light flavor squark, and another that assumes that there are eight light flavor squarks of (approximately) degenerate mass, which implies a production cross section eight times larger. The other top squark decay modes, in which the top decays to (upper left) a bottom quark and $\tilde{\chi}^\pm$, which subsequently decays to a W boson and $\tilde{\chi}_1^0$, (lower) a charm and $\tilde{\chi}_1^0$, and (upper right) either $\tilde{\chi}^\pm$ and a bottom quark or $\tilde{\chi}_1^0$ and a top quark, are shown in Figure 3.14. The charm decay channel is only shown for signal models with small mass splittings, as the top squark would strictly prefer to decay to a top quark and $\tilde{\chi}_1^0$ than to a charm quark and $\tilde{\chi}_1^0$ if kinematically allowed.

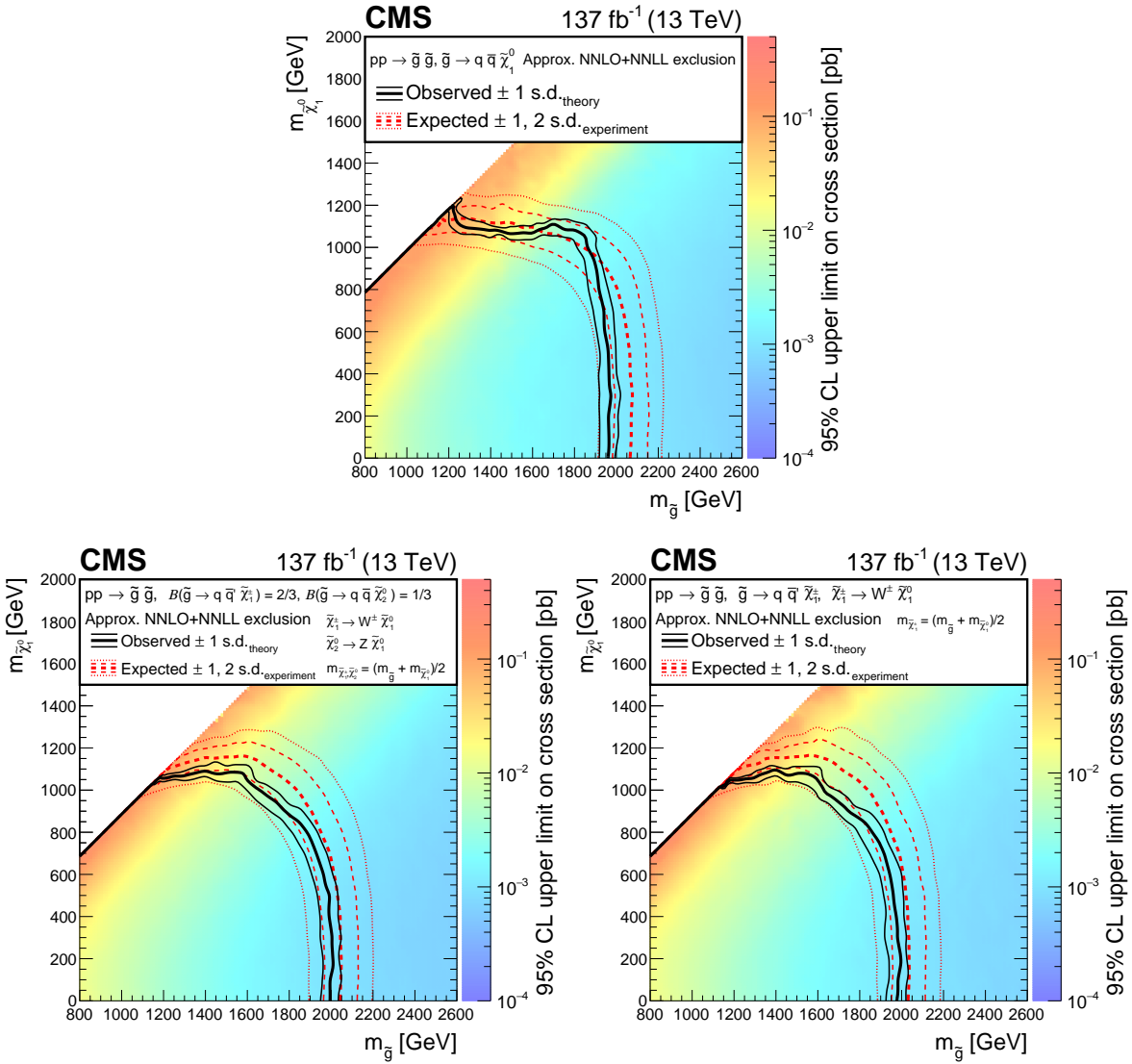


Figure 3.11: Exclusion limits at 95% CL_S for gluino pair production and decay to a pair of light quark jets and (upper) $\tilde{\chi}_1^0$, (lower left) a democratic split between $\tilde{\chi}_1^0, \tilde{\chi}_2^0$, which then decays to a Z boson and $\tilde{\chi}_1^0$, and $\tilde{\chi}^\pm$, which decays to a W boson and $\tilde{\chi}_1^0$, and (lower right) $\tilde{\chi}^\pm$ then W and $\tilde{\chi}_1^0$ with 100% branching fraction. Taken from [5].

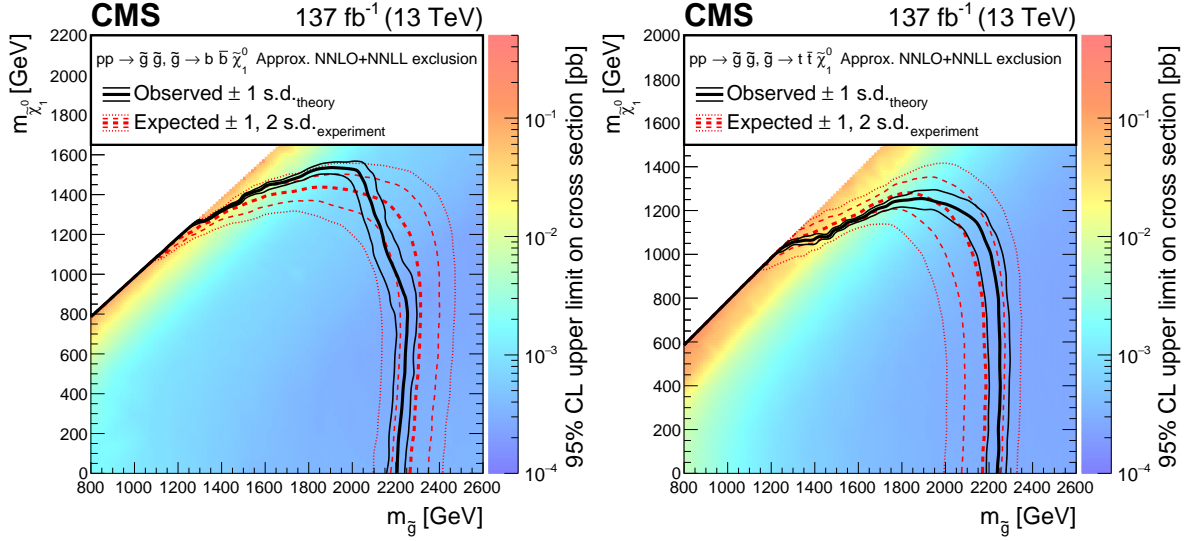


Figure 3.12: Exclusion limits at 95% CL_S for gluino pair production and decay to (left) bottom quarks and (right) top quarks. Taken from [5].

Figure 3.15 shows limits placed on the mono- ϕ model. Here, the horizontal axis is the mass of the singly-produced scalar ϕ , and the vertical axis the mass of the invisible fermion ψ . A star indicates the mass point proposed by the original authors in [1] as most phenomenologically interesting, which is not yet excluded. It is worth emphasizing that the background model is nevertheless consistent with data; this signal is simply very difficult to exclude with the M_{T2} analysis methodology. To save computing resources, the mono- ϕ model is only simulated in the phenomenologically interesting subset of the mass plane, similarly to the top squark to charm model in Figure 3.14 (lower), hence the large white space beneath the considered range of masses.

Figure 3.16 shows limits for leptoquarks decaying to (upper left) a light flavor quark and neutrino, (upper right) a bottom quark and neutrino, and (lower) a top quark and neutrino. As the mass of the neutrinos, in contrast to the mass of $\tilde{\chi}_1^0$, are known to be approximately zero, the leptoquark limits are one dimensional, in the leptoquark masses.

The limits produced by this edition of the classic search improve upon the limits set by the previous edition [9] by hundreds of GeV, and in most cases are the strongest constraints on their respective signal models yet produced by any experiment.

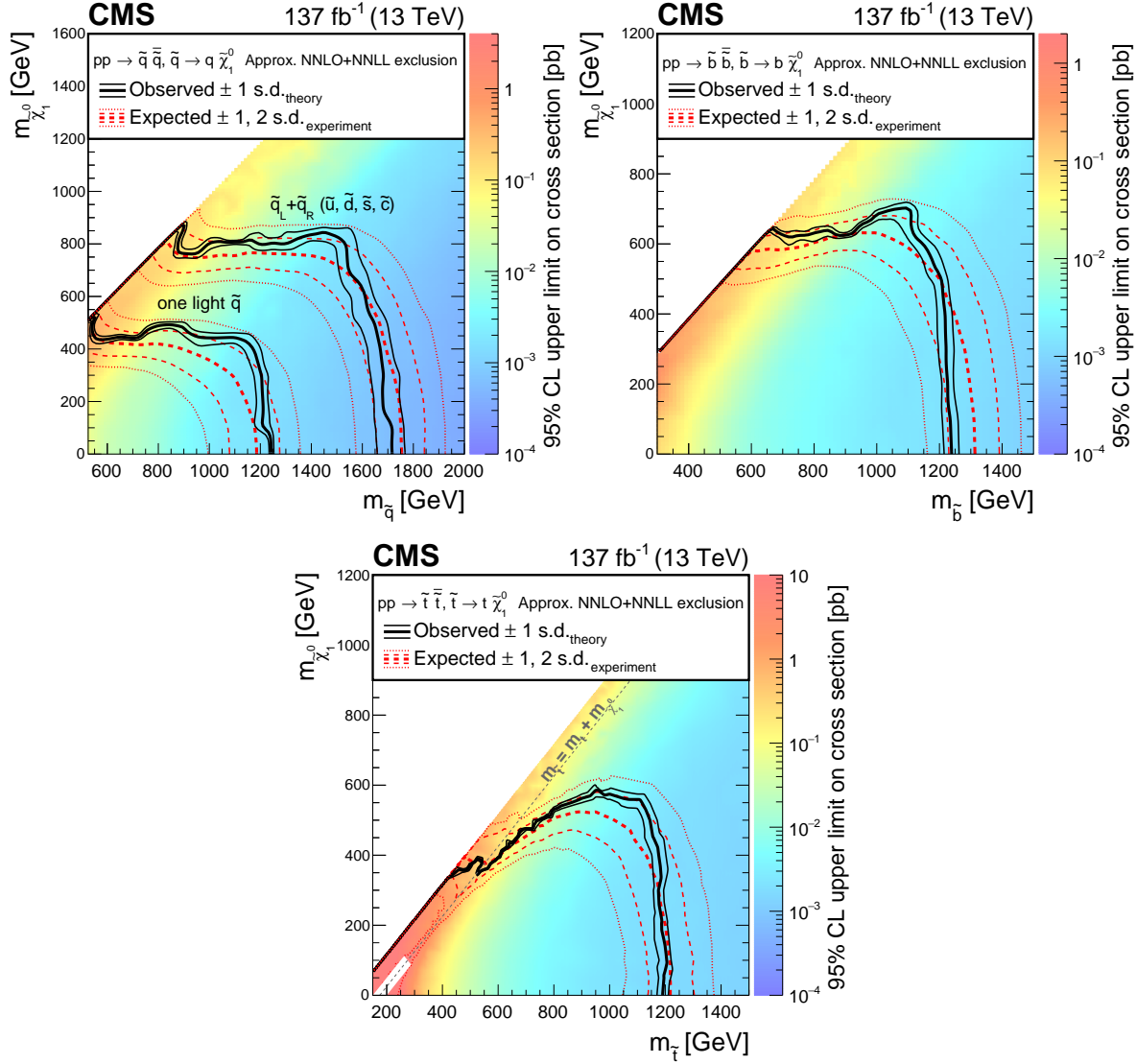


Figure 3.13: Exclusion limit at 95% CL_S for (upper left) light-flavor squark pair production, (upper right) bottom squark pair production, and (lower) top squark pair production. Taken from [5].

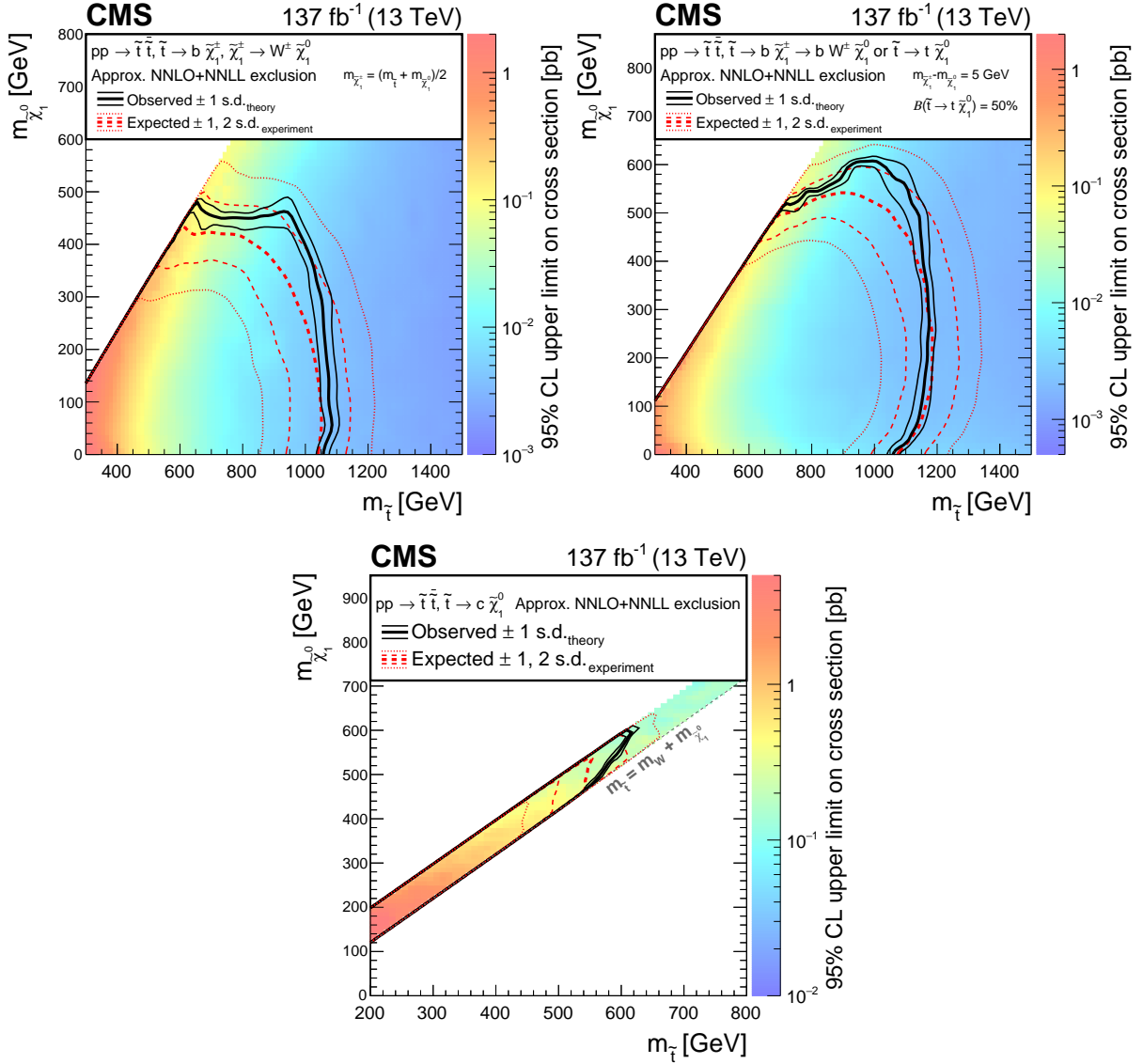


Figure 3.14: Exclusion limits at 95% CLs for top squark pair production and decay to (upper left) a bottom quark and $\tilde{\chi}_1^\pm$, which subsequently decays to a W boson and $\tilde{\chi}_1^0$, (upper right) either a bottom quark and $\tilde{\chi}_1^\pm$ or top quark and $\tilde{\chi}_1^0$, or (lower) a charm quark and $\tilde{\chi}_1^0$. Taken from [5].

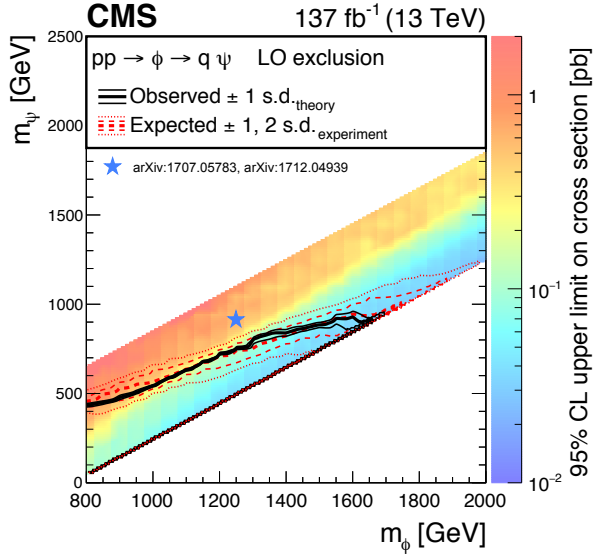


Figure 3.15: Exclusion limit at 95% CL_S for the mono- ϕ model. Only the portion of the mass plane of phenomenological interest was simulated. The star indicates the original authors' proposed best fit mass point, which remains unexcluded. Taken from [5].

3.1.9 Future of the Classic M_{T2} Search

The current limits produced by the classic M_{T2} search are impressive, and are unlikely to improve much in the near future. The pair production cross section for squarks and gluinos drops rapidly with mass, as shown in Figure ???. Generically, a factor of 10 improvement in sensitivity is necessary to push the exclusion limits outward by around 500 GeV along the horizontal axis. At this mature statistical stage, a factor of 10 improvement in sensitivity requires a factor of 100 increase in the integrated luminosity, infeasible in the near future. Improvement along the $\tilde{\chi}_1^0$ axis is similarly difficult due to large backgrounds and low signal efficiency for models with small mass splittings. Therefore, attention in the near future will turn to other new techniques, one of which is discussed in the next section.

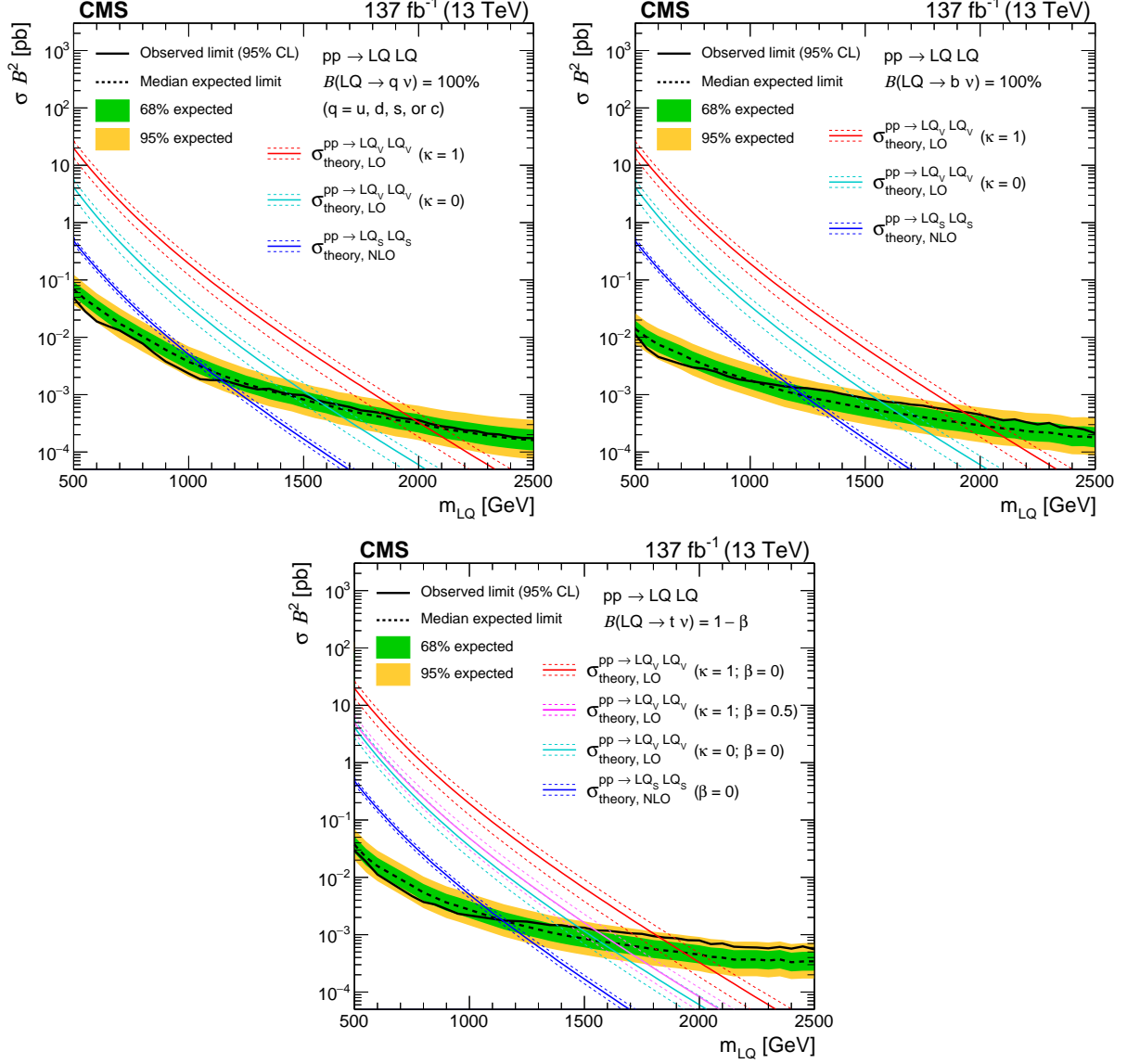


Figure 3.16: Upper limits at 95% CL_S on the leptoquark production cross sections as a function of leptoquark mass. Unlike the limits on supersymmetric models, in which the mass of $\tilde{\chi}_1^0$ is a free parameter, the limits on leptoquarks are 1-dimensional in the leptoquark mass since the neutrino masses are known to be approximately zero. Taken from [5].

3.2 Disappearing Tracks Search

3.2.1 General Description

Define a disappearing track. This search takes the very same events as the classic search, and adds a disappearing track requirement.

Motivation

Why are disappearing track searches interesting? (SUSY can make them, could have new physics right under our noses that we don't see because it looks weird, huge background suppression).

Challenges

Low statistics make it difficult to study background in detail, mysterious sources of background.

Signals

SMS diagrams. Mention that decay lengths can vary, and our sweet spot is decays in the track, 10-100 cm. Signal tends to be isolated, high quality.

Backgrounds

Electrons converting to photons, pions from taus, fakes, and strange baryons. Describe various cleaning selections. Suppress electrons by mapping and vetoing dead ECAL locations, suppress fakes with quality cuts, suppress strange baryons with HCAL energy veto.

3.2.2 Data-Driven Background Estimate

Emphasize that MC should not be trusted to understand a background requiring such detailed detector knowledge.

Short Track Candidates and f_{short}

How do tracks disappear? Who knows: ask the data, for tracks that we are confident are not signal, and remain agnostic of the precise underlying causes. Crucial assumption that the ratio between signal-unlike and signal-like background is flat with MT2.

Validation

Check that background estimate is working at higher MT2, where signal still ought to be relatively rare.

Signal Contamination

Similar to the classic MT2 adjustment for lepton control region contamination, but two-layered. First, need to account for low MT2 ST contamination. Then, need to account for high MT2 STC contamination. Linearize (strictly conservative) so that correction scales appropriately with signal strength.

3.2.3 Results

Show final signal region results. No excesses, and potentially quote most discrepant bins.

3.2.4 Limits

Refer to description of combine statistics procedure in classic search, and show limit scans.

3.2.5 Future

Discuss that, due to small background, disappearing track search scales almost linearly with luminosity, and search is overall heavily dominated by statistical errors. May be worth pursuing in the future at 14 TeV.

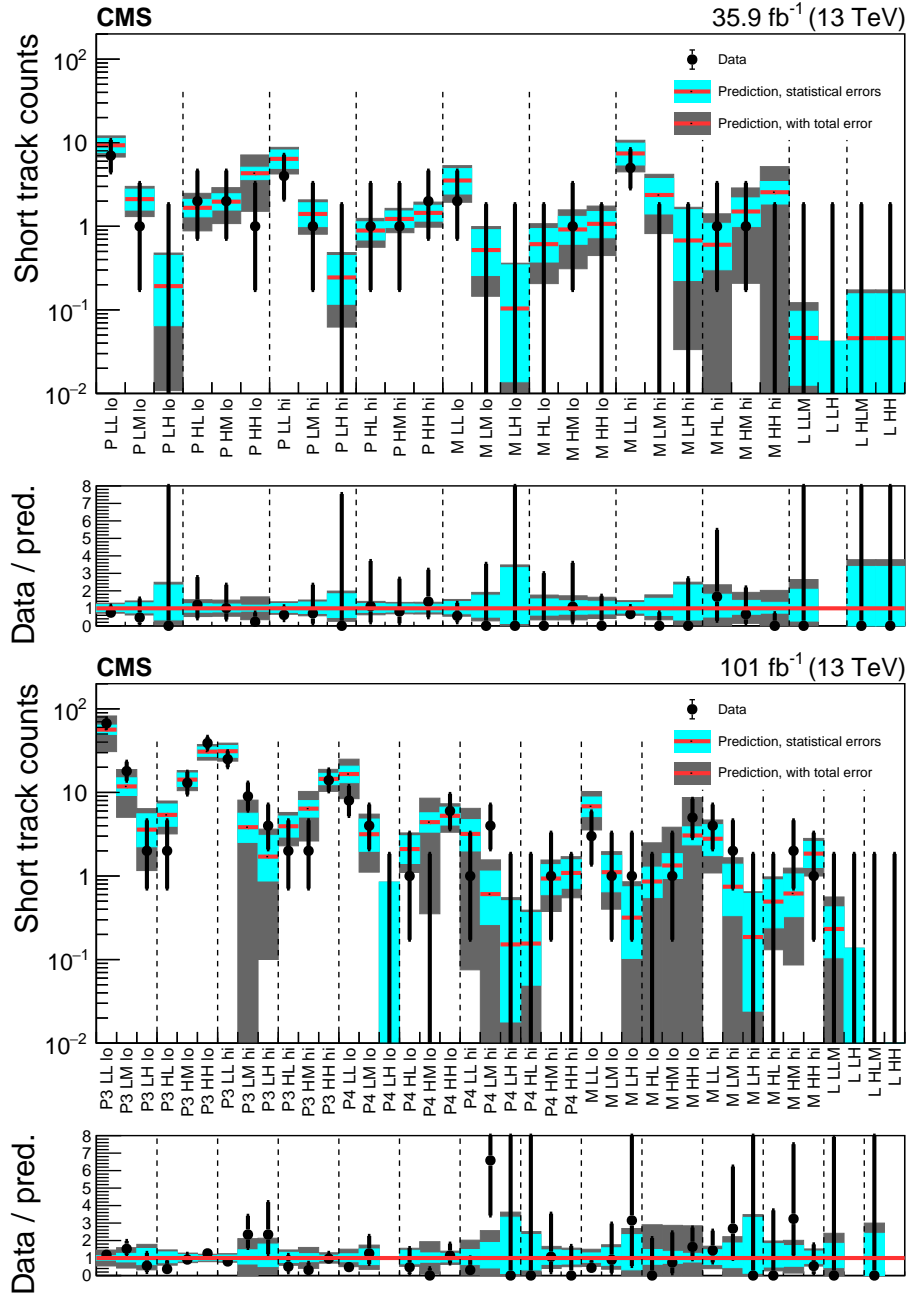


Figure 3.17: Taken from [5]

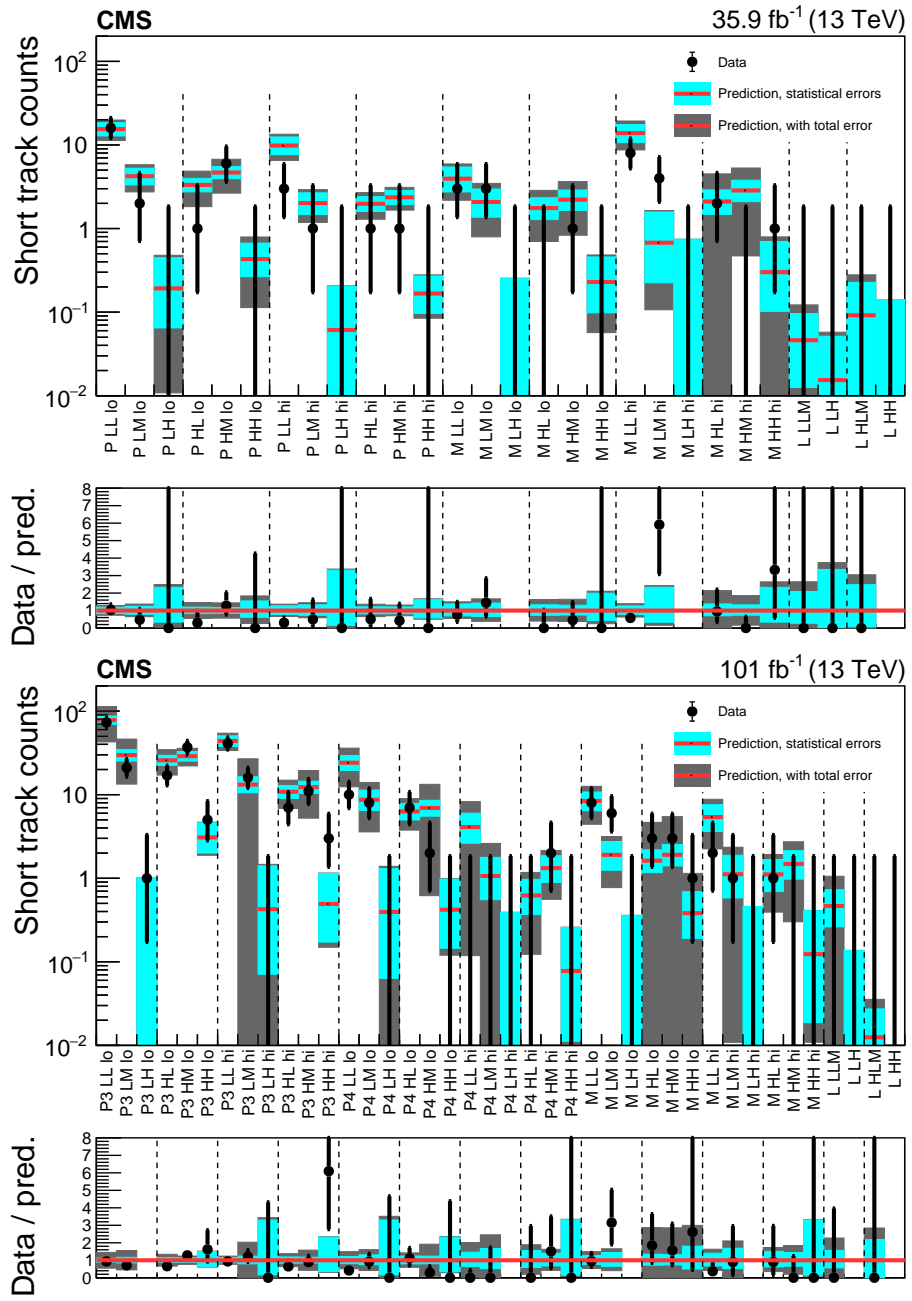


Figure 3.18: Taken from [5]

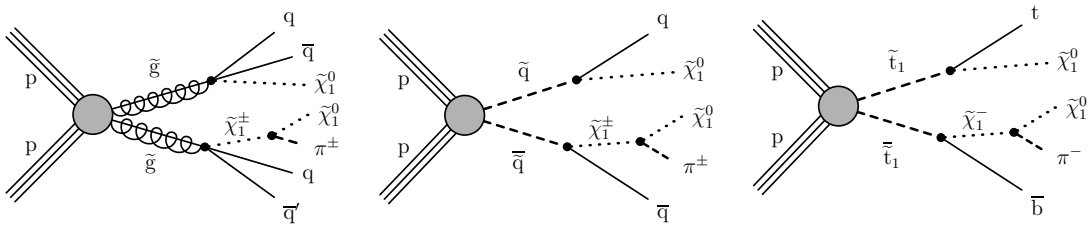


Figure 3.19: Diagrams for (left) gluino, (center) light-flavor squark, and (right) top squark pair production, in which the gluinos and squarks can decay via a long-lived $\tilde{\chi}^\pm$. In this analysis, the gluino is taken to decay with branching fraction 1/3 each to the $\tilde{\chi}_1^0$, $\tilde{\chi}^\pm$ plus, and $\tilde{\chi}^\pm$ minus. Squarks decay with branching fraction 1/2 each to the $\tilde{\chi}_1^0$ and the $\tilde{\chi}^\pm$ allowed by charge conservation. The $\tilde{\chi}^\pm$ mass is greater than the $\tilde{\chi}_1^0$ mass by hundreds of MeV, so that the charged product of the $\tilde{\chi}^\pm$ decay is too soft to be detected. Taken from [5]

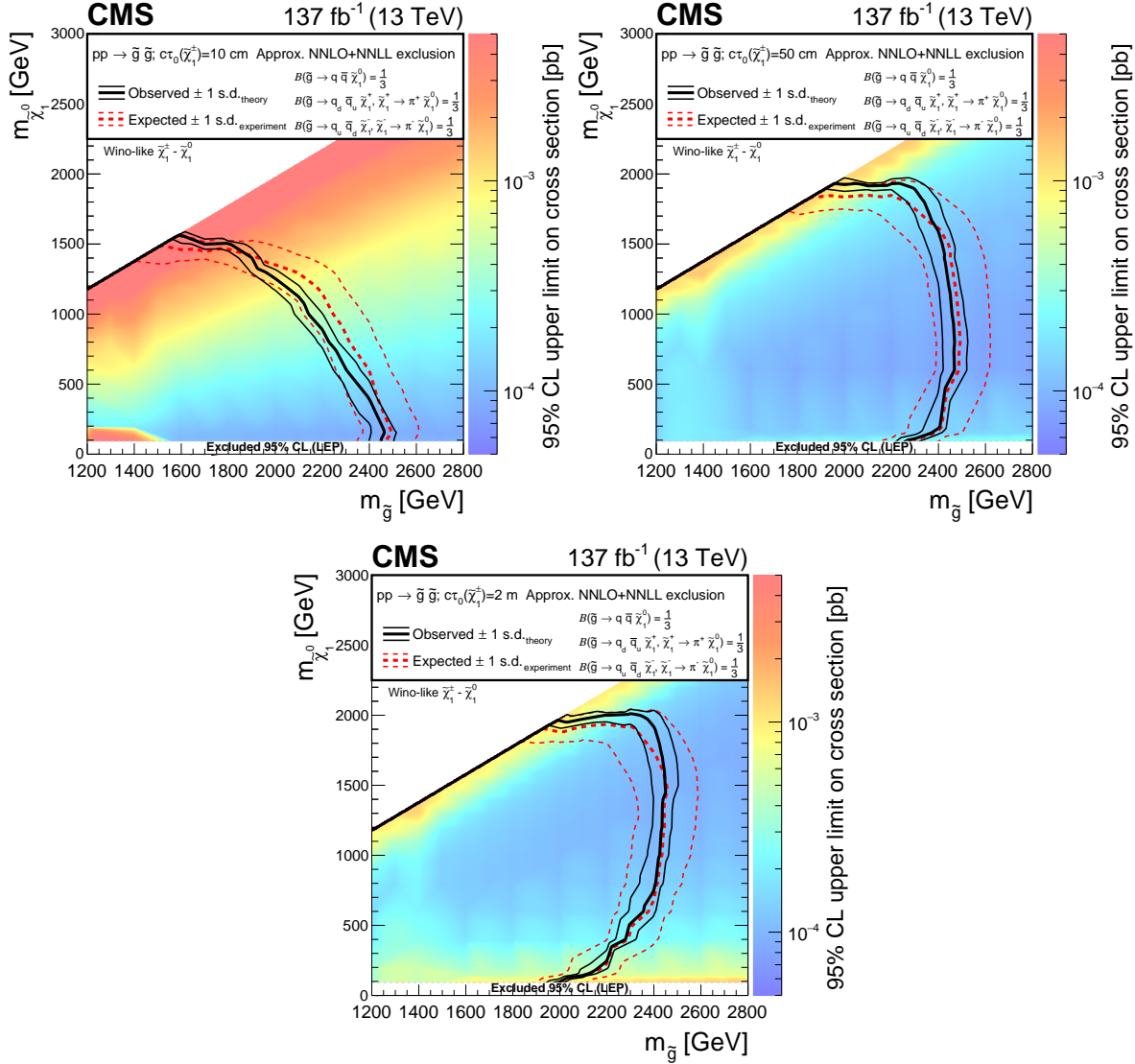


Figure 3.20: Taken from [5]

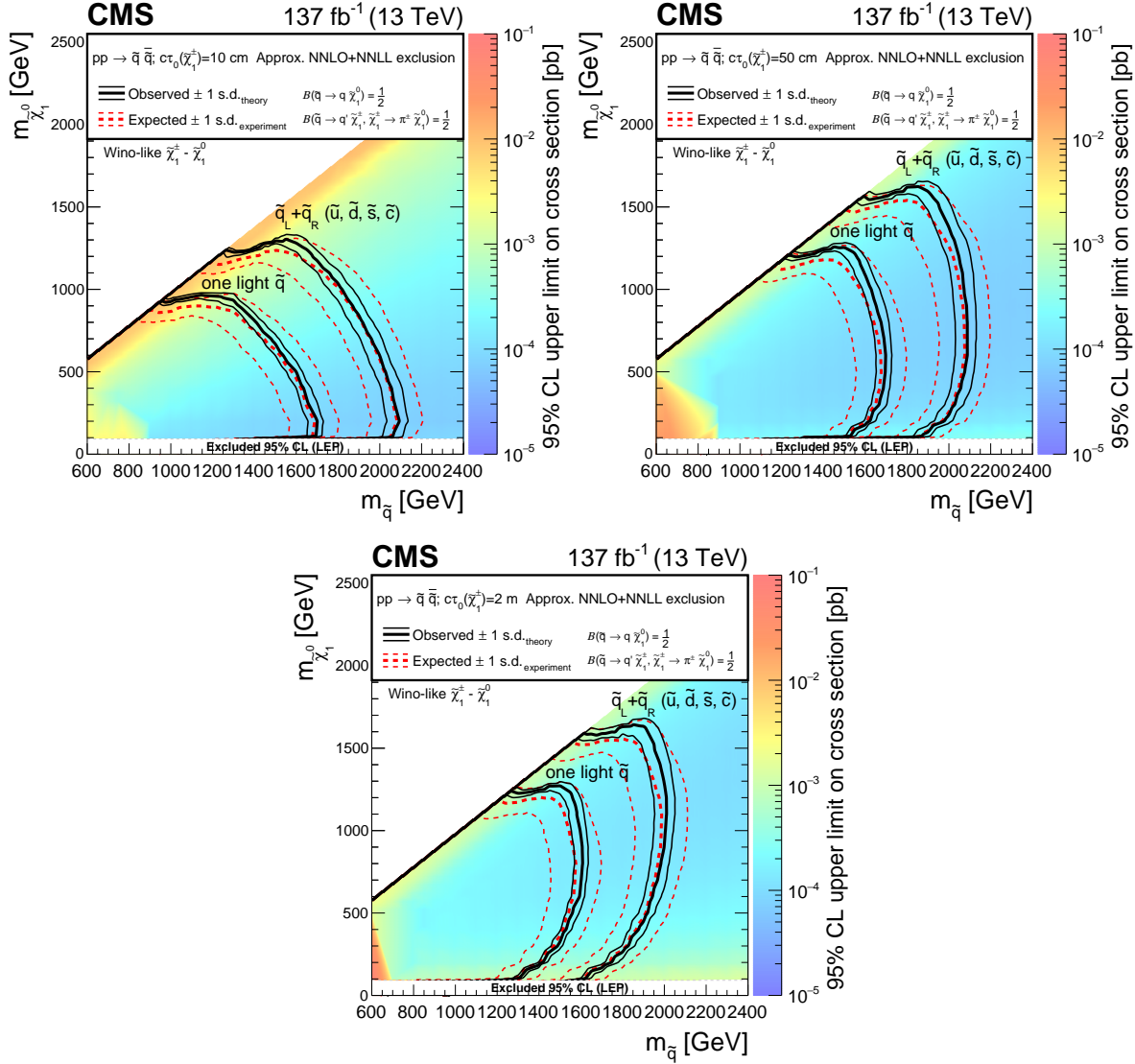


Figure 3.21: Taken from [5]

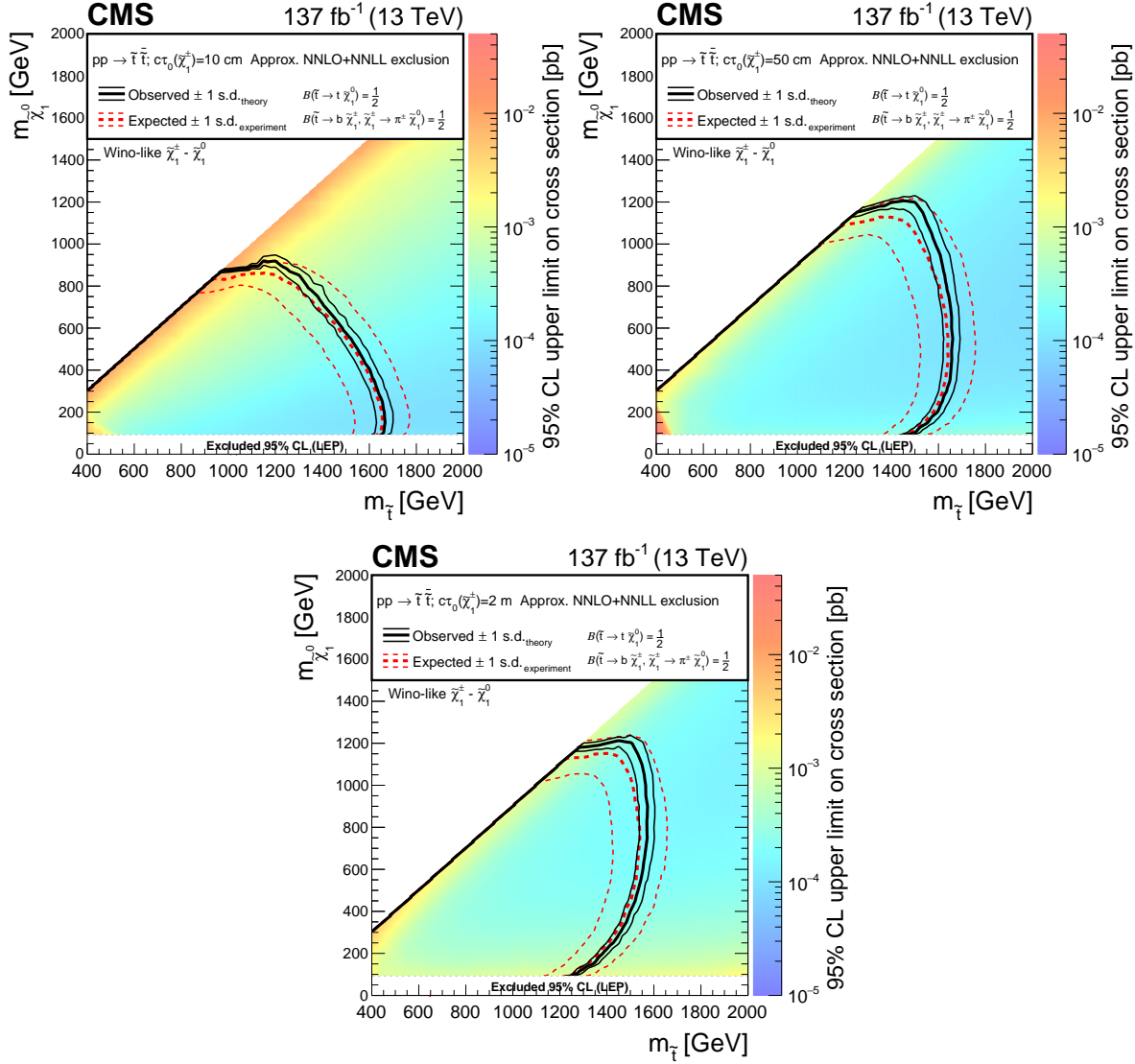


Figure 3.22: Taken from [5]

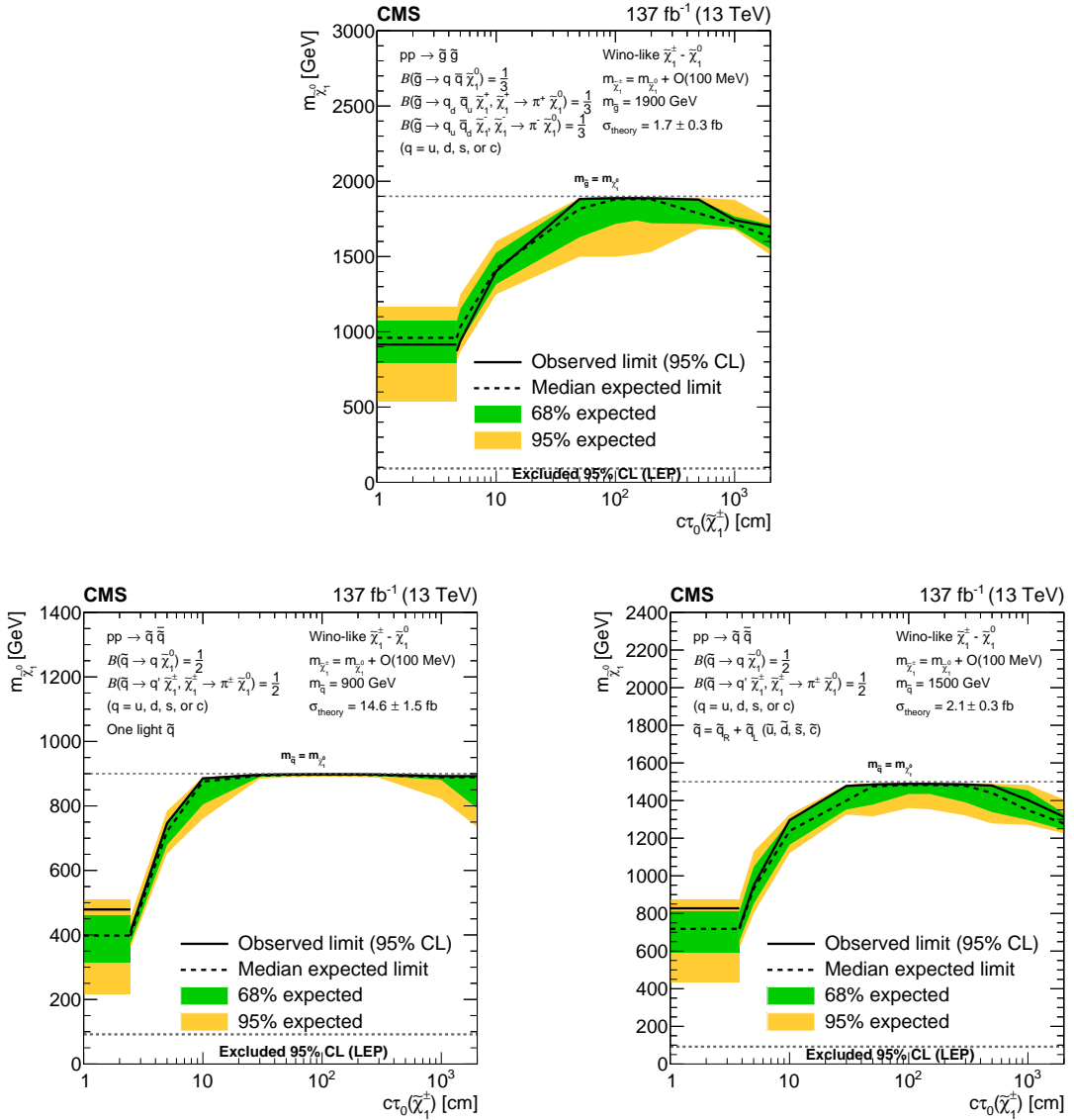


Figure 3.23: Taken from [5]

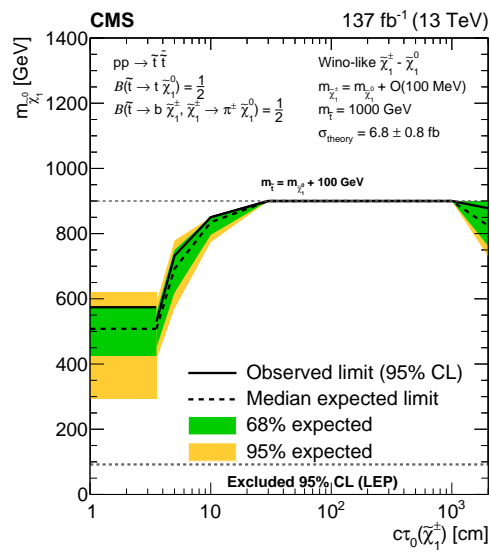


Figure 3.24: Taken from [5]

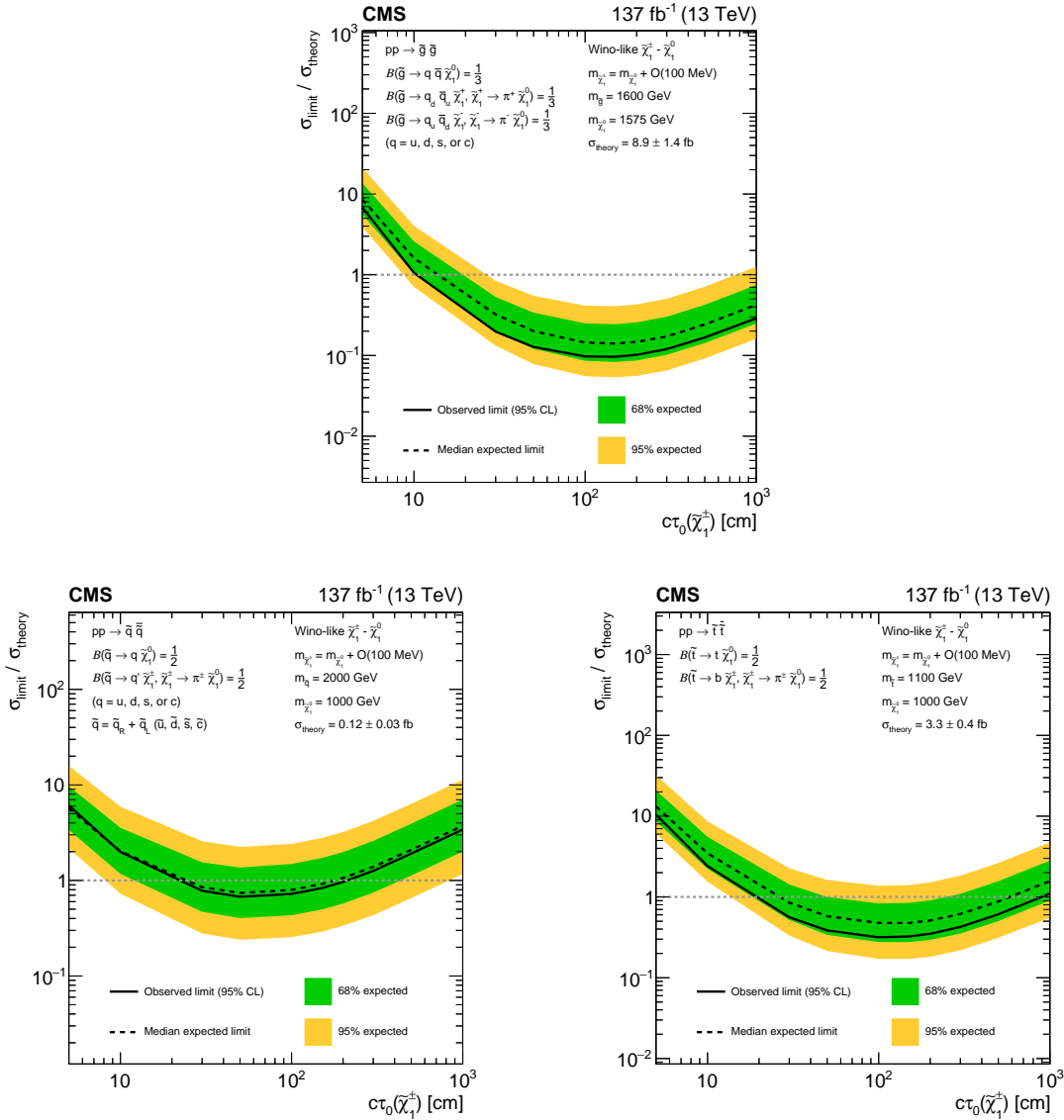


Figure 3.25: Taken from [5]

Chapter 4

Conclusions

SM is robust at low energy physics but has some issues that may have consequences at the weak scale. LHC and CMS are powerful machines that can investigate the weak scale. Performed a pair of searches that are sensitive to pair-produced particles decaying to dark matter, one of these issues, that can constrain SUSY, a solution to the hierarchy problem. One of these searches targets long-lived particles producing disappearing, a challenging final state to study. Produced strongest constraints to date.

Appendix A

Full Classic Binning and Results

Table A.1: Predictions and observations for the 12 search regions with $N_{\text{jet}} = 1$. For each of the background predictions, the first uncertainty listed is statistical (from the limited size of data control samples and Monte Carlo samples), and the second is systematic. Reprinted from [5].

$N_{\text{jet}} = 1$						
$N_{\text{jet}}, N_{\text{b-tag}}$	$p_T^{\text{jet1}} [\text{GeV}]$	Lost lepton	$Z \rightarrow \nu\nu$	Multijet	Total background	Data
1j, 0b	250-350	$70700 \pm 400 \pm 4100$	$167000 \pm 1000 \pm 11000$	$530 \pm 20 \pm 160$	238000 $\pm 1000 \pm 14000$	251941
	350-450	$13440 \pm 130 \pm 790$	$40100 \pm 500 \pm 3100$	$55 \pm 5 \pm 16$	53600 $\pm 500 \pm 3700$	54870
	450-575	$3050 \pm 50 \pm 180$	$10850^{+230}_{-220} \pm 690$	$5.6 \pm 1.1 \pm 1.6$	13910 $\pm 230 \pm 840$	14473
	575-700	$603^{+20}_{-19} \pm 38$	$2590^{+110}_{-100} \pm 160$	$0.38 \pm 0.06 \pm 0.11$	3200 $\pm 110 \pm 190$	3432
	700-1000	$220 \pm 13 \pm 16$	$1076^{+70}_{-66} \pm 66$	$0.12 \pm 0.03 \pm 0.03$	$1295^{+71}_{-67} \pm 79$	1304
	1000-1200	$11.7^{+4.1}_{-3.2} \pm 0.9$	$86^{+23}_{-19} \pm 6$	< 0.01	$98^{+24}_{-19} \pm 7$	98
	≥ 1200	$2.8^{+2.7}_{-1.5} \pm 0.6$	$23^{+12}_{-8} \pm 2$	< 0.01	$26^{+13}_{-9} \pm 2$	30
1j, $\geq 1b$	250-350	$4210 \pm 110 \pm 260$	$9030 \pm 230 \pm 630$	$58 \pm 10 \pm 17$	$13310^{+260}_{-250} \pm 820$	13549
	350-450	$878 \pm 38 \pm 56$	$2180^{+110}_{-100} \pm 170$	$4.6 \pm 0.4 \pm 1.3$	3060 $\pm 110 \pm 220$	3078
	450-575	$211^{+16}_{-15} \pm 13$	$651^{+57}_{-53} \pm 44$	$0.63 \pm 0.18 \pm 0.18$	$863^{+59}_{-55} \pm 53$	810
	575-700	$40.3^{+6.0}_{-5.5} \pm 2.5$	$164^{+30}_{-26} \pm 11$	$0.04 \pm 0.02 \pm 0.02$	$205^{+31}_{-26} \pm 13$	184
	≥ 700	$19.2^{+5.7}_{-4.6} \pm 1.3$	$74^{+21}_{-16} \pm 7$	< 0.01	$94^{+21}_{-17} \pm 7$	83

Table A.2: Predictions and observations for the 30 search regions with $250 \leq H_T < 450$ GeV. For each of the background predictions, the first uncertainty listed is statistical (from the limited size of data control samples and Monte Carlo samples), and the second is systematic. Reprinted from [5].

$250 \leq H_T < 450$ GeV						
$N_{\text{jet}}, N_{\text{b-tag}}$	$M_{\text{T2}} [\text{GeV}]$	Lost lepton	$Z \rightarrow \nu\nu$	Multijet	Total background	Data
2-3j, 0b	200-300	$73700 \pm 500 \pm 5000$	$156000 \pm 1000 \pm 12000$	$580 \pm 20 \pm 140$	$231000 \pm 1000 \pm 16000$	240867
	300-400	$12030 \pm 200 \pm 820$	$31300 \pm 200 \pm 2500$	$50 \pm 5 \pm 10$	$43400 \pm 300 \pm 3200$	44074
	≥ 400	$417^{+51}_{-47} \pm 28$	$1450 \pm 10 \pm 140$	$0.44 \pm 0.09 \pm 0.09$	$1870 \pm 50 \pm 160$	2022
2-3j, 1b	200-300	$12450 \pm 170 \pm 820$	$18700 \pm 300 \pm 1500$	$90 \pm 8 \pm 21$	$31300 \pm 300 \pm 2200$	32120
	300-400	$2380 \pm 80 \pm 160$	$3750 \pm 60 \pm 310$	$6.9 \pm 1.0 \pm 1.5$	$6130 \pm 100 \pm 430$	6258
	≥ 400	$97 \pm 8 \pm 39$	$174 \pm 3 \pm 17$	$0.01 \pm 0.01 \pm 0.00$	$271^{+9}_{-8} \pm 45$	275
2-3j, 2b	200-300	$2240 \pm 70 \pm 150$	$2340^{+110}_{-100} \pm 200$	$9.7 \pm 1.1 \pm 2.3$	$4600^{+130}_{-120} \pm 320$	4709
	300-400	$398^{+34}_{-32} \pm 27$	$469^{+21}_{-20} \pm 39$	$0.68 \pm 0.17 \pm 0.15$	$868^{+40}_{-38} \pm 61$	984
	≥ 400	$13.3 \pm 2.3 \pm 5.4$	$21.7^{+1.0}_{-0.9} \pm 2.2$	< 0.01	$35.0 \pm 2.5 \pm 6.0$	30
2-6j, $\geq 3b$	200-300	$507^{+32}_{-31} \pm 38$	$179^{+35}_{-30} \pm 27$	$1.77 \pm 0.46 \pm 0.46$	$688^{+47}_{-43} \pm 54$	699
	300-400	$69 \pm 6 \pm 15$	$40.0^{+7.8}_{-6.6} \pm 6.0$	$0.16 \pm 0.12 \pm 0.04$	$109^{+10}_{-9} \pm 16$	102
	≥ 400	$1.50 \pm 0.80 \pm 0.61$	$1.43^{+0.28}_{-0.24} \pm 0.25$	< 0.01	$2.92^{+0.85}_{-0.83} \pm 0.67$	0
4-6j, 0b	200-300	$12500 \pm 180 \pm 800$	$21600 \pm 300 \pm 1800$	$250 \pm 17 \pm 58$	$34400 \pm 400 \pm 2400$	35187
	300-400	$2070 \pm 80 \pm 130$	$4660 \pm 70 \pm 410$	$18.2 \pm 3.6 \pm 3.8$	$6750 \pm 110 \pm 510$	6725
	≥ 400	$42 \pm 5 \pm 17$	$155 \pm 2 \pm 64$	$0.06 \pm 0.03 \pm 0.01$	$197 \pm 5 \pm 67$	170
4-6j, 1b	200-300	$5750 \pm 100 \pm 380$	$4300 \pm 150 \pm 360$	$61 \pm 7 \pm 15$	$10120 \pm 180 \pm 680$	10564
	300-400	$784^{+43}_{-42} \pm 52$	$928^{+32}_{-31} \pm 84$	$2.07 \pm 0.29 \pm 0.45$	$1710 \pm 50 \pm 120$	1769
	≥ 400	$14.0 \pm 2.5 \pm 5.7$	$31 \pm 1 \pm 13$	$0.04 \pm 0.02 \pm 0.01$	$45 \pm 3 \pm 14$	40
4-6j, 2b	200-300	$2550^{+70}_{-60} \pm 170$	$921^{+68}_{-63} \pm 87$	$10.0 \pm 1.5 \pm 2.2$	$3480 \pm 90 \pm 230$	3621
	300-400	$220^{+23}_{-21} \pm 15$	$198^{+15}_{-14} \pm 20$	$0.47 \pm 0.15 \pm 0.11$	$419^{+27}_{-25} \pm 31$	496
	≥ 400	$3.2 \pm 0.8 \pm 1.3$	$6.6 \pm 0.5 \pm 2.7$	< 0.01	$9.8 \pm 0.9 \pm 3.1$	14
$\geq 7j, 0b$	200-300	$55^{+15}_{-13} \pm 4$	$61^{+23}_{-17} \pm 26$	$2.64 \pm 0.39 \pm 0.57$	$119^{+28}_{-22} \pm 27$	108
	300-500	$3.8^{+2.1}_{-2.0} \pm 0.8$	$8.1^{+3.1}_{-2.3} \pm 4.3$	$0.08 \pm 0.04 \pm 0.02$	$12.0^{+3.7}_{-3.1} \pm 4.4$	30
	≥ 500	$0.0^{+3.2}_{-0.0} \pm 0.0$	$0.0^{+1.2}_{-0.0} \pm 0.0$	< 0.01	$0.0^{+3.4}_{-0.0} \pm 0.0$	0
$\geq 7j, 1b$	200-300	$48.0^{+9.1}_{-8.2} \pm 3.5$	$19^{+19}_{-11} \pm 10$	$0.33 \pm 0.14 \pm 0.09$	$68^{+21}_{-13} \pm 11$	95
	≥ 300	$3.0 \pm 1.4 \pm 1.2$	$2.5^{+2.4}_{-1.3} \pm 1.7$	$0.03 \pm 0.02 \pm 0.01$	$5.6^{+2.8}_{-1.9} \pm 2.1$	12
$\geq 7j, 2b$	200-300	$41.3^{+7.7}_{-7.0} \pm 3.1$	$6.0^{+5.8}_{-3.2} \pm 3.7$	$0.29 \pm 0.14 \pm 0.06$	$47.6^{+9.7}_{-7.7} \pm 5.0$	30
	≥ 300	$2.15^{+0.78}_{-0.76} \pm 0.87$	$0.74^{+0.72}_{-0.40} \pm 0.57$	< 0.01	$2.9^{+1.1}_{-0.9} \pm 1.1$	1
$\geq 7j, \geq 3b$	200-300	$7.3^{+1.7}_{-1.5} \pm 0.9$	$1.0^{+1.0}_{-0.6} \pm 1.1$	$0.04 \pm 0.04 \pm 0.01$	$8.4^{+1.9}_{-1.6} \pm 1.5$	17
	≥ 300	$0.47 \pm 0.35 \pm 0.20$	$0.12^{+0.11}_{-0.06} \pm 0.14$	< 0.01	$0.59^{+0.37}_{-0.35} \pm 0.24$	0

Table A.3: Predictions and observations for the 40 search regions with $450 \leq H_T < 575$ GeV. For each of the background predictions, the first uncertainty listed is statistical (from the limited size of data control samples and Monte Carlo samples), and the second is systematic. Reprinted from [5].

$450 \leq H_T < 575$ GeV						
$N_{\text{jet}}, N_{\text{b-tag}}$	$M_{\text{T2}} [\text{GeV}]$	Lost lepton	$Z \rightarrow vv$	Multijet	Total background	Data
2-3j, 0b	200-300	$8860 \pm 110 \pm 640$	$20100 \pm 200 \pm 1300$	$69 \pm 13 \pm 16$	29100 $\pm 300 \pm 1900$	28956
	300-400	$4230 \pm 80 \pm 300$	$11770 \pm 140 \pm 790$	$10.6 \pm 0.8 \pm 2.4$	16000 $\pm 200 \pm 1000$	15876
	400-500	$1510 \pm 60 \pm 110$	$5020 \pm 60 \pm 360$	$2.86 \pm 0.62 \pm 0.60$	6540 $\pm 80 \pm 440$	6527
	≥ 500	$121^{+24}_{-21} \pm 9$	$580 \pm 7 \pm 63$	$0.07 \pm 0.03 \pm 0.02$	701^{+25}_{-22} ± 68	740
2-3j, 1b	200-300	$1326 \pm 43 \pm 88$	$2500 \pm 80 \pm 170$	$17.0 \pm 8.4 \pm 3.8$	3840^{+100}_{-90} ± 240	3859
	300-400	$737 \pm 35 \pm 49$	$1464^{+49}_{-48} \pm 99$	$1.62 \pm 0.20 \pm 0.43$	2200 $\pm 60 \pm 140$	2065
	400-500	$259^{+25}_{-23} \pm 19$	$626^{+21}_{-20} \pm 45$	$0.49 \pm 0.10 \pm 0.12$	885^{+32}_{-31} ± 58	907
	≥ 500	$19.1^{+2.8}_{-2.7} \pm 7.8$	$72.4 \pm 2.4 \pm 7.9$	$0.04 \pm 0.02 \pm 0.02$	92 $\pm 4 \pm 11$	79
2-3j, 2b	200-300	$201 \pm 15 \pm 13$	$322^{+31}_{-28} \pm 25$	$1.34 \pm 0.62 \pm 0.47$	524^{+35}_{-32} ± 35	463
	300-400	$83.8^{+9.6}_{-9.1} \pm 9.1$	$188^{+18}_{-17} \pm 15$	$0.26 \pm 0.07 \pm 0.07$	272^{+21}_{-19} ± 20	304
	400-500	$31.8^{+4.1}_{-4.0} \pm 6.7$	$80.4^{+7.7}_{-7.1} \pm 6.6$	$0.02 \pm 0.01 \pm 0.01$	112^{+9}_{-8} ± 10	120
	≥ 500	$2.16^{+0.67}_{-0.66} \pm 0.88$	$9.3^{+0.9}_{-0.8} \pm 1.1$	< 0.01	11.4 $\pm 1.1 \pm 1.4$	15
2-6j, $\geq 3b$	200-300	$232^{+17}_{-16} \pm 15$	$57^{+17}_{-13} \pm 7$	$2.20 \pm 0.70 \pm 0.80$	291^{+24}_{-21} ± 19	297
	300-400	$81^{+12}_{-11} \pm 6$	$33.6^{+9.9}_{-7.8} \pm 4.3$	$0.26 \pm 0.08 \pm 0.08$	115^{+16}_{-14} ± 8	76
	400-500	$10.7^{+2.1}_{-2.0} \pm 2.3$	$11.4^{+3.4}_{-2.7} \pm 1.5$	< 0.01	22.1^{+4.0}_{-3.4} ± 2.8	24
	≥ 500	$1.08 \pm 0.58 \pm 0.44$	$1.03^{+0.30}_{-0.24} \pm 0.17$	< 0.01	2.11^{+0.65}_{-0.62} ± 0.48	0
4-6j, 0b	200-300	$5660 \pm 90 \pm 370$	$8560 \pm 170 \pm 600$	$143 \pm 7 \pm 35$	14360 $\pm 190 \pm 890$	15047
	300-400	$2250 \pm 60 \pm 150$	$4790^{+100}_{-90} \pm 350$	$24.3 \pm 2.6 \pm 6.2$	7060 $\pm 110 \pm 460$	6939
	400-500	$428^{+32}_{-30} \pm 28$	$1220 \pm 20 \pm 110$	$1.42 \pm 0.21 \pm 0.52$	1650 $\pm 40 \pm 130$	1817
	≥ 500	$14.8 \pm 2.2 \pm 6.0$	$86 \pm 2 \pm 35$	$0.04 \pm 0.02 \pm 0.01$	101 $\pm 3 \pm 36$	104
4-6j, 1b	200-300	$2810 \pm 60 \pm 190$	$1880 \pm 80 \pm 130$	$63 \pm 15 \pm 19$	4750 $\pm 100 \pm 300$	4736
	300-400	$937 \pm 36 \pm 63$	$1054^{+45}_{-43} \pm 78$	$5.4 \pm 0.4 \pm 1.4$	2000 $\pm 60 \pm 130$	2039
	400-500	$138^{+17}_{-16} \pm 10$	$269 \pm 11 \pm 25$	$0.36 \pm 0.10 \pm 0.10$	407^{+20}_{-19} ± 31	403
	≥ 500	$7.5 \pm 2.2 \pm 3.0$	$19.1 \pm 0.8 \pm 7.9$	$0.01 \pm 0.01 \pm 0.00$	26.5 $\pm 2.3 \pm 8.5$	27
4-6j, 2b	200-300	$1343^{+38}_{-37} \pm 89$	$414^{+39}_{-35} \pm 33$	$11.5 \pm 1.0 \pm 3.3$	1770 $\pm 50 \pm 110$	1767
	300-400	$418^{+24}_{-23} \pm 29$	$232^{+22}_{-20} \pm 19$	$1.35 \pm 0.35 \pm 0.39$	651^{+32}_{-31} ± 43	636
	400-500	$45.6^{+3.9}_{-3.8} \pm 9.6$	$59.1^{+5.5}_{-5.1} \pm 5.9$	$0.03 \pm 0.02 \pm 0.01$	105^{+7}_{-6} ± 12	120
	≥ 500	$1.59 \pm 0.89 \pm 0.65$	$4.2 \pm 0.4 \pm 1.7$	< 0.01	5.8 $\pm 1.0 \pm 1.9$	7
$\geq 7j, 0b$	200-300	$149^{+17}_{-16} \pm 13$	$169^{+31}_{-27} \pm 34$	$11.5 \pm 0.8 \pm 3.0$	329^{+36}_{-31} ± 38	354
	300-400	$38.9^{+5.8}_{-5.6} \pm 8.2$	$64^{+12}_{-10} \pm 17$	$1.24 \pm 0.42 \pm 0.32$	104^{+13}_{-12} ± 20	110
	≥ 400	$1.28 \pm 0.82 \pm 0.52$	$8.8^{+1.6}_{-1.4} \pm 3.8$	$0.03 \pm 0.02 \pm 0.01$	10.1^{+1.8}_{-1.6} ± 3.8	10
$\geq 7j, 1b$	200-300	$191^{+13}_{-12} \pm 15$	$67^{+19}_{-15} \pm 15$	$4.4 \pm 0.5 \pm 1.2$	262^{+23}_{-19} ± 23	268
	300-400	$37.8^{+3.4}_{-3.3} \pm 8.0$	$25.3^{+7.2}_{-5.7} \pm 7.3$	$0.30 \pm 0.07 \pm 0.08$	63^{+8}_{-7} ± 11	65
	≥ 400	$2.31 \pm 0.69 \pm 0.94$	$3.5^{+1.0}_{-0.8} \pm 1.5$	$0.01 \pm 0.01 \pm 0.00$	5.8^{+1.2}_{-1.0} ± 1.8	3
$\geq 7j, 2b$	200-300	$173^{+12}_{-11} \pm 13$	$19.9^{+5.7}_{-4.5} \pm 5.2$	$1.24 \pm 0.18 \pm 0.33$	194^{+13}_{-12} ± 15	197
	300-400	$26.8 \pm 2.6 \pm 5.7$	$7.6^{+2.2}_{-1.7} \pm 2.4$	$0.09 \pm 0.04 \pm 0.03$	34.6^{+3.4}_{-3.1} ± 6.3	44
	≥ 400	$1.40 \pm 0.44 \pm 0.57$	$1.02^{+0.29}_{-0.23} \pm 0.46$	< 0.01	2.42^{+0.53}_{-0.49} ± 0.73	3
$\geq 7j, \geq 3b$	200-300	$55.4^{+4.8}_{-4.7} \pm 7.3$	$2.3^{+0.7}_{-0.6} \pm 1.1$	$0.15 \pm 0.06 \pm 0.06$	57.8^{+4.8}_{-4.7} ± 7.4	37
	300-400	$6.4 \pm 1.2 \pm 1.5$	$0.86^{+0.25}_{-0.20} \pm 0.46$	$0.01 \pm 0.01 \pm 0.00$	7.3 $\pm 1.2 \pm 1.6$	9
	≥ 400	$0.06 \pm 0.01 \pm 0.03$	$0.12 \pm 0.03 \pm 0.06$	< 0.01	0.18^{+0.04}_{-0.03} ± 0.07	0

Table A.4: Predictions and observations for the 47 search regions with $575 \leq H_T < 1200$ GeV, $N_{\text{jet}} < 7$. For each of the background predictions, the first uncertainty listed is statistical (from the limited size of data control samples and Monte Carlo samples), and the second is systematic. Reprinted from [5].

$575 \leq H_T < 1200$ GeV, $N_{\text{jet}} < 7$						
$N_{\text{jet}}, N_{\text{b-tag}}$	$M_{\text{T2}} [\text{GeV}]$	Lost lepton	$Z \rightarrow vv$	Multijet	Total background	Data
2-3j, 0b	200-300	$5270 \pm 60 \pm 370$	$11550 \pm 160 \pm 790$	$93 \pm 20 \pm 30$	16900 $\pm 200 \pm 1100$	17256
	300-400	$2560 \pm 50 \pm 180$	$7770^{+110}_{-100} \pm 540$	$11.9 \pm 1.3 \pm 4.4$	10340 $^{+120}_{-110} \pm 680$	10145
	400-500	$1101^{+32}_{-31} \pm 77$	$3900 \pm 50 \pm 280$	$1.33 \pm 0.24 \pm 0.41$	5000 $\pm 60 \pm 340$	5021
	500-600	$502^{+24}_{-23} \pm 35$	$2250 \pm 30 \pm 170$	$0.37 \pm 0.07 \pm 0.12$	2760 $\pm 40 \pm 200$	2706
	600-700	$180^{+16}_{-15} \pm 13$	$746 \pm 10 \pm 73$	$0.09 \pm 0.03 \pm 0.03$	926 $^{+19}_{-18} \pm 80$	1066
	700-800	$52.1^{+7.3}_{-6.5} \pm 5.5$	$256 \pm 3 \pm 36$	$0.01 \pm 0.01 \pm 0.00$	308 $^{+8}_{-7} \pm 38$	347
	800-900	$17.7^{+2.6}_{-2.3} \pm 2.2$	$107 \pm 1 \pm 20$	< 0.01	125 $\pm 3 \pm 21$	111
	900-1000	$6.0 \pm 0.9 \pm 1.3$	$39.4 \pm 0.5 \pm 8.5$	$0.01 \pm 0.01 \pm 0.00$	45.4 $^{+1.1}_{-1.0} \pm 8.7$	39
	1000-1100	$3.3^{+1.1}_{-1.0} \pm 1.0$	$13.3 \pm 0.2 \pm 3.9$	< 0.01	16.6 $\pm 1.1 \pm 4.1$	11
	≥ 1100	$0.31^{+0.09}_{-0.08} \pm 0.12$	$2.5 \pm 0.0 \pm 1.1$	< 0.01	2.8 $\pm 0.1 \pm 1.1$	2
2-3j, 1b	200-300	$826^{+27}_{-26} \pm 54$	$1480^{+60}_{-50} \pm 100$	$38 \pm 15 \pm 12$	2340 $\pm 60 \pm 140$	2499
	300-400	$426^{+21}_{-20} \pm 28$	$994^{+38}_{-37} \pm 69$	$2.33 \pm 0.26 \pm 0.84$	1422 $^{+43}_{-42} \pm 90$	1366
	400-600	$282^{+18}_{-17} \pm 20$	$788^{+30}_{-29} \pm 55$	$0.27 \pm 0.06 \pm 0.10$	1071 $^{+35}_{-34} \pm 69$	1057
	600-800	$43.5^{+3.2}_{-3.1} \pm 6.5$	$129 \pm 5 \pm 12$	< 0.01	172 $\pm 6 \pm 15$	225
	800-1000	$4.6 \pm 0.7 \pm 1.3$	$18.8 \pm 0.7 \pm 3.3$	< 0.01	23.4 $\pm 1.0 \pm 3.6$	22
	≥ 1000	$0.34 \pm 0.08 \pm 0.14$	$2.05 \pm 0.08 \pm 0.90$	< 0.01	2.38 $\pm 0.11 \pm 0.91$	1
2-3j, 2b	200-300	$105.1^{+9.2}_{-8.7} \pm 7.6$	$181^{+20}_{-18} \pm 15$	$3.8 \pm 0.5 \pm 1.3$	290 $^{+22}_{-20} \pm 20$	316
	300-400	$55.0^{+6.7}_{-6.3} \pm 7.5$	$122^{+14}_{-12} \pm 10$	$0.27 \pm 0.06 \pm 0.10$	177 $^{+15}_{-14} \pm 14$	159
	400-600	$36.5^{+4.6}_{-4.3} \pm 5.5$	$97^{+11}_{-10} \pm 8$	$0.08 \pm 0.03 \pm 0.03$	133 $^{+12}_{-11} \pm 11$	107
	600-800	$4.7 \pm 0.8 \pm 1.3$	$15.8^{+1.8}_{-1.6} \pm 1.6$	< 0.01	20.6 $^{+1.9}_{-1.8} \pm 2.2$	21
	≥ 800	$0.59 \pm 0.19 \pm 0.24$	$2.56^{+0.29}_{-0.26} \pm 0.45$	< 0.01	3.14 $^{+0.35}_{-0.32} \pm 0.52$	1
2-6j, $\geq 3b$	200-300	$299^{+17}_{-16} \pm 22$	$73^{+15}_{-13} \pm 10$	$6.2 \pm 0.4 \pm 2.1$	379 $^{+22}_{-21} \pm 28$	345
	300-400	$100 \pm 10 \pm 7$	$43.5^{+8.8}_{-7.4} \pm 6.2$	$0.68 \pm 0.09 \pm 0.24$	144 $^{+14}_{-12} \pm 11$	132
	400-600	$32.5^{+6.3}_{-5.6} \pm 2.5$	$31.2^{+6.3}_{-5.3} \pm 4.4$	$0.08 \pm 0.03 \pm 0.03$	63.8 $^{+8.9}_{-7.7} \pm 5.8$	48
	600-800	$3.16^{+0.95}_{-0.90} \pm 0.68$	$5.4^{+1.1}_{-0.9} \pm 0.8$	< 0.01	8.6 $^{+1.4}_{-1.3} \pm 1.1$	4
	≥ 800	$0.10 \pm 0.03 \pm 0.04$	$0.71^{+0.14}_{-0.12} \pm 0.15$	< 0.01	0.81 $^{+0.15}_{-0.12} \pm 0.16$	0
4-6j, 0b	200-300	$6280 \pm 70 \pm 420$	$9470 \pm 160 \pm 650$	$360 \pm 20 \pm 110$	16100 $\pm 180 \pm 1000$	16292
	300-400	$2700 \pm 50 \pm 180$	$5410 \pm 90 \pm 380$	$53 \pm 1 \pm 17$	8160 $\pm 100 \pm 520$	8330
	400-500	$927^{+28}_{-27} \pm 62$	$2420 \pm 40 \pm 180$	$7.7 \pm 0.4 \pm 2.4$	3350 $\pm 50 \pm 230$	3576
	500-600	$324^{+17}_{-16} \pm 22$	$1171^{+20}_{-19} \pm 100$	$1.46 \pm 0.12 \pm 0.46$	1500 $\pm 30 \pm 110$	1516
	600-700	$95.4^{+9.4}_{-8.7} \pm 6.4$	$413 \pm 7 \pm 47$	$0.33 \pm 0.06 \pm 0.10$	509 $^{+12}_{-11} \pm 50$	543
	700-800	$35.6^{+5.0}_{-4.5} \pm 3.6$	$171 \pm 3 \pm 27$	$0.03 \pm 0.02 \pm 0.01$	206 $^{+6}_{-5} \pm 27$	178
	800-900	$13.4^{+2.0}_{-1.8} \pm 1.6$	$64 \pm 1 \pm 11$	$0.02 \pm 0.01 \pm 0.01$	77 $\pm 2 \pm 11$	62
	900-1000	$4.39^{+0.78}_{-0.73} \pm 0.93$	$23.6 \pm 0.4 \pm 5.3$	< 0.01	28.0 $^{+0.9}_{-0.8} \pm 5.4$	20
	1000-1100	$0.64 \pm 0.16 \pm 0.20$	$6.3 \pm 0.1 \pm 2.0$	< 0.01	6.9 $\pm 0.2 \pm 2.0$	3
4-6j, 1b	≥ 1100	$0.78 \pm 0.58 \pm 0.32$	$0.89^{+0.02}_{-0.01} \pm 0.40$	< 0.01	1.68 $\pm 0.58 \pm 0.52$	1
	200-300	$2900 \pm 50 \pm 200$	$2220^{+80}_{-70} \pm 150$	$154 \pm 16 \pm 50$	5270 $\pm 90 \pm 330$	5335
	300-400	$1066 \pm 29 \pm 74$	$1267^{+44}_{-42} \pm 89$	$19.2 \pm 0.9 \pm 6.2$	2350 $\pm 50 \pm 150$	2547
	400-600	$504^{+22}_{-21} \pm 35$	$840^{+29}_{-28} \pm 61$	$2.98 \pm 0.21 \pm 0.93$	1347 $^{+36}_{-35} \pm 88$	1284
	600-800	$35.3^{+5.9}_{-5.2} \pm 2.6$	$138 \pm 5 \pm 14$	$0.09 \pm 0.03 \pm 0.03$	174 $^{+8}_{-7} \pm 16$	151
	800-1000	$3.89^{+0.83}_{-0.77} \pm 0.82$	$19.3^{+0.7}_{-0.6} \pm 4.3$	$0.01 \pm 0.01 \pm 0.00$	23.2 $^{+1.1}_{-1.0} \pm 4.5$	18
4-6j, 2b	≥ 1000	$0.18 \pm 0.07 \pm 0.07$	$1.57 \pm 0.05 \pm 0.65$	< 0.01	1.75 $\pm 0.09 \pm 0.65$	1
	200-300	$1500 \pm 30 \pm 100$	$473^{+36}_{-33} \pm 36$	$42 \pm 2 \pm 13$	2020 $\pm 50 \pm 130$	1968
	300-400	$508 \pm 20 \pm 35$	$270^{+20}_{-19} \pm 21$	$4.9 \pm 0.3 \pm 1.6$	783 $^{+29}_{-28} \pm 50$	788
	400-600	$167 \pm 12 \pm 12$	$179^{+14}_{-13} \pm 14$	$0.57 \pm 0.08 \pm 0.18$	346 $^{+18}_{-17} \pm 23$	354
	600-800	$11.9^{+1.3}_{-1.2} \pm 2.5$	$29.5^{+2.2}_{-2.1} \pm 3.5$	$0.02 \pm 0.01 \pm 0.01$	41.4 $^{+2.6}_{-2.4} \pm 4.6$	37
	≥ 800	$0.91 \pm 0.23 \pm 0.37$	$4.4 \pm 0.56 \pm 1.8$	< 0.01	5.4 $\pm 0.4 \pm 1.9$	7

Table A.5: Predictions and observations for the 34 search regions with $575 \leq H_T < 1200$ GeV, $N_{\text{jet}} \geq 7$. For each of the background predictions, the first uncertainty listed is statistical (from the limited size of data control samples and Monte Carlo samples), and the second is systematic. Reprinted from [5].

$575 \leq H_T < 1200$ GeV, $N_{\text{jet}} \geq 7$						
$N_{\text{jet}}, N_{\text{b-tag}}$	$M_{\text{T2}} [\text{GeV}]$	Lost lepton	$Z \rightarrow vv$	Multijet	Total background	Data
7-9j, 0b	200-300	$589^{+27}_{-26} \pm 39$	$573^{+47}_{-43} \pm 64$	$90 \pm 10 \pm 28$	$1252^{+55}_{-52} \pm 93$	1340
	300-400	$265^{+19}_{-18} \pm 18$	$279^{+23}_{-21} \pm 42$	$14.9 \pm 0.5 \pm 4.7$	$559^{+29}_{-28} \pm 51$	581
	400-600	$92^{+10}_{-9} \pm 6$	$159^{+13}_{-12} \pm 28$	$2.72 \pm 0.18 \pm 0.85$	$253^{+16}_{-15} \pm 30$	243
	600-800	$8.6 \pm 1.2 \pm 1.8$	$22.8^{+1.9}_{-1.7} \pm 6.4$	$0.10 \pm 0.03 \pm 0.03$	$31.6^{+2.2}_{-2.1} \pm 6.8$	32
	≥ 800	$0.51 \pm 0.16 \pm 0.21$	$3.0 \pm 0.2 \pm 1.3$	< 0.01	$3.5 \pm 0.3 \pm 1.3$	2
7-9j, 1b	200-300	$733 \pm 21 \pm 52$	$278^{+28}_{-25} \pm 33$	$48 \pm 3 \pm 16$	$1059^{+35}_{-33} \pm 73$	1052
	300-400	$252^{+13}_{-12} \pm 18$	$135^{+14}_{-12} \pm 21$	$7.7 \pm 0.4 \pm 2.5$	$395^{+19}_{-17} \pm 32$	387
	400-600	$71.3^{+6.9}_{-6.5} \pm 5.2$	$77^{+8}_{-7} \pm 14$	$1.36 \pm 0.13 \pm 0.45$	$150 \pm 10 \pm 16$	131
	600-800	$4.26^{+0.73}_{-0.71} \pm 0.90$	$11.0^{+1.1}_{-1.0} \pm 3.1$	$0.03 \pm 0.02 \pm 0.01$	$15.3^{+1.3}_{-1.2} \pm 3.3$	20
	≥ 800	$0.11 \pm 0.04 \pm 0.05$	$1.48^{+0.15}_{-0.13} \pm 0.63$	< 0.01	$1.60^{+0.15}_{-0.14} \pm 0.63$	1
7-9j, 2b	200-300	$675 \pm 20 \pm 51$	$82^{+8}_{-7} \pm 10$	$20.9 \pm 3.0 \pm 6.7$	$777^{+22}_{-21} \pm 56$	750
	300-400	$211 \pm 11 \pm 16$	$39.8^{+4.0}_{-3.6} \pm 6.4$	$2.42 \pm 0.19 \pm 0.79$	$253^{+12}_{-11} \pm 19$	259
	400-600	$55.4^{+5.5}_{-5.2} \pm 4.2$	$22.7^{+2.3}_{-2.1} \pm 4.2$	$0.50 \pm 0.07 \pm 0.16$	$78.6^{+5.9}_{-5.6} \pm 6.6$	72
	600-800	$3.00^{+0.63}_{-0.62} \pm 0.64$	$3.25^{+0.32}_{-0.30} \pm 0.93$	$0.01 \pm 0.01 \pm 0.01$	$6.3 \pm 0.7 \pm 1.2$	7
	≥ 800	$0.27 \pm 0.20 \pm 0.11$	$0.44 \pm 0.04 \pm 0.19$	< 0.01	$0.71 \pm 0.20 \pm 0.22$	1
7-9j, 3b	200-300	$185 \pm 8 \pm 18$	$11.3^{+1.1}_{-1.0} \pm 1.9$	$3.6 \pm 0.2 \pm 1.2$	$200 \pm 8 \pm 18$	184
	300-400	$52.0 \pm 3.8 \pm 5.0$	$5.5 \pm 0.5 \pm 1.2$	$0.72 \pm 0.12 \pm 0.26$	$58.3^{+3.9}_{-3.8} \pm 5.3$	59
	400-600	$13.6 \pm 1.8 \pm 1.3$	$3.13^{+0.31}_{-0.29} \pm 0.82$	$0.05 \pm 0.02 \pm 0.02$	$16.8 \pm 1.8 \pm 1.6$	14
	≥ 600	$0.49 \pm 0.21 \pm 0.20$	$0.51 \pm 0.05 \pm 0.21$	< 0.01	$1.00 \pm 0.21 \pm 0.29$	2
7-9j, $\geq 4b$	200-300	$38.8 \pm 3.1 \pm 7.4$	$2.01^{+0.20}_{-0.18} \pm 0.71$	$0.55 \pm 0.08 \pm 0.19$	$41.3^{+3.2}_{-3.1} \pm 7.4$	38
	300-400	$14.5^{+2.0}_{-1.9} \pm 2.8$	$0.98^{+0.10}_{-0.09} \pm 0.43$	$0.06 \pm 0.02 \pm 0.02$	$15.6^{+2.0}_{-1.9} \pm 2.8$	16
	≥ 400	$3.75^{+0.98}_{-0.97} \pm 0.70$	$0.65 \pm 0.06 \pm 0.35$	< 0.01	$4.40^{+0.98}_{-0.97} \pm 0.79$	3
$\geq 10j$, 0b	200-300	$11.5 \pm 1.6 \pm 1.0$	$4.4^{+0.4}_{-0.3} \pm 2.3$	$3.1 \pm 0.8 \pm 1.1$	$19.0 \pm 1.8 \pm 2.8$	27
	300-500	$5.6 \pm 1.0 \pm 0.5$	$3.0 \pm 0.2 \pm 1.7$	$0.55 \pm 0.08 \pm 0.20$	$9.1 \pm 1.0 \pm 1.8$	4
	≥ 500	$0.30 \pm 0.11 \pm 0.12$	$0.44^{+0.04}_{-0.03} \pm 0.24$	$0.02 \pm 0.01 \pm 0.01$	$0.76 \pm 0.11 \pm 0.27$	3
$\geq 10j$, 1b	200-300	$21.0 \pm 1.8 \pm 1.6$	$3.5 \pm 0.3 \pm 1.9$	$1.92 \pm 0.18 \pm 0.72$	$26.4 \pm 1.8 \pm 2.7$	32
	300-500	$7.7 \pm 1.0 \pm 0.6$	$2.4 \pm 0.2 \pm 1.4$	$0.45 \pm 0.07 \pm 0.17$	$10.5 \pm 1.1 \pm 1.6$	15
	≥ 500	$0.83^{+0.42}_{-0.41} \pm 0.07$	$0.36^{+0.04}_{-0.03} \pm 0.20$	$0.02 \pm 0.01 \pm 0.01$	$1.20^{+0.42}_{-0.41} \pm 0.22$	0
$\geq 10j$, 2b	200-300	$21.8 \pm 1.8 \pm 1.6$	$1.05 \pm 0.10 \pm 0.66$	$0.64 \pm 0.08 \pm 0.24$	$23.5 \pm 1.8 \pm 1.8$	26
	300-500	$8.8 \pm 1.2 \pm 0.6$	$0.69^{+0.07}_{-0.06} \pm 0.45$	$0.16 \pm 0.04 \pm 0.06$	$9.6^{+1.3}_{-1.2} \pm 0.8$	9
	≥ 500	$0.22 \pm 0.13 \pm 0.02$	$0.10 \pm 0.01 \pm 0.06$	< 0.01	$0.32 \pm 0.13 \pm 0.07$	0
$\geq 10j$, 3b	200-300	$9.9 \pm 1.3 \pm 1.2$	$0.25 \pm 0.02 \pm 0.20$	$0.29 \pm 0.05 \pm 0.12$	$10.4 \pm 1.3 \pm 1.2$	14
	≥ 300	$1.59 \pm 0.50 \pm 0.18$	$0.19 \pm 0.02 \pm 0.16$	$0.02 \pm 0.01 \pm 0.01$	$1.80 \pm 0.50 \pm 0.25$	2
$\geq 10j$, $\geq 4b$	≥ 200	$3.9 \pm 1.2 \pm 0.8$	$0.00^{+0.17}_{-0.00} \pm 0.00$	$0.05 \pm 0.02 \pm 0.02$	$4.0 \pm 1.2 \pm 0.8$	6

Table A.6: Predictions and observations for the 37 search regions with $1200 \leq H_T < 1500$ GeV, $N_{\text{jet}} < 7$. For each of the background predictions, the first uncertainty listed is statistical (from the limited size of data control samples and Monte Carlo samples), and the second is systematic. Reprinted from [5].

$1200 \leq H_T < 1500$ GeV, $N_{\text{jet}} < 7$						
$N_{\text{jet}}, N_{\text{b-tag}}$	M _{T2} [GeV]	Lost lepton	Z → vv	Multijet	Total background	Data
2-3j, 0b	200-400	$315 \pm 15 \pm 21$	$656^{+51}_{-47} \pm 73$	$39 \pm 16 \pm 12$	$\mathbf{1009}^{+55}_{-52} \pm 85$	1128
	400-600	$43.0^{+5.2}_{-4.7} \pm 4.9$	$185^{+14}_{-13} \pm 30$	$0.03 \pm 0.02 \pm 0.01$	$\mathbf{228}^{+15}_{-14} \pm 31$	207
	600-800	$14.1^{+2.1}_{-2.0} \pm 1.7$	$64 \pm 5 \pm 17$	< 0.01	$\mathbf{78} \pm 5 \pm 17$	83
	800-1000	$6.4^{+1.1}_{-1.0} \pm 1.3$	$32.5^{+2.5}_{-2.3} \pm 7.6$	< 0.01	$\mathbf{38.9}^{+2.7}_{-2.5} \pm 7.8$	36
	1000-1200	$3.23^{+0.61}_{-0.59} \pm 0.99$	$17.5 \pm 1.3 \pm 5.2$	< 0.01	$\mathbf{20.7}^{+1.5}_{-1.4} \pm 5.3$	19
	≥ 1200	$0.87^{+0.14}_{-0.13} \pm 0.35$	$6.0^{+0.5}_{-0.4} \pm 2.6$	< 0.01	$\mathbf{6.9} \pm 0.5 \pm 2.6$	4
2-3j, 1b	200-400	$61.5^{+7.2}_{-6.5} \pm 4.2$	$78^{+19}_{-16} \pm 10$	$9.7 \pm 0.7 \pm 3.0$	$\mathbf{149}^{+21}_{-17} \pm 12$	157
	400-600	$10.1 \pm 1.4 \pm 1.0$	$21.9^{+5.4}_{-4.4} \pm 3.8$	$0.03 \pm 0.02 \pm 0.01$	$\mathbf{32.0}^{+5.6}_{-4.6} \pm 4.1$	27
	600-800	$2.36^{+0.36}_{-0.35} \pm 0.41$	$7.5^{+1.9}_{-1.5} \pm 2.0$	< 0.01	$\mathbf{9.8}^{+1.9}_{-1.6} \pm 2.1$	9
	800-1000	$0.78^{+0.16}_{-0.15} \pm 0.19$	$3.84^{+0.95}_{-0.78} \pm 0.93$	< 0.01	$\mathbf{4.62}^{+0.97}_{-0.79} \pm 0.96$	6
	1000-1200	$0.43 \pm 0.08 \pm 0.14$	$2.13^{+0.53}_{-0.43} \pm 0.64$	< 0.01	$\mathbf{2.56}^{+0.54}_{-0.44} \pm 0.66$	2
	≥ 1200	$0.14^{+0.05}_{-0.04} \pm 0.06$	$0.71^{+0.18}_{-0.14} \pm 0.31$	< 0.01	$\mathbf{0.86}^{+0.18}_{-0.15} \pm 0.31$	0
2-3j, 2b	200-400	$4.8^{+2.0}_{-1.6} \pm 0.3$	$11^{+11}_{-6} \pm 2$	$1.38 \pm 0.13 \pm 0.43$	$\mathbf{18}^{+11}_{-6} \pm 2$	18
	400-600	$0.61^{+0.30}_{-0.25} \pm 0.07$	$3.2^{+3.1}_{-1.7} \pm 0.7$	< 0.01	$\mathbf{3.8}^{+3.1}_{-1.8} \pm 0.7$	5
	600-800	$0.21^{+0.11}_{-0.09} \pm 0.04$	$1.1^{+1.1}_{-0.6} \pm 0.4$	< 0.01	$\mathbf{1.3}^{+1.1}_{-0.6} \pm 0.4$	2
	800-1000	$0.07^{+0.04}_{-0.03} \pm 0.02$	$0.56^{+0.55}_{-0.31} \pm 0.18$	< 0.01	$\mathbf{0.63}^{+0.55}_{-0.31} \pm 0.18$	1
	≥ 1000	$0.03 \pm 0.02 \pm 0.01$	$0.42^{+0.41}_{-0.23} \pm 0.18$	< 0.01	$\mathbf{0.46}^{+0.41}_{-0.23} \pm 0.18$	1
2-6j, ≥ 3b	200-400	$22.6^{+4.7}_{-4.2} \pm 1.8$	$0.0^{+6.6}_{-0.0} \pm 0.0$	$4.4 \pm 0.2 \pm 1.5$	$\mathbf{27.0}^{+8.1}_{-4.2} \pm 2.4$	25
	400-600	$1.58^{+0.51}_{-0.48} \pm 0.34$	$0.0^{+1.6}_{-0.0} \pm 0.0$	$0.02 \pm 0.01 \pm 0.01$	$\mathbf{1.6}^{+1.7}_{-0.5} \pm 0.3$	3
	≥ 600	$0.47^{+0.27}_{-0.26} \pm 0.19$	$0.00^{+0.94}_{-0.00} \pm 0.00$	< 0.01	$\mathbf{0.47}^{+0.98}_{-0.26} \pm 0.19$	4
4-6j, 0b	200-400	$606^{+21}_{-20} \pm 41$	$909^{+63}_{-59} \pm 90$	$208 \pm 12 \pm 64$	$\mathbf{1720}^{+70}_{-60} \pm 130$	1768
	400-600	$84.3^{+7.4}_{-6.9} \pm 5.8$	$234^{+16}_{-15} \pm 34$	$0.88 \pm 0.09 \pm 0.27$	$\mathbf{319}^{+18}_{-17} \pm 36$	301
	600-800	$21.1^{+3.2}_{-2.9} \pm 2.3$	$75 \pm 5 \pm 17$	$0.06 \pm 0.02 \pm 0.02$	$\mathbf{96} \pm 6 \pm 17$	99
	800-1000	$7.6^{+1.2}_{-1.1} \pm 1.1$	$35.2^{+2.4}_{-2.3} \pm 8.0$	$0.01 \pm 0.01 \pm 0.00$	$\mathbf{42.7}^{+2.7}_{-2.5} \pm 8.2$	41
	1000-1200	$2.23^{+0.36}_{-0.33} \pm 0.61$	$14.1^{+1.0}_{-0.9} \pm 4.2$	< 0.01	$\mathbf{16.3} \pm 1.0 \pm 4.2$	15
	≥ 1200	$0.47^{+0.10}_{-0.09} \pm 0.19$	$3.0 \pm 0.2 \pm 1.3$	< 0.01	$\mathbf{3.5} \pm 0.2 \pm 1.3$	5
4-6j, 1b	200-400	$278^{+15}_{-14} \pm 20$	$254^{+33}_{-30} \pm 28$	$97 \pm 2 \pm 30$	$\mathbf{629}^{+36}_{-33} \pm 50$	579
	400-600	$30.3^{+4.0}_{-3.7} \pm 2.7$	$65^{+9}_{-8} \pm 10$	$0.33 \pm 0.06 \pm 0.10$	$\mathbf{96}^{+9}_{-8} \pm 11$	79
	600-800	$8.2^{+1.4}_{-1.3} \pm 1.0$	$21.0^{+2.8}_{-2.5} \pm 4.8$	$0.02 \pm 0.01 \pm 0.01$	$\mathbf{29.2}^{+3.1}_{-2.8} \pm 5.0$	16
	800-1000	$2.36^{+0.56}_{-0.54} \pm 0.50$	$9.8^{+1.3}_{-1.1} \pm 2.3$	$0.01 \pm 0.01 \pm 0.00$	$\mathbf{12.2}^{+1.4}_{-1.3} \pm 2.4$	9
	1000-1200	$1.00 \pm 0.24 \pm 0.31$	$4.0 \pm 0.5 \pm 1.2$	< 0.01	$\mathbf{5.0}^{+0.6}_{-0.5} \pm 1.2$	6
	≥ 1200	$0.07 \pm 0.02 \pm 0.03$	$0.86^{+0.11}_{-0.10} \pm 0.37$	< 0.01	$\mathbf{0.92}^{+0.11}_{-0.10} \pm 0.37$	1
4-6j, 2b	200-400	$120.4^{+9.1}_{-8.7} \pm 9.8$	$45^{+18}_{-13} \pm 5$	$26.0 \pm 0.6 \pm 8.1$	$\mathbf{191}^{+20}_{-16} \pm 15$	194
	400-600	$11.9 \pm 1.4 \pm 1.5$	$11.5^{+4.6}_{-3.4} \pm 1.8$	$0.11 \pm 0.03 \pm 0.04$	$\mathbf{23.4}^{+4.8}_{-3.7} \pm 2.6$	27
	600-800	$3.49 \pm 0.83 \pm 0.75$	$3.7^{+1.5}_{-1.1} \pm 1.0$	< 0.01	$\mathbf{7.2}^{+1.7}_{-1.4} \pm 1.3$	7
	800-1000	$0.66 \pm 0.16 \pm 0.20$	$1.73^{+0.69}_{-0.51} \pm 0.48$	< 0.01	$\mathbf{2.38}^{+0.71}_{-0.54} \pm 0.53$	3
	≥ 1000	$0.15 \pm 0.04 \pm 0.06$	$0.84^{+0.34}_{-0.25} \pm 0.36$	< 0.01	$\mathbf{1.00}^{+0.34}_{-0.25} \pm 0.36$	0

Table A.7: Predictions and observations for the 31 search regions with $1200 \leq H_T < 1500$ GeV, $N_{\text{jet}} \geq 7$. For each of the background predictions, the first uncertainty listed is statistical (from the limited size of data control samples and Monte Carlo samples), and the second is systematic. Reprinted from [5].

$1200 \leq H_T < 1500$ GeV, $N_{\text{jet}} \geq 7$						
$N_{\text{jet}}, N_{\text{b-tag}}$	$M_{\text{T2}} [\text{GeV}]$	Lost lepton	$Z \rightarrow vv$	Multijet	Total background	Data
7-9j, 0b	200-400	$120.4^{+9.8}_{-9.2} \pm 9.0$	$108^{+26}_{-21} \pm 21$	$91 \pm 3 \pm 29$	$\mathbf{319}^{+28}_{-24} \pm 38$	379
	400-600	$16.5^{+1.9}_{-1.8} \pm 2.0$	$25.8^{+6.3}_{-5.1} \pm 5.7$	$0.80 \pm 0.09 \pm 0.25$	$\mathbf{43.1}^{+6.5}_{-5.4} \pm 6.3$	45
	600-800	$2.94 \pm 0.42 \pm 0.63$	$8.6^{+2.1}_{-1.7} \pm 2.1$	$0.06 \pm 0.02 \pm 0.02$	$\mathbf{11.6}^{+2.1}_{-1.8} \pm 2.2$	17
	800-1000	$0.77^{+0.14}_{-0.13} \pm 0.24$	$2.90^{+0.70}_{-0.58} \pm 1.00$	$0.01 \pm 0.01 \pm 0.00$	$\mathbf{3.7}^{+0.7}_{-0.6} \pm 1.0$	3
	≥ 1000	$0.11 \pm 0.03 \pm 0.05$	$1.09^{+0.26}_{-0.22} \pm 0.50$	< 0.01	$\mathbf{1.21}^{+0.27}_{-0.22} \pm 0.50$	0
7-9j, 1b	200-400	$133.8^{+8.0}_{-7.7} \pm 9.8$	$36^{+13}_{-10} \pm 8$	$58 \pm 2 \pm 18$	$\mathbf{228}^{+15}_{-13} \pm 23$	247
	400-600	$16.6^{+2.9}_{-2.7} \pm 1.3$	$8.7^{+3.2}_{-2.4} \pm 2.1$	$0.46 \pm 0.07 \pm 0.14$	$\mathbf{25.8}^{+4.3}_{-3.6} \pm 2.7$	23
	600-800	$1.83^{+0.43}_{-0.41} \pm 0.28$	$2.9^{+1.1}_{-0.8} \pm 0.8$	$0.03 \pm 0.02 \pm 0.01$	$\mathbf{4.8}^{+1.1}_{-0.9} \pm 0.8$	7
	800-1000	$0.65^{+0.24}_{-0.23} \pm 0.18$	$0.95^{+0.34}_{-0.26} \pm 0.34$	$0.02 \pm 0.01 \pm 0.01$	$\mathbf{1.62}^{+0.42}_{-0.35} \pm 0.39$	2
	≥ 1000	$0.22 \pm 0.19 \pm 0.09$	$0.36^{+0.13}_{-0.10} \pm 0.17$	< 0.01	$\mathbf{0.58}^{+0.23}_{-0.21} \pm 0.19$	0
7-9j, 2b	200-400	$124.0^{+7.6}_{-7.4} \pm 9.1$	$9.9^{+3.6}_{-2.7} \pm 2.5$	$21.4 \pm 0.5 \pm 6.9$	$\mathbf{155} \pm 8 \pm 12$	162
	400-600	$15.0^{+2.8}_{-2.6} \pm 1.3$	$2.41^{+0.87}_{-0.66} \pm 0.67$	$0.12 \pm 0.03 \pm 0.04$	$\mathbf{17.5}^{+3.0}_{-2.7} \pm 1.5$	18
	600-800	$2.47^{+0.78}_{-0.76} \pm 0.53$	$0.81^{+0.29}_{-0.22} \pm 0.26$	$0.01 \pm 0.01 \pm 0.00$	$\mathbf{3.29}^{+0.83}_{-0.79} \pm 0.60$	1
	≥ 800	$0.24 \pm 0.11 \pm 0.10$	$0.36^{+0.13}_{-0.10} \pm 0.16$	< 0.01	$\mathbf{0.60}^{+0.17}_{-0.15} \pm 0.19$	1
7-9j, 3b	200-400	$30.0 \pm 2.6 \pm 3.2$	$1.89^{+0.68}_{-0.52} \pm 0.64$	$5.0 \pm 0.3 \pm 1.8$	$\mathbf{36.9}^{+2.7}_{-2.6} \pm 3.8$	46
	400-600	$4.1^{+1.1}_{-1.0} \pm 0.6$	$0.45^{+0.16}_{-0.12} \pm 0.18$	$0.02 \pm 0.01 \pm 0.01$	$\mathbf{4.6}^{+1.1}_{-1.0} \pm 0.6$	2
	≥ 600	$0.92^{+0.50}_{-0.49} \pm 0.38$	$0.23^{+0.08}_{-0.06} \pm 0.11$	< 0.01	$\mathbf{1.15} \pm 0.50 \pm 0.40$	1
7-9j, $\geq 4b$	200-400	$9.1 \pm 1.6 \pm 1.8$	$0.26^{+0.10}_{-0.07} \pm 0.23$	$0.88 \pm 0.10 \pm 0.32$	$\mathbf{10.3} \pm 1.6 \pm 1.9$	9
	≥ 400	$0.44^{+0.24}_{-0.23} \pm 0.08$	$0.10^{+0.04}_{-0.03} \pm 0.09$	< 0.01	$\mathbf{0.53} \pm 0.24 \pm 0.12$	0
$\geq 10j$, 0b	200-400	$7.7^{+1.2}_{-1.1} \pm 0.8$	$2.7^{+0.6}_{-0.5} \pm 2.8$	$8.3 \pm 0.9 \pm 3.0$	$\mathbf{18.7}^{+1.6}_{-1.5} \pm 4.1$	17
	400-600	$1.00 \pm 0.32 \pm 0.22$	$0.56^{+0.13}_{-0.11} \pm 0.62$	$0.11 \pm 0.03 \pm 0.04$	$\mathbf{1.66}^{+0.35}_{-0.34} \pm 0.66$	1
	≥ 600	$0.10^{+0.35}_{-0.04} \pm 0.04$	$0.14^{+0.08}_{-0.03} \pm 0.14$	$0.01 \pm 0.01 \pm 0.00$	$\mathbf{0.24}^{+0.36}_{-0.05} \pm 0.15$	0
$\geq 10j$, 1b	200-400	$15.2 \pm 1.8 \pm 1.4$	$1.1^{+0.4}_{-0.3} \pm 1.2$	$5.3 \pm 0.2 \pm 1.9$	$\mathbf{21.6}^{+1.9}_{-1.8} \pm 2.7$	22
	400-600	$1.27^{+0.38}_{-0.36} \pm 0.11$	$0.22^{+0.08}_{-0.06} \pm 0.26$	$0.05 \pm 0.02 \pm 0.02$	$\mathbf{1.55}^{+0.39}_{-0.37} \pm 0.29$	6
	≥ 600	$0.03 \pm 0.02 \pm 0.01$	$0.05^{+0.10}_{-0.01} \pm 0.05$	< 0.01	$\mathbf{0.07}^{+0.11}_{-0.02} \pm 0.05$	0
$\geq 10j$, 2b	200-400	$16.9 \pm 1.8 \pm 1.5$	$0.44^{+0.16}_{-0.12} \pm 0.50$	$2.7 \pm 0.2 \pm 1.0$	$\mathbf{20.1} \pm 1.8 \pm 1.9$	16
	400-600	$2.62^{+0.71}_{-0.68} \pm 0.30$	$0.09 \pm 0.03 \pm 0.11$	$0.01 \pm 0.01 \pm 0.00$	$\mathbf{2.73}^{+0.71}_{-0.68} \pm 0.32$	2
	≥ 600	$0.23 \pm 0.15 \pm 0.10$	$0.02^{+0.08}_{-0.01} \pm 0.02$	< 0.01	$\mathbf{0.25}^{+0.17}_{-0.15} \pm 0.10$	0
$\geq 10j$, 3b	200-400	$5.58^{+0.86}_{-0.85} \pm 0.61$	$0.12^{+0.11}_{-0.03} \pm 0.16$	$1.04 \pm 0.10 \pm 0.42$	$\mathbf{6.74}^{+0.87}_{-0.86} \pm 0.76$	6
	≥ 400	$0.51 \pm 0.22 \pm 0.06$	$0.03^{+0.11}_{-0.01} \pm 0.04$	< 0.01	$\mathbf{0.54}^{+0.25}_{-0.22} \pm 0.08$	0
$\geq 10j$, $\geq 4b$	≥ 200	$2.59 \pm 0.82 \pm 0.62$	$0.10^{+0.13}_{-0.03} \pm 0.13$	$0.31 \pm 0.06 \pm 0.13$	$\mathbf{3.00}^{+0.83}_{-0.82} \pm 0.65$	7

Table A.8: Predictions and observations for the 30 search regions with $H_T \geq 1500$ GeV, $N_{\text{jet}} < 7$. For each of the background predictions, the first uncertainty listed is statistical (from the limited size of data control samples and Monte Carlo samples), and the second is systematic. Reprinted from [5].

$H_T \geq 1500$ GeV, $N_{\text{jet}} < 7$						
$N_{\text{jet}}, N_{\text{b-tag}}$	M_{T2} [GeV]	Lost lepton	$Z \rightarrow vv$	Multijet	Total background	Data
2-3j, 0b	400-600	$27.2^{+4.4}_{-3.9} \pm 2.5$	$150^{+14}_{-13} \pm 19$	$0.16 \pm 0.04 \pm 0.05$	$177^{+15}_{-13} \pm 20$	125
	600-800	$7.8^{+1.4}_{-1.2} \pm 0.8$	$38.7^{+3.6}_{-3.3} \pm 8.4$	< 0.01	$46.5^{+3.9}_{-3.6} \pm 8.6$	37
	800-1000	$2.29^{+0.39}_{-0.34} \pm 0.35$	$17.2^{+1.6}_{-1.5} \pm 3.4$	< 0.01	$19.5^{+1.7}_{-1.5} \pm 3.4$	19
	1000-1200	$1.20^{+0.21}_{-0.19} \pm 0.26$	$9.0 \pm 0.8 \pm 1.8$	< 0.01	$10.2^{+0.9}_{-0.8} \pm 1.9$	14
	1200-1400	$0.80^{+0.16}_{-0.14} \pm 0.22$	$4.9^{+0.5}_{-0.4} \pm 1.3$	< 0.01	$5.7^{+0.5}_{-0.4} \pm 1.4$	4
	1400-1800	$0.43^{+0.09}_{-0.08} \pm 0.15$	$2.80^{+0.26}_{-0.24} \pm 0.98$	< 0.01	$3.23^{+0.28}_{-0.26} \pm 0.99$	3
	≥ 1800	$0.05 \pm 0.02 \pm 0.02$	$0.41^{+0.04}_{-0.03} \pm 0.19$	< 0.01	$0.46 \pm 0.04 \pm 0.19$	0
2-3j, 1b	400-600	$5.2^{+1.1}_{-1.0} \pm 0.6$	$13.4^{+4.9}_{-3.7} \pm 1.9$	$0.09 \pm 0.03 \pm 0.03$	$18.7^{+5.0}_{-3.8} \pm 2.1$	23
	600-800	$1.52^{+0.43}_{-0.41} \pm 0.27$	$3.5^{+1.3}_{-1.0} \pm 1.0$	< 0.01	$5.0^{+1.3}_{-1.0} \pm 1.0$	3
	800-1000	$0.38 \pm 0.09 \pm 0.10$	$1.53^{+0.55}_{-0.42} \pm 0.35$	< 0.01	$1.90^{+0.56}_{-0.43} \pm 0.37$	3
	1000-1200	$0.10 \pm 0.03 \pm 0.03$	$0.81^{+0.29}_{-0.22} \pm 0.24$	< 0.01	$0.91^{+0.29}_{-0.22} \pm 0.24$	4
	≥ 1200	$0.19 \pm 0.06 \pm 0.08$	$0.73^{+0.26}_{-0.20} \pm 0.31$	< 0.01	$0.92^{+0.27}_{-0.21} \pm 0.32$	0
2-3j, 2b	≥ 400	$0.63^{+0.49}_{-0.36} \pm 0.26$	$0.0^{+3.0}_{-0.0} \pm 0.0$	< 0.01	$0.6^{+3.0}_{-0.4} \pm 0.3$	2
2-6j, $\geq 3b$	400-600	$1.72^{+0.73}_{-0.68} \pm 0.42$	$1.1^{+2.4}_{-0.9} \pm 0.3$	$0.03 \pm 0.02 \pm 0.01$	$2.8^{+2.5}_{-1.1} \pm 0.6$	1
	≥ 600	$0.37^{+0.19}_{-0.18} \pm 0.16$	$0.5^{+1.2}_{-0.4} \pm 0.2$	< 0.01	$0.9^{+1.2}_{-0.5} \pm 0.2$	0
4-6j, 0b	400-600	$46.4^{+5.6}_{-5.1} \pm 3.6$	$176^{+15}_{-14} \pm 23$	$1.62 \pm 0.13 \pm 0.46$	$224^{+16}_{-15} \pm 24$	207
	600-800	$10.6^{+2.3}_{-1.9} \pm 1.2$	$45.5^{+4.0}_{-3.7} \pm 9.9$	$0.07 \pm 0.03 \pm 0.02$	$56^{+5}_{-4} \pm 10$	62
	800-1000	$4.5^{+1.1}_{-1.0} \pm 0.5$	$20.3^{+1.8}_{-1.6} \pm 3.9$	< 0.01	$24.8^{+2.1}_{-1.9} \pm 4.1$	31
	1000-1200	$1.35^{+0.30}_{-0.26} \pm 0.24$	$10.6 \pm 0.9 \pm 2.1$	< 0.01	$11.9^{+1.0}_{-0.9} \pm 2.2$	12
	1200-1400	$0.89^{+0.27}_{-0.25} \pm 0.23$	$5.7 \pm 0.5 \pm 1.5$	< 0.01	$6.6^{+0.6}_{-0.5} \pm 1.6$	9
	1400-1600	$0.20 \pm 0.05 \pm 0.07$	$2.64^{+0.23}_{-0.21} \pm 0.92$	< 0.01	$2.84^{+0.24}_{-0.22} \pm 0.92$	3
	≥ 1600	$0.09 \pm 0.03 \pm 0.04$	$1.18 \pm 0.10 \pm 0.51$	< 0.01	$1.27^{+0.11}_{-0.10} \pm 0.51$	2
4-6j, 1b	400-600	$21.0^{+3.7}_{-3.3} \pm 2.0$	$32.6^{+7.0}_{-5.8} \pm 5.5$	$0.81 \pm 0.09 \pm 0.23$	$54.5^{+7.9}_{-6.7} \pm 6.3$	72
	600-800	$4.79^{+0.91}_{-0.83} \pm 0.62$	$8.4^{+1.8}_{-1.5} \pm 2.3$	$0.02 \pm 0.01 \pm 0.01$	$13.2^{+2.0}_{-1.7} \pm 2.5$	20
	800-1000	$1.27^{+0.26}_{-0.24} \pm 0.27$	$3.71^{+0.79}_{-0.66} \pm 0.92$	$0.03 \pm 0.02 \pm 0.01$	$5.01^{+0.84}_{-0.71} \pm 0.97$	8
	1000-1400	$0.89^{+0.21}_{-0.20} \pm 0.28$	$3.00^{+0.64}_{-0.54} \pm 0.93$	< 0.01	$3.89^{+0.68}_{-0.57} \pm 0.98$	6
	≥ 1400	$0.40^{+0.34}_{-0.33} \pm 0.16$	$0.72^{+0.15}_{-0.13} \pm 0.31$	< 0.01	$1.12^{+0.37}_{-0.36} \pm 0.36$	3
4-6j, 2b	400-600	$7.2^{+1.2}_{-1.1} \pm 1.1$	$4.3^{+2.9}_{-1.9} \pm 1.4$	$0.17 \pm 0.04 \pm 0.05$	$11.7^{+3.2}_{-2.2} \pm 1.9$	11
	600-800	$1.66^{+0.41}_{-0.40} \pm 0.46$	$1.12^{+0.76}_{-0.48} \pm 0.55$	$0.01 \pm 0.01 \pm 0.00$	$2.79^{+0.86}_{-0.63} \pm 0.73$	3
	≥ 800	$0.32 \pm 0.13 \pm 0.13$	$0.99^{+0.67}_{-0.43} \pm 0.52$	< 0.01	$1.31^{+0.68}_{-0.45} \pm 0.54$	4

Table A.9: Predictions and observations for the 21 search regions with $H_T \geq 1500$ GeV, $N_{\text{jet}} \geq 7$. For each of the background predictions, the first uncertainty listed is statistical (from the limited size of data control samples and Monte Carlo samples), and the second is systematic. Reprinted from [5].

$H_T \geq 1500$ GeV, $N_{\text{jet}} \geq 7$						
$N_{\text{jet}}, N_{\text{b-tag}}$	M_{T2} [GeV]	Lost lepton	$Z \rightarrow vv$	Multijet	Total background	Data
7-9j, 0b	400-600	$14.3^{+1.8}_{-1.7} \pm 1.7$	$32.3^{+7.5}_{-6.2} \pm 4.3$	$1.50 \pm 0.13 \pm 0.44$	48.1 $^{+7.7}_{-6.4} \pm 5.0$	36
	600-800	$3.77^{+0.56}_{-0.55} \pm 0.69$	$8.3^{+1.9}_{-1.6} \pm 2.2$	$0.18 \pm 0.04 \pm 0.05$	12.3 $^{+2.0}_{-1.7} \pm 2.3$	9
	800-1000	$1.16^{+0.18}_{-0.17} \pm 0.30$	$3.70^{+0.86}_{-0.71} \pm 0.83$	$0.01 \pm 0.01 \pm 0.00$	4.86 $^{+0.88}_{-0.73} \pm 0.90$	6
	1000-1400	$0.58 \pm 0.11 \pm 0.19$	$2.96^{+0.69}_{-0.57} \pm 0.86$	$0.01 \pm 0.01 \pm 0.00$	3.55 $^{+0.69}_{-0.58} \pm 0.89$	4
	≥ 1400	$0.05 \pm 0.01 \pm 0.02$	$0.71^{+0.17}_{-0.14} \pm 0.30$	< 0.01	0.76 $^{+0.17}_{-0.14} \pm 0.30$	2
7-9j, 1b	400-600	$12.8^{+2.5}_{-2.3} \pm 1.6$	$9.2^{+4.2}_{-3.0} \pm 1.4$	$0.82 \pm 0.09 \pm 0.24$	22.9 $^{+4.9}_{-3.8} \pm 2.3$	25
	600-800	$3.49^{+0.94}_{-0.89} \pm 0.76$	$2.4^{+1.1}_{-0.8} \pm 1.0$	$0.06 \pm 0.02 \pm 0.02$	5.9 $^{+1.4}_{-1.2} \pm 1.2$	7
	≥ 800	$1.09^{+0.34}_{-0.32} \pm 0.45$	$2.10^{+0.96}_{-0.69} \pm 0.93$	< 0.01	3.2 $^{+1.0}_{-0.8} \pm 1.0$	2
7-9j, 2b	400-600	$8.1^{+1.8}_{-1.6} \pm 1.0$	$2.4^{+1.1}_{-0.8} \pm 0.4$	$0.35 \pm 0.06 \pm 0.10$	10.9 $^{+2.1}_{-1.8} \pm 1.2$	10
	600-800	$1.78^{+0.54}_{-0.52} \pm 0.40$	$0.62^{+0.28}_{-0.20} \pm 0.25$	$0.02 \pm 0.01 \pm 0.01$	2.41 $^{+0.61}_{-0.56} \pm 0.49$	5
	≥ 800	$0.40^{+0.19}_{-0.18} \pm 0.17$	$0.55^{+0.25}_{-0.18} \pm 0.25$	$0.01 \pm 0.01 \pm 0.00$	0.96 $^{+0.31}_{-0.26} \pm 0.30$	0
7-9j, 3b	400-800	$2.40^{+0.74}_{-0.72} \pm 0.29$	$0.32^{+0.15}_{-0.10} \pm 0.12$	$0.10 \pm 0.03 \pm 0.03$	2.82 $^{+0.76}_{-0.72} \pm 0.32$	2
	≥ 800	$0.16 \pm 0.09 \pm 0.07$	$0.08^{+0.04}_{-0.03} \pm 0.04$	< 0.01	0.24 $\pm 0.09 \pm 0.08$	0
7-9j, $\geq 4b$	≥ 400	$0.52^{+0.23}_{-0.22} \pm 0.08$	$0.07^{+0.03}_{-0.02} \pm 0.06$	$0.02 \pm 0.01 \pm 0.01$	0.61 $^{+0.23}_{-0.22} \pm 0.10$	1
$\geq 10j$, 0b	400-800	$1.41 \pm 0.38 \pm 0.33$	$1.52^{+0.35}_{-0.29} \pm 0.34$	$0.23 \pm 0.05 \pm 0.08$	3.17 $^{+0.52}_{-0.48} \pm 0.49$	11
	≥ 800	$0.05 \pm 0.02 \pm 0.02$	$0.37^{+0.09}_{-0.07} \pm 0.17$	$0.01 \pm 0.01 \pm 0.00$	0.43 $^{+0.09}_{-0.08} \pm 0.17$	0
$\geq 10j$, 1b	400-800	$2.16^{+0.71}_{-0.69} \pm 0.25$	$0.56^{+0.25}_{-0.18} \pm 0.16$	$0.14 \pm 0.04 \pm 0.05$	2.85 $^{+0.76}_{-0.71} \pm 0.31$	3
	≥ 800	$0.55 \pm 0.30 \pm 0.22$	$0.13^{+0.06}_{-0.04} \pm 0.07$	< 0.01	0.68 $^{+0.31}_{-0.30} \pm 0.23$	0
$\geq 10j$, 2b	≥ 400	$1.98^{+0.69}_{-0.67} \pm 0.24$	$0.30^{+0.14}_{-0.10} \pm 0.12$	$0.05 \pm 0.02 \pm 0.02$	2.33 $^{+0.70}_{-0.68} \pm 0.28$	0
$\geq 10j$, 3b	≥ 400	$0.77 \pm 0.35 \pm 0.09$	$0.00^{+0.45}_{-0.00} \pm 0.00$	$0.05 \pm 0.03 \pm 0.02$	0.82 $^{+0.57}_{-0.35} \pm 0.09$	1
$\geq 10j$, $\geq 4b$	≥ 400	$0.09 \pm 0.05 \pm 0.01$	$0.00^{+0.45}_{-0.00} \pm 0.00$	< 0.01	0.09 $^{+0.45}_{-0.05} \pm 0.01$	0

Bibliography

[1]

- [2] Morad Aaboud et al. Search for long-lived charginos based on a disappearing-track signature in pp collisions at $\sqrt{s} = 13$ TeV with the ATLAS detector. *JHEP*, 06:022, 2018.
- [3] Georges Aad et al. Search for charginos nearly mass degenerate with the lightest neutralino based on a disappearing-track signature in pp collisions at $\sqrt{s}=8$ TeV with the ATLAS detector. *Phys. Rev.*, D88(11):112006, 2013.
- [4] Christoph Borschensky, Michael Krmer, Anna Kulesza, Michelangelo Mangano, Sanjay Padhi, Tilman Plehn, and Xavier Portell. Squark and gluino production cross sections in

pp

p p collisions at

$$\sqrt{s} = 13, 14, 33$$

$s = 13, 14, 33$ and

100

100 tev. *The European Physical Journal C*, 74(12), Dec 2014.

- [5] CMS Collaboration. Searches for physics beyond the standard model with the m_{T2} variable in hadronic final states with and without disappearing tracks in proton-proton collisions at $\sqrt{s} = 13$ tev, 2019.
- [6] V. Khachatryan et al. Search for disappearing tracks in proton-proton collisions at $\sqrt{s} = 8$ TeV. *JHEP*, 01:096, 2015.
- [7] V. Khachatryan, A. M. Sirunyan, A. Tumasyan, W. Adam, E. Asilar, T. Bergauer, J. Brandstetter, E. Brondolin, M. Dragicevic, and et al. Search for new physics with the m_{t2} variable in all-jets final states produced in pp collisions at $s = 13$

$$\sqrt{s} = 13$$

tev. *Journal of High Energy Physics*, 2016(10), Oct 2016.

- [8] V. Khachatryan, A.M. Sirunyan, A. Tumasyan, W. Adam, E. Asilar, T. Bergauer, J. Brandstetter, E. Brondolin, M. Dragicevic, J. Er, and et al. Jet energy scale and resolution in the cms experiment in pp collisions at 8 tev. *Journal of Instrumentation*, 12(02):P02014P02014, Feb 2017.
- [9] Albert M Sirunyan et al. Search for new phenomena with the M_{T2} variable in the all-hadronic final state produced in protonproton collisions at $\sqrt{s} = 13$ TeV. *Eur. Phys. J.*, C77(10):710, 2017.
- [10] Albert M Sirunyan et al. Search for disappearing tracks as a signature of new long-lived particles in proton-proton collisions at $\sqrt{s} = 13$ TeV. *JHEP*, 08:016, 2018.
- [11] Albert M Sirunyan et al. Search for natural and split supersymmetry in proton-proton collisions at $\sqrt{s} = 13$ TeV in final states with jets and missing transverse momentum. *JHEP*, 05:025, 2018.
- [12] Albert M Sirunyan et al. Inclusive search for supersymmetry in pp collisions at $\sqrt{s} = 13$ TeV using razor variables and boosted object identification in zero and one lepton final states. *JHEP*, 03:031, 2019.
- [13] Albert M Sirunyan et al. Search for supersymmetry in proton-proton collisions at 13 TeV in final states with jets and missing transverse momentum. 2019.